TECHNISCHE UNIVERSITÄT WIEN

Energy Economics Group

Master Thesis

for the achievement of the academic degree

Diplom-Ingenieur

in the field of study Energie- und Automatisierungstechnik
at TU Wien

Large-scale heat pumps in Europe: A review of the status quo and the competitiveness of different heat sources

submitted at
Institute of Energy Systems and Electrical Drives

Supervisor: Ao. Univ. Prof. Univ. Prof. Dipl.-Ing. Dr.techn. Reinhard Haas
Assistent: Ali Kök, MSc

by

Lukas Steinwender, BSc
51831841

Wien, June 2024

Statutory Declaration

I declare that I have authored this thesis independently, that I have not used other than the declared sources/resources, and that I have explicitly marked all material which has been quoted either literally or by content from the used sources.

Wien, _____ _____

Date Signature

Eidesstattliche Erklärung

Ich erkläre an Eides statt, dass ich die vorliegende Arbeit selbstständig verfasst, andere als die angegebenen Quellen/Hilfsmittel nicht benutzt, und die den benutzten Quellen wörtlich und inhaltlich entnommenen Stellen als solche kenntlich gemacht habe.

Wien, am _____ _____

Datum Unterschrift

Danksagung

An dieser Stelle möchte ich mich bei all denjenigen bedanken, die mich während der Anfertigung dieser Masterarbeit unterstützt und motiviert haben.

Ich möchte mich zunächst bei Senior Scientist Dipl.-Ing. Dr.techn. Lukas Kranzl und Ali Kök, M.Sc. für die kompetente Betreuung, hilfreiche Anregungen und die rasche Unterstützung bei allen wichtigen Fragen bedanken.

Ebenso möchte ich meiner Familie und besonders meinen Eltern für die moralische und finanzielle Unterstützung während des gesamten Studiums danken. Auch meinen Freunden möchte ich danken, besonders Martin und Andy, deren Motivation mir auch in den schwersten Prüfungen geholfen hat.

Lukas Steinwender

Abstract

Large-scale heat pumps are regarded as a key technology for decarbonizing district heating systems. This work investigates the current status and potential contribution of large-scale heat pumps (LSHP) in European district heating systems under varying conditions of heat source availability and technology portfolios. The core objective is to assess the techno-economic viability of LSHP, particularly focusing on different refrigerants, sizes, and climate conditions. The methodology involves the creation of a database for large-scale heat pumps to assess their current status in terms of various parameters like size, location and temperature levels. It is followed by a scenario development using a district heat supply model. The data collection indicates that the installation of large-scale heat pumps has grown rapidly in recent years, along with an increasing diversity of heat sources in EU member states. Out of the simulated portfolios, large-scale heat pumps can cover from 47% to 68% of the total heat demand under various conditions when industrial process heat is used as a heat source, while this share is more fluctuating for ambient heat sources. Their economic viability is heavily influenced by the type of refrigerant and the scale of implementation, with larger heat pump units having significant economies of scale effects. Additionally, climatic conditions play a crucial role, with southern and central European climates showing higher efficiency and utilization rates compared to northern Europe. In conclusion, large-scale heat pumps are a promising technology for covering a high share of the heat demand in district heating systems under current conditions. Apart from the impact of electricity prices, which is not a focus of this thesis, their competitiveness depends on optimizing the choice of refrigerants, utilizing economies of scale, and diversifying heat sources to ensure reliability under specific climatic conditions.

Kurzfassung

Großwärmepumpen gelten als Schlüsseltechnologie zur Dekarbonisierung von Fernwärmesystemen. Diese Arbeit untersucht den aktuellen Stand und den potenziellen Beitrag von Großwärmepumpen in europäischen Fernwärmesystemen unter verschiedenen Berücksichtigung der Verfügbarkeit von Wärmequellen in verschiedenen Technologieportfolios. Das Hauptziel der Arbeit besteht darin, zu bewerten, wann die Installation von Großwärmepumpen technisch und ökonomisch sinnvoll ist, wobei der Fokus auf verschiedenen Kältemitteln, Größen und klimatischen Bedingungen liegt. Hierzu wird zunächst eine Datenbank für Großwärmepumpen erstellt, um den aktuellen Stand verschiedener Parameter wie Größe, Standort und Temeperaturniveaus zu erfassen. Dies wird durch die Entwicklung von Szenarien in einem Optimierungsmodell für die Einsatzplanung in Fernwärmenetzen ergänzt. Die Datenerhebung zeigt, dass die Installation von Großwärmepumpen in den letzten Jahren stark zugenommen hat, zusammen mit einer zunehmenden Vielfalt an Wärmequellen in den EU-Mitgliedstaaten. In den simulierten Portfolios können Großwärmepumpen unter verschiedenen Bedingungen 47% bis 68% der gesamten Wärmenachfrage decken, wenn industrielle Prozesswärme als Wärmequelle genutzt wird, während dieser Anteil bei Umgebungswärmequellen stärker schwankt. Die Rentabilität wird stark von der Art des Kältemittels beeinflusst, wobei größere Wärmepumpeneinheiten erhebliche Skaleneffekte aufweisen. Zusätzlich spielen klimatische Bedingungen eine entscheidende Rolle, wobei südliche und zentraleuropäische Klimazonen höhere Effizienz- und Nutzungsraten im Vergleich zu Nordeuropa zeigen. Zusammenfassend lässt sich sagen, dass Großwärmepumpen eine vielversprechende Technologie darstellen, um einen hohen Anteil des Wärmebedarfs in Fernwärmesystemen unter aktuellen Bedingungen zu decken. Abgesehen von den Strompreisen, die nicht im Fokus dieser Arbeit stehen, hängt ihre Wettbewerbsfähigkeit von der Optimierung der Wahl der Kältemittel, der Nutzung von Skaleneffekten und der Diversifizierung der Wärmequellen ab, um die Zuverlässigkeit unter bestimmten klimatischen Bedingungen sicherzustellen.

Contents

Abbreviations

The following abbreviations are used in the text. The different variables used in equations are explained in their respective sections.

CAPEX **C**apital **Ex**penditure
CHP **C**ombined **H**eat and **P**ower
COP **C**oefficient **Of** **P**erformance
DH **D**istrict **H**eating
DHC **D**istrict **H**eating and **C**ooling
GWP **G**lobal **W**arming **P**otential
HP **H**eat **P**umps
LCOH **L**evelized **C**ost **o**f **H**eat
LSHP **L**arge-**S**cale **H**eat **P**umps
MILP **M**ixed **I**nteger **L**inear **P**rogram
OPEX **O**perational **Ex**penditure
TCI **T**otal **C**ost of **I**nvestment
TES **T**hermal **E**nergy **S**torage

1 Introduction

In the *Paris Agreement* (2015), the goal of keeping the rise in mean global temperature well below 2 °C above pre-industrial levels has been set. To meet this goal and reach net zero by 2050, it is crucial to reduce the global CO_2-emissions caused by human primary energy consumption in a way, that is economical, feasible, and credible (Dolphin et al., 2023), and therefore widely accepted.

Vaclav (2023) shows the small and slow progress in reaching this goal, with the coronavirus pandemic being the first significant reduction (fig. 1.1) in global primary energy consumption. The *Renewables Global Status Report* (2019) states that the heating and cooling sector accounts for 50% of the global primary energy consumption in 2019. In Gilbert et al. (2023), this share is broken down further (fig. 1.2):

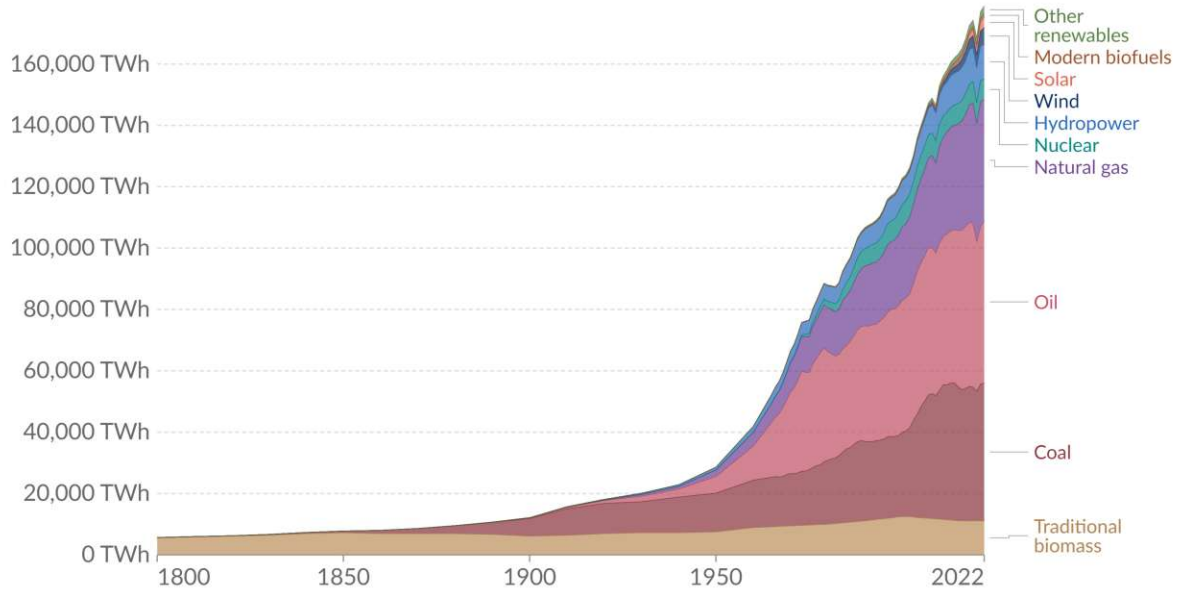

Figure 1.1: Global primary energy consumption by source (Vaclav, 2023)

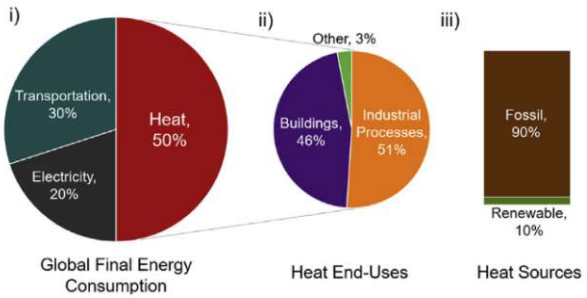

Figure 1.2: Breakdown of global final energy use by sector (Gilbert et al., 2023)

"About 90% of energy currently used for heating originates from fossil fuels and results in significant carbon emissions" (Gilbert et al., 2023)

This highlights the need for a sustainable heat supply. As a part of the Heat Roadmap Europe studies, Paardekooper et al. (2018) investigates this issue and estimates a potential increase of the district heating share to 50% of the entire heat demand by 2050, with approximately 25–30% of it being supplied using large-scale electric heat pumps.

Together with the knowledge gap in the literature on the topic of quantity and quality of excess and ambient heat sources (Arpagaus et al., 2018) and their technical utilization and economic potential (Jesper et al., 2021), this leads to the research question:

> "What is the current status and the potential contribution of large-scale heat pumps in European district heating systems under different conditions in terms of heat source availability and technology portfolio?"

The research question leads to the following sub-questions:

- What are the potentials of heat sources currently in terms of size, temperature levels, fluctuations, and regulatory aspects?
- Which technologies and framework conditions provide synergies with **L**arge-**S**cale **H**eat **P**umps (LSHP), and which are competing?
- How to improve the modeling (e.g. the **C**oefficient **O**f **P**erformance (COP)) of LSHP in a **D**istrict **H**eating (DH) supply optimization model?

The following points fall under the scope of this work:

- The definition of LSHP in this work is the same as in David et al. (2017) as all heat pumps with an output heating capacity $> 1 MW_{th}$ in total, where multiple units in series or parallel are summed up.
- The implementation of LSHP in 3^{rd} and 4^{th} generation DH systems with supply temperatures of 50°C – 120°C, also including industrial heat pumps which can provide heat in this temperature range and could be connected to DH.

To answer the research question, a 2-stage methodology is applied, which can be seen in detail in fig. 3.1: In the first stage, a literature review and data collection of various online resources is performed to asses current qualitative and quantitative aspects of LSHP in Europe. In the second stage, this data is used as input for the DH Supply Model HotMaps (2024). Here, scenarios are developed and conclusions can be drawn.

The work is divided in the following chapters:

- **Chapter 1: Introduction**
  Here, the general context is given and the relevance of the research question is highlighted. Based on this, sub-questions are presented and a brief methodological overview is given.

- **Chapter 2: State of the Art**
  Existing studies with a similar methodology or in a similar field of research are presented and the differences and similarities to this thesis are highlighted.

- **Chapter 3: Methodology**
  The methodology is presented in detail and starting from the main data sources, the data categorization is developed. The input data, adaptions to HotMaps (2024) and the scenarios developed are described in this chapter.

- **Chapter 4: Current status of large-scale heat pumps in European district heating systems**
  The literature review results and data collection about LSHP in Europe are presented and interpreted in this chapter.

- **Chapter 5: Results**
  This chapter shows the simulation results and scenarios developed in HotMaps (2024).

- **Chapter 6: Conclusion**
  Based on the results of chapters 4 and 5, conclusions to answer the research question are drawn in this chapter.

2 State of the Art

To make the subject of large-scale heat pumps in district heating more tangible, the most relevant literature regarding the advantages and disadvantages of LSHP, the assessment of the current status of LSHP in district heating and how LSHP are implemented in optimization models are discussed in this chapter. Additional background information regarding the working principle of a typical compression heat pump and the temperature levels used can be found in section 3.1.2, where the database categorization is explained.

2.1 Barriers and opportunities of large scale heat pumps in literature

Since the first generation of steam-powered district heating systems in the 1880s with a flow temperature of over 200°C, they evolved to have lower distribution temperatures with every generation (*District heating generations explained* 2024). Current systems feature flow temperatures below 100°C, which makes the whole system more efficient. Lowering the flow temperatures also opens up the opportunity to capture heat from low-temperature sources (Sulzer et al., 2021). LSHP are the best means to implement these low-temperature heat sources into DH systems, as the heat pump's COP improves when the temperature lift, which it has to overcome, is lower. O'Shea et al. (2019) lists common advantages of using existing local heat sources in a DH network, such as increased security of supply, lower carbon emissions of heating and lower cost or free heat, as it is already being lost to the environment and thus improving the economy of the DH system. A more detailed examination of heat sources could then lead to better exploitation of these advantages, which is done in this thesis in section 3.4.3 and section 4.1.

Apart from the heat source temperatures, the chosen refrigerant plays a major role in assessing the economic viability, performance, and environmental impact of LSHP. The results and evaluation on this topic can be found in section 4.3. Vannoni et al. (2023) conducted a techno-economic analysis regarding the impact of refrigerant fluid selection on cost and COP with optimization of Pareto fronts. In this paper, 6 low global warming potential fluids are benchmarked against R134a, the most common refrigerant in LSHP for different source and supply temperature ranges and for 7 different large-scale heat pump sizes.

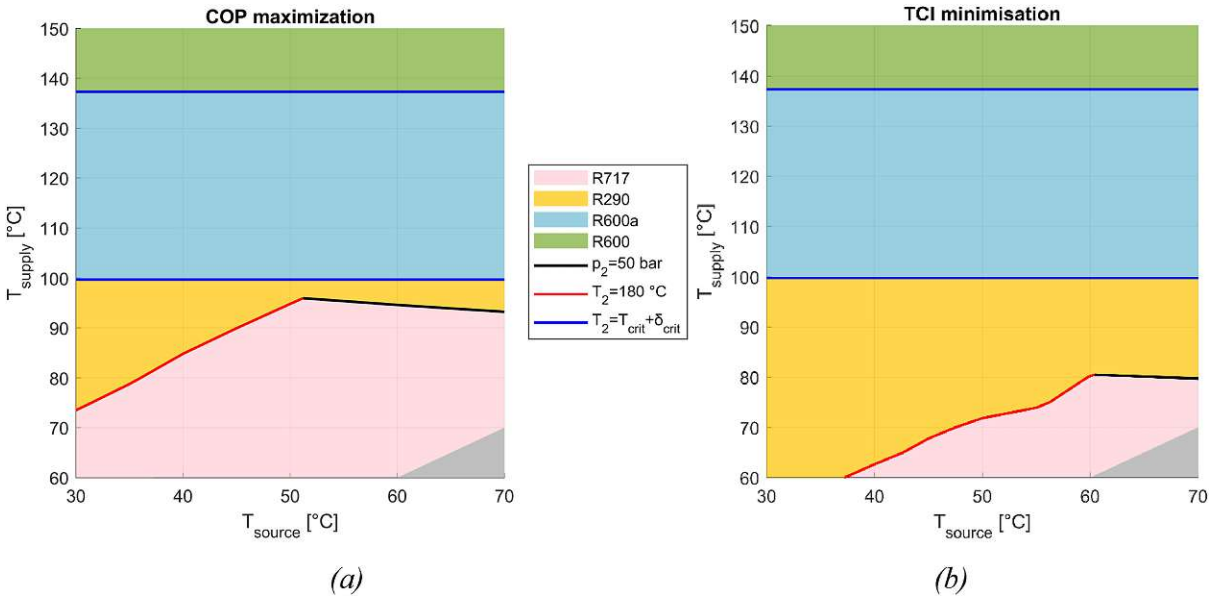

Figure 2.1: Merit order of working fluids for a 1MW heat pump (Vannoni et al., 2023)

In fig. 2.1, the most favorable refrigerants for any combination of source- and supply temperatures are presented. It shows that ammonia (R717) is the best option for low to medium-temperature heat pumps, while propane (R290) is the best for supply temperatures of up to 100 °C and n-butane (R600, R600a) is best suited for supply temperatures over 100 °C. Cost functions for estimating total investment cost and COP depending only on the temperatures and the installed capacity are developed in Vannoni et al. (2023), which is used in this work in section 3.3.1.

The integration of LSHP can be beneficial for the electricity system as well, as the renewable share in the electricity mix worldwide and especially in the EU is growing rapidly, low-carbon electricity becomes a viable solution to decarbonize the heating sector (Gaur, Fitiwi, and Curtis, 2021). LSHP can therefore be used on one side to integrate renewable energy sources and provide flexibility in the electricity market for a stable and economic operation of power grids. (Fischer and Madani, 2017).

Even though LSHP are a promising technology, Jesper et al. (2021) identified 3 main barriers that hinder a wide uptake of large-scale heat pumps:

1. Technical barriers like the limitation of the heat sink temperature and the availability of refrigerants with a low global warming potential (GWP)
2. The missing knowledge on the topic of using excess heat and heat pumps
3. Economical barriers that include the high ratio of electricity prices compared to gas and oil prices, especially in Germany.

In a recent study by Agora Energiewende (2023), the potential of LSHP in German district heating systems is discussed. They are estimated to cover 70% of the heating demand by 2045, thus replacing a large portion of natural gas. However, another barrier to the uptake of LSHP mentioned are complex planning and approval procedures, as well as high additional fees for electricity prices, confirming point 3 in (Jesper et al., 2021).

2.2 Assessing the current status of large-scale heat pumps in Europe

Due to the significant future potential of LSHP, the scientific community has been eager to explore their barriers and opportunities. In Sulzer et al. (2021), the number of scientific documents about **D**istrict **H**eating and **C**ooling (DHC) in title, abstract, or keywords that have been published annually since 1970 are shown.

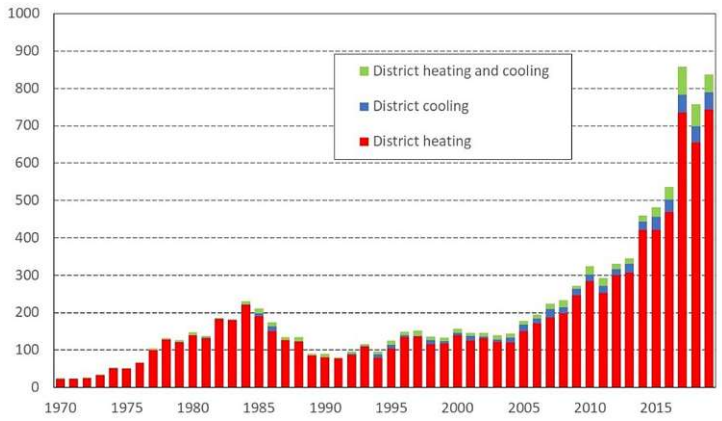

Figure 2.2: Number of annual scientific documents about district heating and cooling (Sulzer et al., 2021)

The first emergence of works in the 1980s was due to the oil crisis in the 1970s (Jesper et al., 2021). In the last 20 years, the number of publications has been increasing exponentially because of the high pressure to curb greenhouse gas emissions (Gaur, Fitiwi, and Curtis, 2021). Interestingly, the progression in fig. 2.2 corresponds to the total number of installed LSHP units in the timeline collected in this work (fig. 4.2). David et al. (2017) gave a comprehensive overview of the status of LSHP $> 1 MW_{th}$ in Europe as a part of the Heat Roadmap Europe studies in the year 2017. Compared to and building upon David et al. (2017), which collected 149 LSHP units with a total heating capacity of 1580 MW_{th}, a total of 315 large-scale heat pump projects with a total heating capacity of 4032 MW_{th} have been collected in this work. In fig. 2.3, the distribution of this capacity across Europe is compared to a recent publication of (Piel et al., 2022) published in the international network for district energy, "Euroheat & Power", showing the contribution of this work to the state of knowledge.

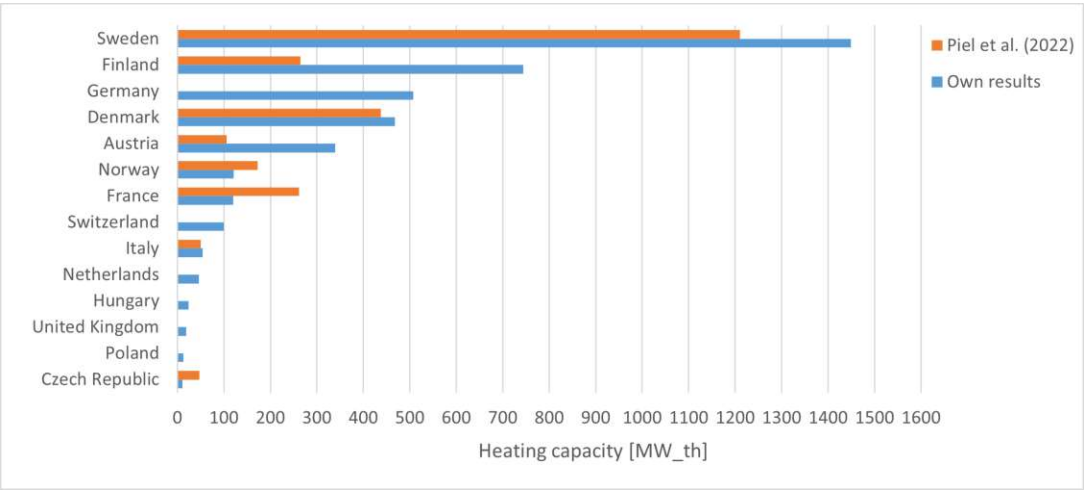

Figure 2.3: Comparison of the total heating capacity per country of the own results with Piel et al. (2022)

2.3 Modelling the implementation of large-scale heat pumps in district heating

In Pieper, Mašatin, et al. (2019), a modeling framework to plan the integration of LSHP in DH is presented. The city of Tallinn, Estonia is used as a case study. It features 6 different heat sources and 13 potential locations of LSHP within the city's district heating network. Similarly, a mixed integer linear program (MILP) with hourly resolution is used in GAMS to minimize the total cost of ownership, including investment and operational costs. Highlights of the methodology include:

- Modeling the COP using an approach by Ommen et al. (2019), that depends on the characteristics of heat source and heat sink temperatures, as well as characteristics of the compressor, the heat exchanger, and the refrigerant. The use of a constant COP is not adequate because of fluctuating temperature levels in the heat sources and the DH network, therefore the COP is constantly changing. This issue is dealt with in this thesis by using temperature sensitivities of COP.
- Using design conditions for a LSHP for calculating COP and the maximal heat source capacities. Design conditions are represented as conditions of a winter day with the highest heat sink and the lowest heat source temperature.

The goals are to identify the most suitable heat sources to be used by LSHP, the optimum heat pump capacity to be installed for each heat source, and the optimal hourly operation of the chosen LSHP to minimize costs. All of these goals are also pursued in this thesis and can be found in chapter 5. Key findings are that it is economically optimal to install 122 MW of additional HP capacity for Tallinn (440 000 inhabitants), without compromising existing base-load units. Further, the installation of these heat pumps could lead to significant cost savings by reducing the need for more expensive heating options like natural gas boilers.

In Popovski et al. (2019), different decarbonization scenarios for an existing DH network are discussed. The focus lies on LSHP, among other renewable heat energy technologies. The methodology consists of two steps. First, the heat demand of the city of Herten in Germany and the potential to extend its DH system were estimated by constructing and applying a building stock simulation model. Secondly, a supply dispatch model is used to calculate scenarios and sensitivities. As input for the model, heat demand profiles were generated: The heat demand profiles were modeled as linearly dependent on air temperature to account for space heating for 80% of the demand. For the remaining 20%, when the demand consists mainly of hot water, it is modeled independent from air temperature. A similar approach is used in this work in section 3.4.3. While the scenarios consist of comparing the current situation with different renovation and heat generator scenarios, an analysis of the cost-competitiveness of heat pumps was achieved by varying the most influential factors such as **C**apital **E**xpenditure (CAPEX), interest rate, size, heat supply and heat source temperatures and COP and also the electricity price. By incrementally varying these parameters, cases were constructed in which the **L**evelized **C**ost **o**f **H**eat (LCOH) of LSHP is cost-competitive to coal-fired CHP plants, which is currently the main heat source in Herten. Among the findings are that LSHP are not cost competitive with coal-fired CHP, but they could be by increasing full load hours, reducing supply temperatures, lowering electricity prices, reducing CAPEX and operating the HP based on hourly spot market prices.

Compared to the presented studies, this thesis does not only feature a sensitivity analysis of one city but rather a comparison of the effect of different refrigerants, climate conditions as well as economics of scale and different system sizes on the viability of LSHP. The investment cost is also differentiated based on refrigerant, which is neglected in the other studies. Additionally, this thesis features 7 different heat sources, of which 4 differ in each climate condition.

3 Methodology

In fig. 3.1, a flowchart of the methodology is shown. It consists of the following 2 main parts: After defining the research question and scope in chapter 1, the current state of large-scale heat pumps is assessed by conducting a literature review and data collection, which is presented in chapter 4. Then, the research question is answered by using the collected data to develop scenarios in the DH Supply Model HotMaps (2024) to quantify the competitiveness of LSHP under current conditions in Europe.

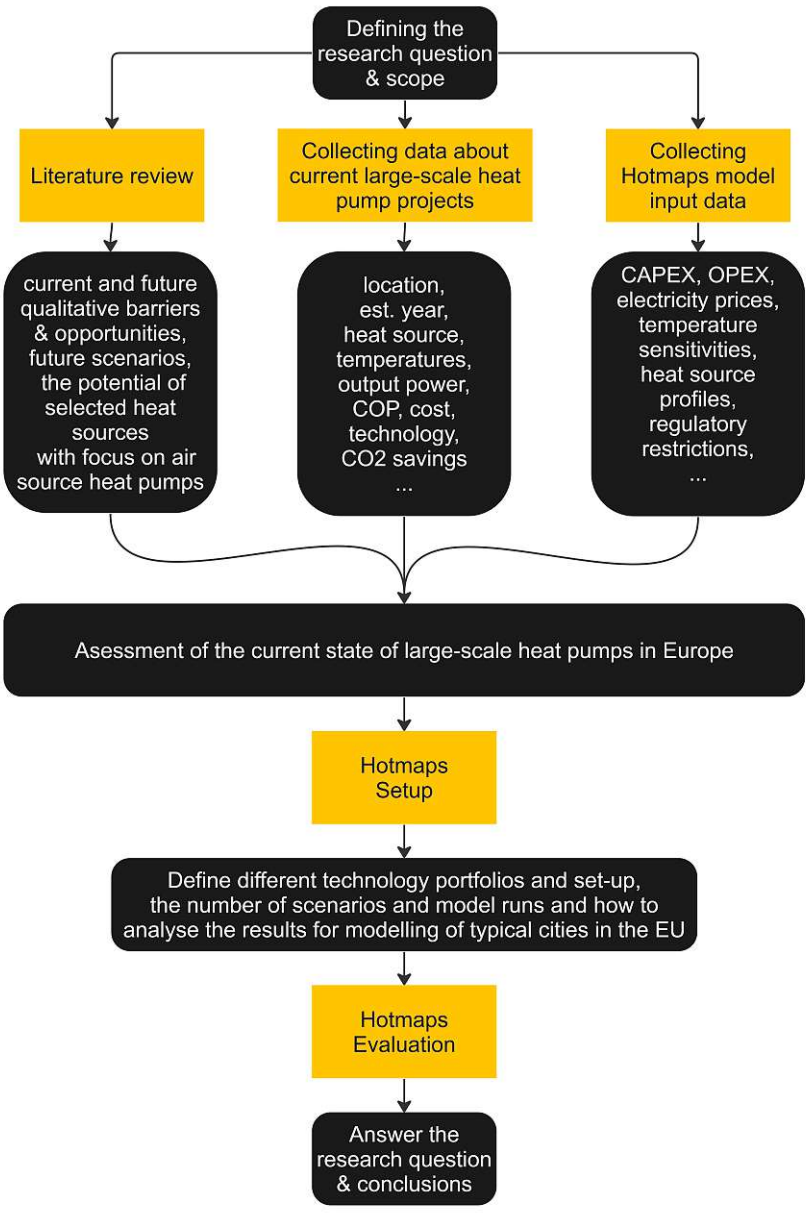

Figure 3.1: Flowchart of the methodology

3.1 The current state of large-scale heat pump installations in Europe

3.1.1 Main Data Sources

The data collection was conducted through online research, with data sheets from heat pump manufacturers or on websites from utility companies, as well as by reviewing conferences. The database consists of the following sources, where major sources are assigned a number in the database. The number of heat pumps can be counted in different ways:

- The number of **projects (315)** counts the independent heat pump projects, each located at unique locations. However, the sum of the number of installations included (349) in table 3.1 is larger because some projects are mentioned in multiple sources. Multiple sources in a single project are included because data validity can be checked and missing data from one source may be found in a different source.

- As mentioned in chapter 1, the heating capacity of multiple heat pump units in series or parallel at a single location has to be larger than 1 MW **when summed up** to be included in this database. The number of these **heat pump units** is **469** in total.

Table 3.1: Main Data Sources

Nr	Title	Installations included	Source
1	ANNEX 47 Heat Pumps in District Heating and Cooling systems Task 2	21	(Geyer et al., 2019)
2	ANNEX 47 Heat Pumps in District Heating and Cooling systems Task 3	16	(Marguerite et al., 2019)
3	Heat Roadmap Europe : Large-Scale Electric Heat Pumps in District Heating Systems	81	(David et al., 2017)
4	Wärmeversorgung mit Wärmepumpen im Wohnquartier – Vom Stand der Technik zu neuen Ansätzen	12	(Xiao et al., 2020)
5	Planenergi - Large Heatpumps in Denmark	68	(Odgaard et al., 2020)
6	Integration von Wärmepumpen in industrielle Produktionssysteme – Potenziale und Instrumente zur Potenzialerschließung	9	(Wolf, 2018)
7	Friotherm	16	(Friotherm, 2023)
8	A review of common faults in large-scale heat pumps	17	(Aguilera et al., 2022)
	Individual projects from various other sources	109	

3.1.2 Data Base Categories

David et al. (2017), as seen in table 3.1, has the most comprehensive database of the main sources. Its categorization consists of the following categories:

- Country
- Name (Location)
- Source
- Refrigerant
- Output Capacity (MW)
- Units
- COP
- Source Temperature [°C] (called T_{SI} here)
- Supply Temperature [°C] (called T_F here)
- Temperature Range [°C] (called ΔT here)
- Cooling
- Established Year
- Reference

For this work, an expanded categorization is developed, which can be seen in the following table 3.2. To fully understand table 3.2, a closer look at the typical heat pump process is necessary: In the following fig. 3.2, the 4-step cycle of an ambient air source heat pump is shown to explain the different temperature levels. It is representative for all compression heat pumps, which make up more than 90% of the units collected in this work (see fig. 4.22).

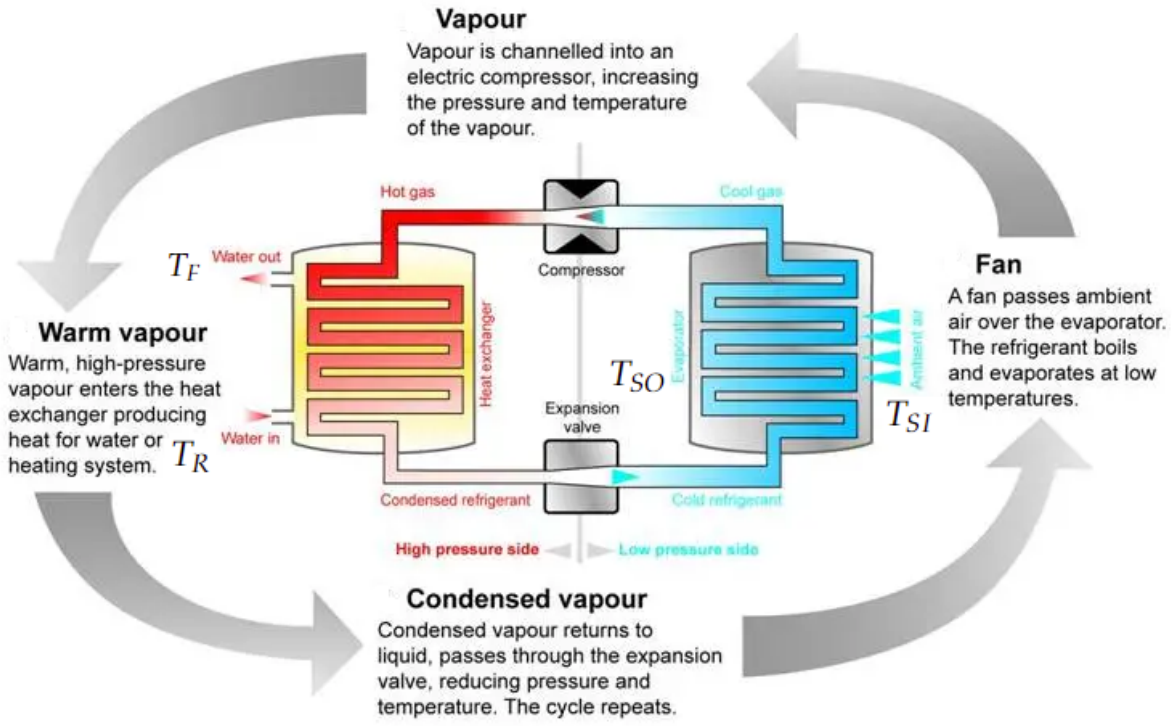

Figure 3.2: Exemplary compression heat pump cycle, adapted from *Heat Pump* (2013)

Throughout the research, it became evident, that there are 4 temperatures to focus on. These are the temperatures that can be measured from outside the heat pump. While the heat pump can be treated as a black box for this thesis, it is still important to know the inner workings for drawing conclusions.

Starting at the compressor on the top, it is the only part of the heat pump where electrical energy is used to compress the refrigerant and therefore increasing its temperature. The hot and gaseous refrigerant then goes into a heat exchanger in which it transfers its heat to the DH grid and condenses in the process. The rate of heat exchange depends apart from the heat exchanger area, on the temperature of the water returning from the DH network T_R and the temperature of the water going into the DH network T_F, more specifically the difference between the two, called $\Delta T_{High} = T_F - T_R$.

The now liquid refrigerant gets depressurized by an expansion valve, which cools it down to the lowest temperature in the cycle. In a second heat exchanger, the heat source, entering with T_{SI} gives off its heat to the cool refrigerant and leaves the heat exchanger with the temperature T_{SO}. The difference between these two is called $\Delta T_{Low} = T_{SI} - T_{SO}$.

Finally, the refrigerant gets compressed again and the cycle continues. The efficiency of the heat pump is determined among others by the temperature difference between the high and low side, which is called $\Delta T = T_F$ - T_{SI} (see eq. (4.1)) This definition is following the standard EN 14511-2 as seen in Schlosser et al. (2020). Further details on the analysis of the temperatures and COP can be found in section 4.1.

The categories of table 3.2 are grouped into 4 main categories, which are general information, technical information, economic information and sources. The column "Fullness" gives a measure of available data in each category calculated as the share of available data in all data points. It can be seen that by using this approach, categories like "Heat Source 1" or "Output capacity heating" are almost filled, while there is only sparse economic information available.

Table 3.2: Database categories

	Category	**Description**	**Fullness [%]**
GENERAL INFORMATION	Country	Name of the country the heat pump is installed	100.0
	Country (ISO 3166-2)	ISO 3166-2 code of the country	100.0
	Latitude	Latitude derived from the city location	98.7
	Longitude	Longitude derived from the city location	98.7
	City	Name of the city the heat pump is installed	98.7
	Name	More detailed description of the project	100.0
	Established Year	Year when the heat pump went into operation	96.5

TECHNICAL INFORMATION	Heat source 1	Primary heat source	100.0
	Heat source 2	Secondary heat source	17.6
	Heat sink	Determines if the heat sink is district heating (DH) or not (see fig. 4.25)	100.0
	Utilization	A more detailed description of the heat sink if not connected to DH (see fig. 4.26)	25.6
	T_R [°C]	Return temperature	28.1
	T_F [°C]	Flow temperature (here, missing values are filled up with country specific temperatures)	100
	T_{SI} [°C]	Temperature source in is the temperature of the heat source before entering the heat exchanger	54.6
	T_{SO} [°C]	Temperature source out is the temperature of the heat source after leaving the heat exchanger	28.1
	ΔT [°C]	$\Delta T = T_F$ - T_{SI}	68.8
	ΔT_{High} [°C]	$\Delta T_{High} = T_F - T_R$	68.8
	ΔT_{Low} [°C]	$\Delta T_{Low} = T_{SI} - T_{SO}$	68.8
	HP manufacturer	Heat pump manufacturer	14.4
	HP technology	Heat pump technology	100
	Refrigerant	Refrigerant (ASHRAE number)	53.4
	Output capacity heating [MW_{th}]	Heating capacity	97.8
	Annual heat production [MWh_{th}]	Annual heat production	13.4
	Output capacity cooling [MW_{th}]	Cooling capacity	12.1
	Units [-]	Number of heat pumps installed in one location	100
	$COP_{heating}$ [-]	Coefficient of performance in heating mode	51.4
	$COP_{cooling}$ [-]	Coefficient of performance in cooling mode	3.8
	Cooling?	Determines if the installation has cooling capability (see fig. 4.24)	48.7
	annual CO2 emission savings [t]	Annual CO2 emission savings	15.3

	Active?	Determines if the installation is operating and active today (see fig. 4.21)	100
ECONOMIC INFORMATION	spec. Inv. costs [€/MW]	Specific investment costs	13.4
	Investment costs [M€]	Total Investment costs	13.4
	Annual operation hours [h]	Annual operation hours	2.9
	Annual energy savings [MWh]	Annual Energy savings in MWh	3.8
	Annual energy savings [€]	Annual Energy savings in €	2.6
SOURCES	Source 1	Primary source	100
	Source 2	Secondary source	33.5
	Note	Further notes and descriptions	20.1
	Additional	Additional information	12.4

3.1.3 Heat Source Categorization

The classification of heat sources used in this work is adapted and expanded from O'Shea et al. (2019): Items marked with a ● are included both in O'Shea et al. (2019) and in this work,
items marked with a ✶ are new categories in this work,
items marked with a ❊ are included in other categories in this work and
items marked with a ❍ are included in O'Shea et al. (2019) but not in this work.

A short explanation of each heat source is given here, while further information can be found in chapter 4.

Commercial Sources

- ● Flue gas heat recovery
  The heat from flue gases produced by combustion can be captured and used to power LSHP.

- ● Industrial process heat recovery
  Many industrial processes produce waste heat, but no exhaust gases and are included in this category.

- ● Commercial / Industrial CHP
  Commercial and industrial sites can have on-site combined heat and power (CHP) units that can be utilized by LSHP.

- ✶ Data center
  Data centers can provide a reliable heat source for LSHP throughout the year and are included in this category.

- ✶ Cooling plant
  The waste heat of a plant, that is designed for cooling a building or industrial processes, can be used as a heat source for heat pumps when both heat and cooling demand occur at the same time.

- ✶ Cooling network
  When there is a district heating as well as a district cooling network, it is possible to use a heat pump to provide excess cold to the district cooling network, using it effectively as a heat source (Marguerite et al., 2019).

- ❊ Commercial / Industrial cooling
  Due to different temperatures, this category has been split into data center, cooling plant and cooling network.

Infrastructural Sources

- ● Sewage water
  This category includes all sites that use heat obtained from sewage water, either from pipes or directly at the sewage water treatment facility.

- ✶ HVDC, metro, mine water, **T**hermal **E**nergy **S**torage (TES), unknown
  The waste heat from high voltage DC stations, as well as exhaust air from a metro system or water from mines, as well as the use of a booster heat pump with thermal energy storage as a heat source have been found. Due to the small sample size, they have been grouped into this category.
- ❉ Power plant
  This heat source is included in Flue gas heat recovery and Commercial / Industrial CHP.
- ❉ Sewage pipes waste heat
  This heat source is included in the Sewage water category.
- ❍ Landfill (biogas & waste heat)
  This heat source is too small to be used by LSHP and no units have been found.
- ❍ WWTW (waste heat, biogas/sludge incineration)
  This heat source is too small to be used by LSHP and no units have been found.

Environmental Sources

The following heat sources are characterized by not using additional facilities but rather relying on heat from the environment directly. This makes them highly dependent on the geographic location. They are also characterized by having more fluctuating temperature profiles in general, which will be investigated further in section 3.4.3.

- ● Ambient air
- ● Lake water
- ● River water
- ● Sea water
- ● Ground water
- ● Deep geothermal
- ✶ Solar thermal
- ❉ Mine water
  Due to the small sample size, this heat source has been included in a combined category.

3.2 HotMaps District Heat Supply Model

> "The HotMaps Dispatch Model is a web user interface to develop energy system models. It is based on Pyomo for modeling and bokeh for visualization and interaction. The primary focus is flexible model creation with/and without the web user interface, and a high temporal resolution (hourly based) for the optimization. It has also the ability to execute and create many scenarios. "
> (Havlicek and Hasani, 2020)

This section will cover the most important parts of the Hotmaps DH Supply Model (also known as the HotMaps dispatch model) which is used to evaluate the cost-optimal investments and dispatch of a district heating system. It is a **M**ixed **I**nteger **L**inear **P**rogram (MILP) and features a scenario mode and an investment mode. In this work, the investment mode is used to determine the optimal installed capacity for each heat generator. The scenario mode is then used to evaluate the competitiveness of LSHP under different circumstances. Further details can be studied in Havlicek and Hasani (2020). The model is also available on GitHub under HotMaps (2024).

3.2.1 Indices

The following indices describe the heat generators used in this work, the heat storage and the time steps of HotMaps (2024):

Table 3.3: Definition and properties of the model indices

Index	Description
j	$\in \{\text{generators}\} =$ $\in \{\text{gas CHP}, \text{biomass CHP}, \text{geothermal heat pump},$ $\text{ground water heat pump}, \text{lake water heat pump}, \text{sea water heat pump},$ $\text{sewage water heat pump},$ $\text{industrial excess heat pump}, \text{ambient air heat pump}\}$
hs	$\in \{\text{heat storage}\}$
t	Timestep in hours $\{t \in \mathbb{N}_{\geq 0} \mid t \geq 1, t \leq 8760\}$

3.2.2 Variables

Typically for a MILP, the variables are located both in the domain of positive real numbers $\mathbb{R}_{\geq 0}$ and also in binary integers $\{0, 1\}$, which are used to turn generators or options on or off.

Table 3.4: Definition and properties of the most important model variables

Variable	Domain	Description	Unit
$x_{th,j,t}$	$\in \mathbb{R}_{\geq 0}$	heat generation of generator j in hour t	MWh_{th}
$x_{el,j,t}$	$\in \mathbb{R}_{\geq 0}$	electricity generation of generator j in hour t	MWh_{el}
$x_{load,hs,t}$	$\in \mathbb{R}$	thermal energy transferred to heat storage hs in hour t (> 0 : loading, < 0 : unloading)	MWh_{th}
Cap_j	$\in \mathbb{R}_{\geq 0}$	heating capacity of generator j	MWh_{th}
Cap_{hs}	$\in \mathbb{R}_{\geq 0}$	heat storage capacity	MWh_{th}
$coldstart_{j,t}$	$\in \{0,1\}$	coldstart	1
$Active_{j,t}$	$\in \{0,1\}$	active	1

3.2.3 Parameters

In contrast to the variables, the following parameters are fixed and do not change during the optimization process.

Table 3.5: Definition and properties of the most important model parameters

Symbols of Parameters	Description
$\text{demand}_{th,t}$	thermal demand, time-dependent
$\text{temp}_{sea,lake}$	temperature of sea and lake water
temp_{ww}	temperature of waste water
temp_{flow}	flow temperature
temp_{return}	return temperature
$\text{temp}_{ambient}$	ambient temperature
maxdemand	maximum demand
potential_j	potential of the heat generator j
IK_j	investment costs (IK) of heat generator j
$\text{OP}_{fix,j}$	fixed operational costs of heat generator j
$\eta_{el,j}$	electrical efficiency of heat generator j
$\text{elPrice}_{j,t}$	electricity price for heat generator j, time-dependent
$\text{mc}_{j,t}$	variable costs
$\eta_{th,j,t}$	thermal efficiency of heat generator j, time-dependent
$HPRF_{j,t}$	heat pump restriction factor of heat pump j, time-dependent
$P_{th,min.j}$	minimal thermal power of heat generator j
$\text{x}_{th,cap,j}$	maximal thermal power of heat generator j
α_j	annuity of heat generator j
loadcap_{hs}	load capacity of heat storage hs
unloadcap_{hs}	unload capacity of heat storage hs
η_{hs}	efficiency of heat storage hs
loss_{hs}	losses of heat storage hs
IK_{hs}	investment costs (IK) of heat storage hs
cap_{hs}	capacity of heat storage hs
$\text{c}_{ramp,chp}$	ramp costs for CHP

Symbols of Parameters	Description
$c_{ramp,waste}$	ramp costs for waste incineration
$c_{coldstart,j}$	coldstart costs of heat generator j
α_{hs}	annuity of heat storage hs
$OP_{var,j}$	Variable operational costs of heat generator j
$temperature_t$	time-dependent temperature
$sale_{electricityprice,j,t}$	sale electricity price
$OP_{fix,hs}$	Fixed operational costs of heat storage hs
p_{CO2}	CO2 price
$caploss_{hs}$	capacity losses of heat storage hss
$\eta_{th,nom,j,t}$	thermal, normative efficiency of heat generator j, time-dependent
$s_{source,j}$	source temperature sensitivity of the COP
$s_{flow,j}$	flow temperature sensitivity of the COP
$s_{return,j}$	return temperature sensitivity of the COP
$COP_{nom,j}$	nominal heat pump COP at nominal temperatures

3.2.4 Objective Function

HotMaps (2024) aims to minimize the total cost of the system minus the generated revenue, which is expressed in the objective function:

$$min\ c_{tot} - rev_{gen,el} \tag{3.1}$$

Where c_{tot} are the total costs:

$$c_{tot} = c_{inv} + c_{var} + c_{op,fix} + c_{op,var} + c_{cold} \tag{3.2}$$

The revenue generated from selling electricity is the amount of generated electricity times its price:

$$rev_{gen,el} = \sum_{j,t} x_{el,j,t} \cdot sale_{electricityprice,j,t} \tag{3.3}$$

The total costs are composed of annualized investment costs c_{inv}, which are calculated from the investment cost IK for generators j and heat storage hs, where Cap is the newly installed heating capacity and $x_{th,cap,j}$ the already existing capacity. In this work, there is no pre-installed capacity. When investment mode is turned off, $Cap_j = x_{th,cap,j}$ and $Cap_{hs} = cap_{hs}$, and in investment mode $Cap_j \geq x_{th,cap,j}$ and $Cap_{hs} \geq cap_{hs}$.

$$c_{inv} = \sum_{j}(Cap_j - x_{th,cap,j}) \cdot IK_j \cdot \alpha_j + \sum_{hs}(Cap_{hs} - cap_{hs}) \cdot IK_{hs} \cdot \alpha_{hs} \tag{3.4}$$

Other costs are calculated based on the heat $x_{th,j,t}$ generated at time step t for generator j, like variable costs c_{var}:

$$c_{var} = \sum_{j,t} x_{th,j,t} \cdot mc_{j,t} \tag{3.5}$$

and variable operational costs $c_{op,var}$:

$$c_{op,var} = \sum_{j,t} x_{th,j,t} \cdot OP_{var,j} \tag{3.6}$$

Fixed operational costs $c_{op,fix}$ are based on installed capacity:

$$c_{op,fix} = \sum_{j} Cap_j \cdot OP_{fix,j} + \sum_{hs} Cap_{hs} \cdot OP_{fix,hs} \tag{3.7}$$

For total coldstart costs c_{cold}, the number of coldstarts are counted and multiplied with the specific coldstart costs $c_{coldstart,j}$:

$$c_{cold} = \sum_{j,t} coldstart_{j,t} \cdot c_{coldstart,j} \tag{3.8}$$

3.2.5 Constraints

In the following section, the most important constraints are described. The optimal solution of the model must be within these constraints.

Heating generation covers demand
At all times, the heating demand must be covered by the heat generation, with the possibility of loading or unloading the heat storage *hs*:

$$\sum_{j,t} x_{th,j,t} - \sum_{hs} x_{load,hs,t} = demand_{th,t} \tag{3.9}$$

Electrical power generation
To convert thermal to electrical energy, the efficiencies η are used:

$$x_{el,j,t} = \frac{x_{th,j,t}}{\eta_{th,j,t}} \cdot \eta_{el,j} \tag{3.10}$$

Capacity restriction rules
The maximum capacity of a generator can either be

$$Cap_j \leq max_{demand} \tag{3.11}$$

if the inv_{flag} is set true, or otherwise

$$Cap_j = x_{th,cap,j} \tag{3.12}$$

Generation rules

The amount of heat generated must not exceed the installed capacities. Depending on whether the generator is a heat pump or not, this leads to 2 equations, because the heat pump´s maximum output capacity depends on $\eta_{th,j,t}$ (COP). For other generators, it is:

$$x_{th,j,t} \leq Cap_j \cdot Active_{j,t} \tag{3.13}$$

For heat pumps, it is:

$$x_{th,j,t} \leq Cap_j \cdot \eta_{th,j,t} \cdot Active_{j,t} \cdot HPRF_{th,j,t} \tag{3.14}$$

The heat pump restriction factor $HPRF_{th,j,t}$ is used to implement a power fade-out at certain heat source temperatures $\theta_{s,j,t}$, which is described in section 3.4. It is defined by the following 3 equations using a fade out temperature $\theta_{s,j,fo}$ and a minimal possible temperature $\theta_{s,j,min}$:

$$\theta_{s,j,t} < \theta_{s,j,min} \quad HPRF = 0 \tag{3.15a}$$

$$\theta_{s,j,min} \leq \theta_{s,j,t} < \theta_{s,j,fo} \quad HPRF = \frac{\theta_{s,j,t} - \theta_{s,j,min}}{\theta_{s,j,fo} - \theta_{s,j,t}} \tag{3.15b}$$

$$\theta_{s,j,t} \geq \theta_{s,j,fo} \quad HPRF = 1 \tag{3.15c}$$

The heat pump COP is temperature-dependent. This is modeled using sensitivities *s* to account for deviations from the nominal conditions (see section 3.3.3).

$$\eta_{th,j,t} = COP_{nom,j} + s_{source_j} \cdot (\theta_{s,j,t} - \theta_{s,nom_j}) + s_{flow_j} \cdot (\theta_{f,j,t} - \theta_{f,nom_j}) + s_{return_j} \cdot (\theta_{r,j,t} - \theta_{r,nom_j}) \tag{3.16}$$

All generators can have a minimum operating power.

$$x_{th,j,t} \geq P_{th,min,j} \cdot Active_{j,t} \tag{3.17}$$

For heat pumps, the rule is again adopted to account for COP:

$$x_{th,j,t} \geq P_{th,min,j} \cdot \eta_{th,j,t} \cdot Active_{j,t} \tag{3.18}$$

Coldstart rule
If $t = 1$, then $coldstart_{j1} == 1$, otherwise $coldstart_{j,t}$ is only true for cold starts:

$$coldstart_{j,t} \geq ((Active_{j,t}(j,t) - Active_{j,t}(j,t-1) \tag{3.19}$$

Heat storage rules
The heat storage level equals the old level plus loading minus unloading. Depending on the value of t there is one special condition rule so that the heat storage level is the same at the first and last time step. If t is equal to 1, 3.20a is taken, otherwise 3.20b.

$$storelevel_{hs,t}(hs,1) = storelevel_{hs,t}(hs,8760) \tag{3.20a}$$
$$storelevel_{hs,t}(hs,t) = storelevel_{hs,t-1}(hs,8760) \cdot (1 - caploss_{hs}) + x_{load,hs,t}(hs,t-1) \cdot \eta_{hs} \tag{3.20b}$$

Installed capacities must be greater or equal to the pre-installed capacities. If the inv_{flag} is set, then 3.21a is taken, otherwise 3.21b.

$$Cap_{hs} \geq cap_{hs} \tag{3.21a}$$
$$Cap_{hs} = cap_{hs} \tag{3.21b}$$

The actual storage level must be smaller than the installed storage:

$$storelevel_{hs,t}(hs,t) \leq Cap_{hs} \tag{3.22}$$

The loading power must be less than the maximum loading power:

$$x_{load,hs,t}(hs,t) \leq load_{cap,hs} \tag{3.23}$$

If the investment flag is set, then the 3.24 is taken, otherwise 3.25.

$$x_{load,hs,t}(hs,t) \geq -unload_{cap,hs} \tag{3.24}$$
$$x_{load,hs,t}(hs,t) \geq -storelevel_{hs,t}(hs,t) \tag{3.25}$$

3.3 Heat generator input data

This section presents the input data for the heat generators to HotMaps (2024). First, the economic input data is presented, as it is the most important for investment decisions. It is followed by the COP calculation and the electricity profiles used. The environmental data such as temperature profiles are presented in scenario 3 of section 3.4.3.

3.3.1 Economic heat generator input data

For LSHP, the main cost factors are **T**otal **C**ost of **I**nvestment (TCI) [€/MW], which is another word for CAPEX for initial expenses. Ongoing expenses are split into fixed **O**perational **E**xpenditure (OPEX) [€/MWa] depending on the installed capacity and variable OPEX [€/MWh] depending on the produced energy.

The following table shows fixed and variable OPEX, as well as cold start costs for the heat generators, which are also found in table 3.3:

Table 3.6: Operational Expenditure and Coldstart Costs

Heat generator	**OPEX fixed (EUR/MWa)**	**OPEX variable (EUR/MWh)**	**Coldstart Costs (EUR/Start)**
CHP Biomass	65929	1.83	1622
Peak Boiler	2127	1.17	41.23
Heat pump Air, Sewage, Lake, Industrial process heat, Ground water	2127	2.86	10.63
Heat pump Geothermal	18792	2.02	10.63
Heat pump Sea	4253	1.27	10.63

The data in table 3.6 is obtained from the danish energy agency catalog (DEA, 2023), which is a comprehensive technology data catalog for technologies used for centralized and decentralized production of electricity and district heat. Coldstart costs for for the Peak boiler and CHP biomass are obtained in Lok, Ng, and Andiappan (2020). Fixed and variable OPEX are in a similar range for heat pumps using different heat sources, except for geothermal and sea water. A reason for this is the additional cost of pumping deep geothermal water, as well as measures against corrosion for sea water and geothermal. Therefore, the focus lies on differentiating TCI based on the heat sources of LSHP and how the size of a LSHP unit affects the specific investment cost due to economies of scale.

TCI are commonly evaluated by either carrying out field studies to assess the cost of real LSHP projects, which was done in Pieper, Ommen, et al. (2018) or by creating a thermodynamic heat pump model and verifying it with real data, which was done in Vannoni et al. (2023).

While the first approach has the benefit of accessing real data directly, only a minimal number of projects can be found in the literature. Additionally, cost can be highly project-specific and hard to generalize. This is also why the economic data collection for the database (table 2) is not used for this evaluation. The second approach has the benefit of having more room for variation of parameters and deriving cost functions. In the following section, findings from these approaches are compared.

Real projects

Pieper, Ommen, et al. (2018) examines the investment costs of 26 LSHP in Denmark using natural refrigerants and developed linear cost correlations in Matlab. The heat sources air, flue gas, excess heat, groundwater, and sewage water are investigated and broken down to the cost of heat pump, heat source connection, construction, electricity and consulting, as shown in the following graph:

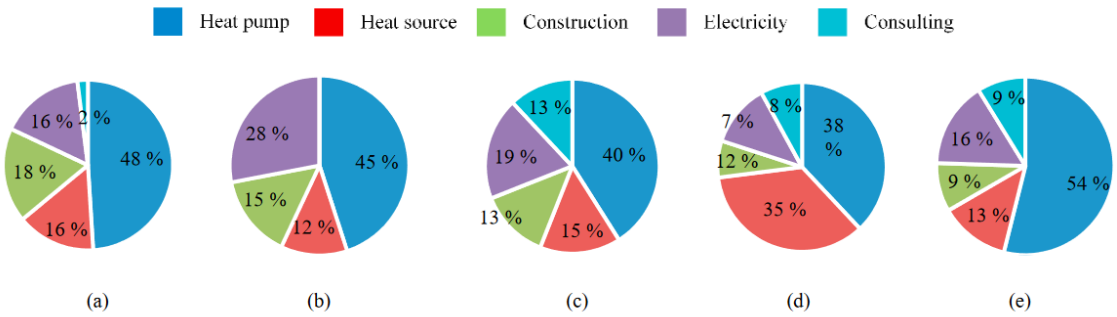

Figure 3.3: Breakdown of total investment cost for the heat sources (a) air; (b) flue gas; (c) excess heat; (d) groundwater; (e) sewage water (Pieper, Ommen, et al., 2018)

It can be seen that the heat pump itself accounts for 38% - 54% of the total investment cost, whereas the heat source is in a narrow range of 12% - 16% for the sources air, flue gas, excess heat and sewage water, except for groundwater, which accounts for 35% due to drilling cost. Further, in DEA (2023), the share of the cost of the heat source is assessed for the sources deep geothermal (92%) and seawater (20%). This share of the heat source $s_h s$ on total cost will be used later for cost calculation.

For the heat pump itself, TCI are also dependent on the refrigerant and the nominal temperatures used to design the heat pump (Nielsen et al., 2018), Vannoni et al. (2023). Because there is no further information in DEA (2023) and Pieper, Ommen, et al. (2018) regarding these parameters, cost functions are used to calculate TCI, which are presented in the following section.

Application of cost functions

In Vannoni et al. (2023), a thermodynamic large-scale heat pump model is developed using the software "WTEMP EVO". It first optimizes each component of the heat pump for maximum COP and then the relative purchased equipment cost is estimated. The total cost of investment is calculated by multiplying the sum of purchased equipment cost by a factor of 4.16 from Bejan, Tsatsaronis, and Moran (1995) to account for installation, piping, instrumentation, electrical equipment engineering, supervision, as well as start-up and working capital (e.g., working fluid), but **not** for the heat source. The model is then validated by the database from David et al. (2017). Finally, cost functions are derived for 7 different working fluids, which allow the calculation of TCI_{1000} and the nominal COP_{nom} for the average 1000 kW heat pump, without using the detailed thermodynamic model. TCI can be scaled using power functions with an exponent α for larger heat pumps with a size X in MW, accounting for economies of scale. This variation is done for the sub-scenario 2 in section 3.4.2. The COP depends primarily on the temperatures and does not change with size.

In this work, these functions are used for the refrigerants R134a, R290 and R600a with the parameters from Vannoni et al. (2023) and median heat source temperatures from the own database, which can also be found in section 4.1. The design flow temperature is 90°C.

$$TCI_{1000} = D + E \cdot \Delta T_{lift} + F \cdot T_{flow} \tag{3.26}$$

$$TCI_X = TCI_{1000} \cdot X[MW_{th}]^{\alpha} \tag{3.27}$$

$$COP_{nom} = G + H \cdot \Delta T_{lift} + I \cdot T_{flow} + J \cdot \Delta T_{lift}^2 + K \cdot \Delta T_{lift} \cdot T_{flow} \tag{3.28}$$

An overview of the relevant parameters used is given in the following table:

Table 3.7: Parameters for the refrigerants R134a, R290, and R600a (Vannoni et al., 2023)

Parameters	**R134a**	**R290**	**R600a**
$\alpha[-]$	0.78443	0.76557	0.76098
$D[€]$	1.3223×10^6	5.4505×10^5	2.2529×10^6
$E[€/K]$	4.6581×10^3	3.2472×10^3	6.2829×10^3
$F[€/K]$	-3.0343×10^3	-866.83	-5.6106×10^3
$G[-]$	-3.0202	-7.8830	3.0708
$H[K^{-1}]$	-0.094519	0.10353	-0.13482
$I[K^{-1}]$	0.03198	0.043282	0.012003
$J[K^{-2}]$	8.6747×10^{-4}	6.5222×10^{-4}	4.3302×10^{-4}

The following table shows the resulting nominal COP_{nom} for the refrigerants and heat sources used.

Table 3.8: Nominal COP of large-scale heat pumps using various heat sources for R134a, R290, and R600a (own calculation)

Heat Source	$\mathbf{T_{source}}$ **[°C]**	$\mathbf{\Delta T_{Lift}}$ **[°C]**	$\mathbf{COP_{nom,R134a}}$	$\mathbf{COP_{nom,R290}}$	$\mathbf{COP_{nom,R600a}}$
HP Air	0	90	2.95	2.61	2.03
HP Sewage water	11	79	2.88	2.68	2.31
HP Sea	4	86	2.90	2.62	2.12
HP Lake	6	84	2.88	2.63	2.17
HP Geothermal	55	35	4.73	4.55	4.50
HP Industrial process heat	35	55	3.47	3.39	3.30
HP Ground water	8	82	2.88	2.64	2.23

While the nominal values for COP_{nom} are rather low, they will be increased by the temperature sensitivities (section 3.3.3) when the heat pump is not in its nominal operating mode. For instance, the input temperatures are higher than the nominal temperatures (section 3.4.3) and the flow temperatures are usually lower than 90°C (fig. 3.12), both resulting in a COP increase. The resulting highest possible COP can be seen in fig. 5.25, while an exemplary yearly COP profile can be found in fig. 5.26.

To take account for the additional cost of the different heat sources, the following approach is used in this work:

1. Calculate TCI from eq. (3.26), accounting for the total capital investment cost without the heat source.
2. Calculate the cost of the heat source c_{hs} by dividing the average TCI with the share of the heat source s_{hs} on total cost derived from Pieper, Ommen, et al. (2018) and DEA (2023). By using the average TCI, there is no dependency on the refrigerant for the cost of the heat source.
$$c_{hs} = \frac{\overline{TCI}}{(1 - s_{hs})/s_{hs}} \tag{3.29}$$
3. Add the cost of the heat source to TCI for the specific refrigerant.

The following graphs in fig. 3.4 and fig. 3.5 show a comparison of TCI for a 1 MW heat pump and a 10 MW heat pump for all heat sources used in HotMaps (2024).

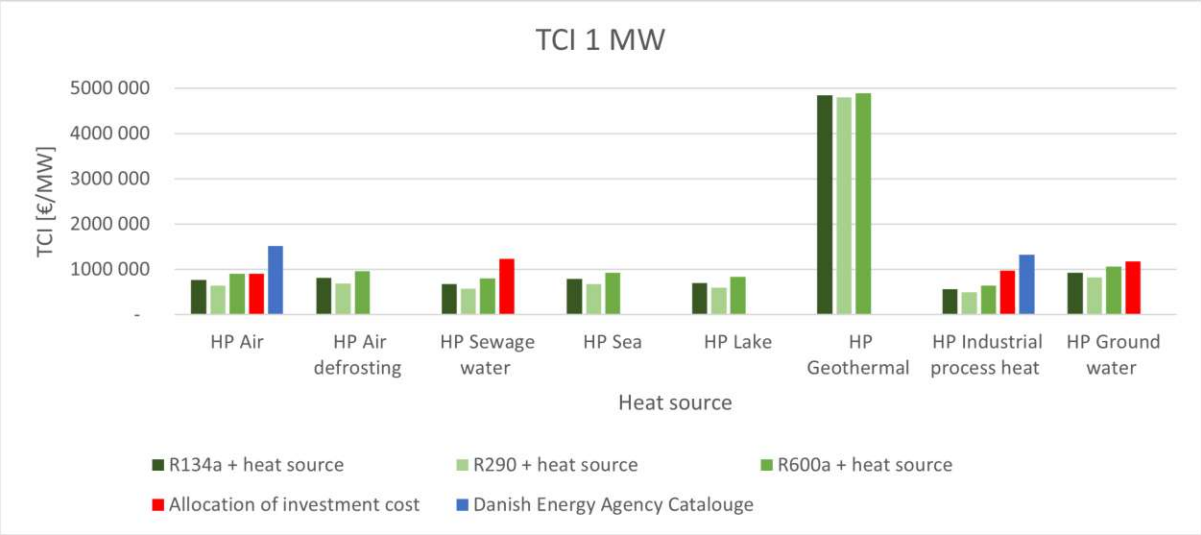

Figure 3.4: TCI comparison of own cost calculation with Pieper, Ommen, et al. (2018) and DEA (2023) for a 1 MW heat pump

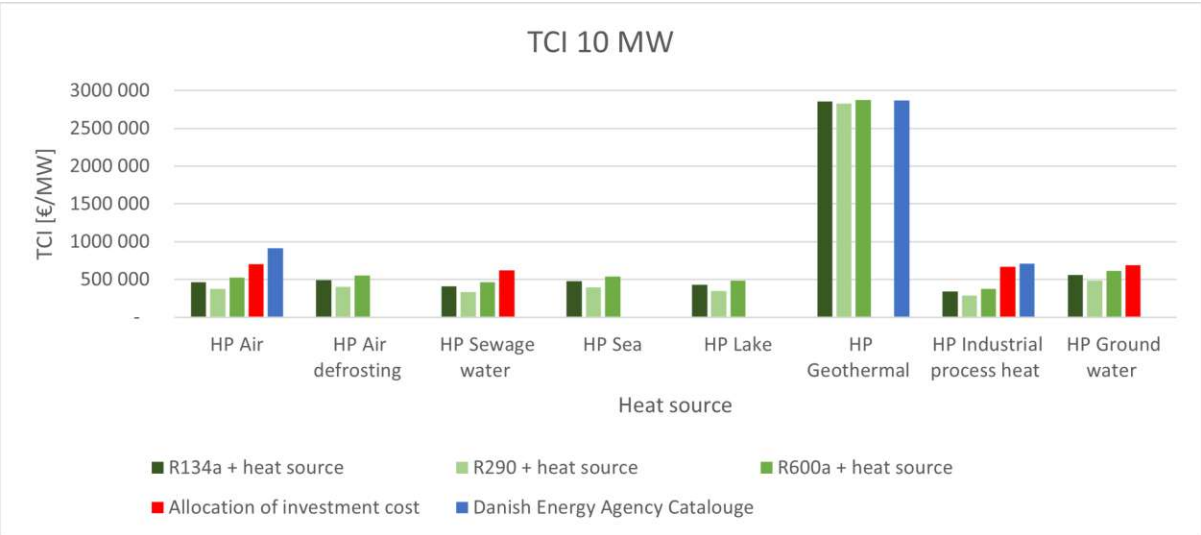

Figure 3.5: TCI comparison of own cost calculation with Pieper, Ommen, et al. (2018) and DEA (2023) for a 10 MW heat pump

While R290 features a lower TCI than R134a and R600a, the calculated TCI is generally lower than the 2 other sources. This indicates that it could be an optimistic cost calculation, or that the used refrigerants in the case studies, which are not further specified may lead to higher costs. Nevertheless, this method features a consistent way to calculate TCI for all heat sources and is therefore chosen.

For the additional heat generators, the TCI and efficiencies are obtained from DEA (2023):

Table 3.9: Efficiencies and Total Capital Investment of additional heat generators (DEA, 2023)

Name	Thermal Efficiency (-)	Electrical Efficiency (-)	TCI (€/MW_{th})
CHP Biomass	0.67	0.32	2 392 589
Peak Boiler	0.97	0.00	63 802

3.3.2 Heat storage

A heat storage is implemented to buffer the varying heat generation and demand, provide peak load management and optimize heat pump use. Typical storage sizes and their respective charge and discharge capacity can be found in Pursiheimo et al. (2022) for Helsinki. While the size of the heat storage gets optimized (see eq. (3.21a)), typical loading and unloading power for a big and small city can be found together with the maximal heat pump capacity in table 3.13. The loading and unloading efficiency is 80%, which is a common value for heat storages to account for heat loss. The investment cost of storage capacity can vary widely and a storage capacity cost for investment in additional heat storage based on the system of Braedstrup in Denmark of 800 €/MWh is taken (Yang et al., 2021). Additionally, hourly heat losses of 1% are assumed. The heat storage has OPEX of 0.1 €/MWh due to the low maintenance cost of heat storages.

3.3.3 Modelling COP using temperature sensitivities

To capture the temperature dependency of COP, temperature sensitivities $s[\frac{1}{°C}]$ are implemented in HotMaps (2024). The sensitivities can be calculated for flow temperature s_{flow}, return temperature s_{return} and source temperature s_{source} by linear approximation, where the indexed temperature is changed while the other temperatures are kept the same using eq. (3.28). For example, source temperature sensitivity is calculated using:

$$s_{source} = \frac{\Delta COP}{\Delta T_{source}} \tag{3.30}$$

This way, additional sensitivities for the refrigerants R134a, R290 and R600a are added to HotMaps (2024), whereas R600, R717 and R744 are already implemented. The following figure shows the sensitivity calculation for R290a with a flow temperature of constantly 90°C and a varying source temperature from 0°C to 50°C. The resulting sensitivity is the slope of the linear function that cuts the COP evaluated at the temperatures 0°C and 50°C (fig. 3.6).

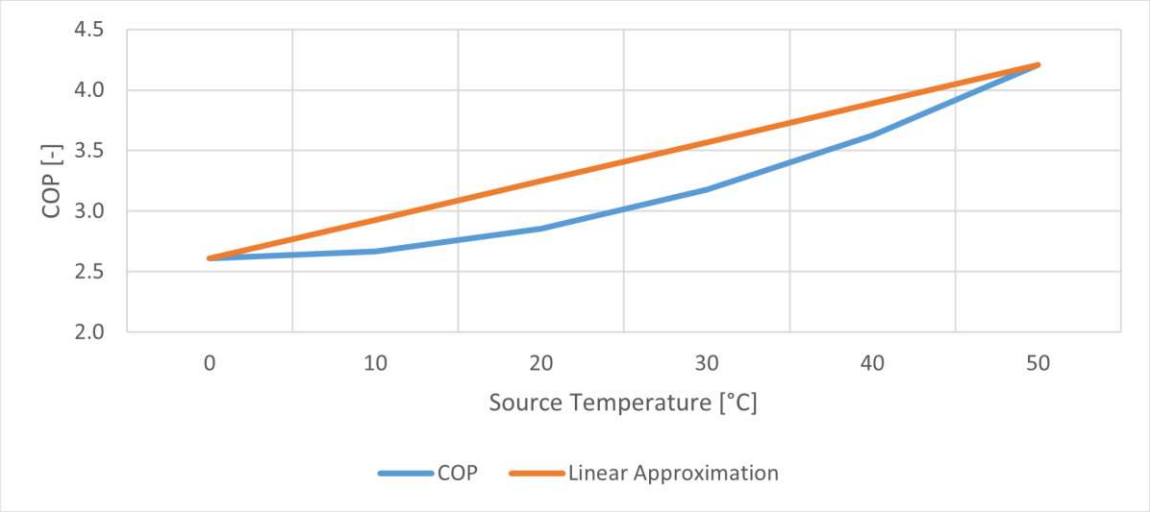

Figure 3.6: COP for R290a at source temperatures from 0°C to 50°C and resulting sensitivity from the linear approximation (own calculation)

The sensitivities for the refrigerants are as follows:

Table 3.10: COP sensitivities (own calculation)

	R134a	**R290**	**R600a**
s_{source}	0.028	0.032	0.043
s_{flow}	-0.026	-0.025	-0.025
s_{return}	-0.010	-0.010	-0.010

No source temperature sensitivity is needed for heat sources with a constant source temperature. The COP for any combination of temperatures θ at time t is obtained by adding these sensitivities to the nominal COP, which is calculated in eq. (3.28). In HotMaps (2024), the sensitivities are implemented by the following equation:

$$\eta_{th,j,t} = COP_{nom,j} + s_{source_j} \cdot (\theta_{s,j,t} - \theta_{s,nom_j}) + s_{flow_j} \cdot (\theta_{f,j,t} - \theta_{f,nom_j}) + s_{return_j} \cdot (\theta_{r,j,t} - \theta_{r,nom_j}) \tag{3.31}$$

3.3.4 Energy carrier prices

In contrast to national CO_2 prices, which are often implemented as a static carbon tax, large greenhouse gas emitters, such as energy companies fall under the European Union Emissions Trading System (ETS). It caps the total level of greenhouse gas emissions and allows industries with lower emissions to sell their extra allowances to larger emitters. This results in a dynamic price determined by supply and demand. As of January 2024, this price is 80€/t, which is used as a model input (*Carbon Price Tracker* 2024). With the emission factor, the CO_2-emissions per MWh are calculated: For gas, this factor is 0.2 t_{CO2}/MWh (Juhrich, 2022). For electricity in a country with a high percentage of renewables like Austria, the factor is 0.064 t_{CO2}/MWh (*Stromkennzeichnung* 2024). For biomass, it is a question of debate whether to assign a price for the CO_2-emissions for farming equipment or even to assume a negative CO_2 balance because biomass CHP gets to replace fossil CHP plants (Bundestag, 2007). For this reason, no CO_2-emissions are assigned to biomass. For the gas price, the quarterly average spot price for

the EU from the first quarter of 2023 is used, which is 53.32 €/MWh (Commission, 2023). For the wood pellets, which fuel the Biomass CHP, the price of 38.38 €/MWh from the same time period is used (*Argus Biomass Markets (2023-04-26).pdf* 2024).

For CHP plants selling electricity, the hourly stock exchange electricity price profile for Germany from the year 2023 is used (Ewen, 2024). It can be seen in the following fig. 3.7:

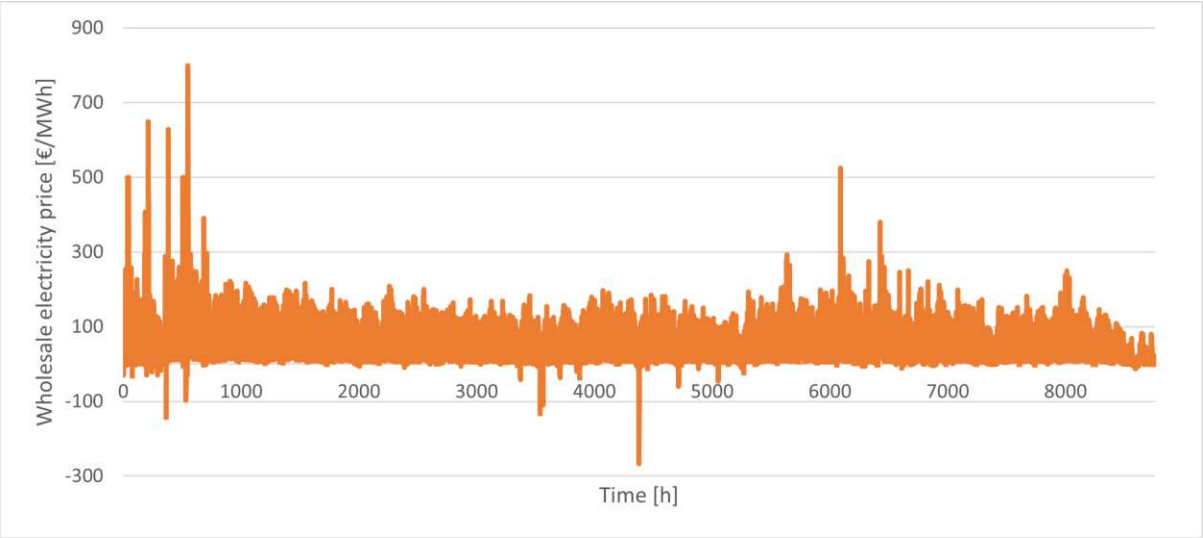

Figure 3.7: Wholesale electricity price for Germany for the year 2023 (Ewen, 2024)

With an average price of 81.61 €/MWh, it is relatively high compared to the average price of the years 2006-2019, which is 41.42 €/MWh, although way below the record year of 2022 with 230.57 €/MWh (*Durchschnittliche Börsenstrompreise — Energy-Charts* 2024). However, according to Schmitt (2022), the average, unweighted baseload prices of the EU will be in a range from 69 €/MWh to 78 €/MWh between 2030 and 2050 (fig. 3.8). Baseload prices are the annual average prices across all hourly prices of the year. This makes it an accurate value for the implementation in future scenarios.

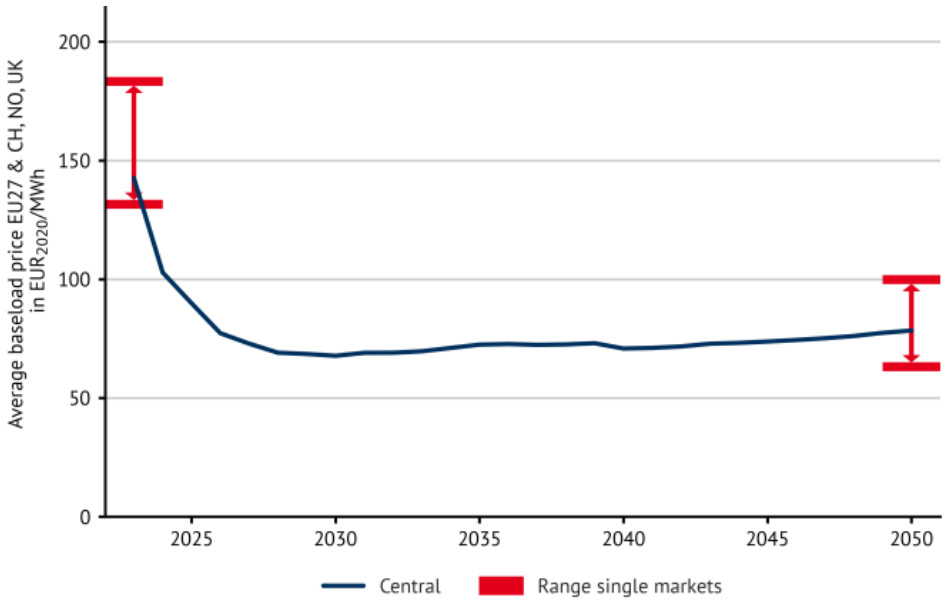

Figure 3.8: Annual baseload prices and range of fluctuation of national individual markets on average (Schmitt, 2022)

For heat pumps, which consume electricity, the price from Ewen (2024) is increased by 56.66 €/MWh over the whole year, accounting for taxes, grid usage charge, CHP surcharge, etc. (AGFW, 2024) in particular for LSHP in Germany. This also takes into account that the EEG surcharge is omitted by 2023 (*Wegfall der EEG-Umlage entlastet Stromkunden — Bundesregierung* 2022).

3.3.5 Other input data

In the following table, additional input data regarding lifetime, interest rate and part load capabilities is presented. For a single LSHP unit, a minimum output power factor of 0.25 is found in literature (DEA, 2023). This takes into account the limited part-load abilities of LSHP. However, a high minimum output power factor severely increases the model runtime. Additionally, the load will be covered by many LSHP units in reality, whereas it is modeled as a single unit in HotMaps (2024). Therefore, the sum of the heat pump units must have a smaller minimum output power than the single units. For these reasons, a minimum output power factor of 0.1 is set.

Table 3.11: Other input data (DEA, 2023)

Parameter	**Value**
Life time [years]	25
Interest rate [%]	5
Minimum output power factor heat pumps and CHP [0-1]	0.1

3.4 Applying the HotMaps district heat supply model to develop scenarios

To answer the research question "What is the current status and the potential contribution of large-scale heat pumps in district heating under different conditions in terms of heat source availability and technology portfolio?", 3 exemplary heat generation portfolios are defined in the first step. To evaluate the competitiveness of different heat sources of LSHP under various circumstances, the model input parameters are varied in the next step. In HotMaps (2024), the portfolios are implemented as scenarios, while different circumstances are implemented as sub-scenarios. To allocate the optimal installed capacity of each heat generator to each case, all model runs are performed in investment mode with no initial installed capacity. As the installed capacity of each heat generator will have a major impact on the overall cost of the system, this step is crucial for evaluating economic competitiveness. In summary, the following parameters are varied in the sub-scenarios:

- **Sub-scenario 1: The impact of different refrigerants**
  The choice of refrigerant influences the COP, the temperature sensitivities of the COP, and the investment cost of LSHP.
- **Sub-scenario 2: The impact of the size of the city and heat pump unit**
  This variation takes into account the economies of scale effects for different heat pump unit sizes as well as different maximum heat demands under the assumption that larger heat pump units will be installed in larger cities.
- **Sub-scenario 3: The impact of climate conditions**
  In this sub-scenario, 3 exemplary climate conditions in northern, central, and southern Europe are implemented to evaluate the effects of the climate condition on LSHP. This includes using different temperature profiles as well as having differently shaped heat demand profiles.

Apart from LSHP, as mentioned in Gerhardt (2021), CHP plants will play a major role in current and future DH systems. Therefore, all portfolios consist of a biomass CHP plant and also a gas boiler for peak loads (Peak Boiler). For LSHP, the most common heat sources found in the database (see fig. 4.3) are used. Portfolios 2 and 3 feature cases, where no large water body or no sewage water system is available to use as a heat source. While the heat sources air, sewage water, sea water, and lake water all have varying temperature profiles over the year (see section 3.4.3), the heat sources geothermal, industrial process heat, and groundwater show a constant temperature at different levels. The portfolios are shown in table 3.12.

Table 3.12: Heat generator portfolios

Portfolio 1	**Portfolio 2**	**Portfolio 3**
CHP Biomass	CHP Biomass	CHP Biomass
Peak Boiler	Peak Boiler	Peak Boiler
HP Air defrosting	HP Air	HP Air defrosting
HP Sewage water	HP Sewage water	
HP Sea		HP Lake
HP Geothermal (T_{source} = 55°C)	HP Industrial process heat (T_{source} = 35°C)	HP Ground water (T_{source} = 8°C)

Additionally, defrosting effects are implemented for air source heat pumps, which will be explained in the following section.

Shutoff temperature & defrosting

To prevent the build-up of unacceptable ice crystal formation, the operating temperature range heat pumps must be limited. The typical temperature difference between the inlet and the outlet of the heat exchanger is around 3 K (*MVV Mannheim Wärmepumpe* 2024), (DECC, 2015) for freshwater heat pumps. This makes a shutoff temperature of 4 °C necessary to be well above the freezing point. For sewage water heat pumps, defrosting is usually no issue as the temperatures stay above 5 °C for the whole year, even in the northern European climate (see fig. 3.16). Due to the salinity of seawater, the freezing point is -1.7 °C (Zheng et al., 2015). This results in a lower shutoff temperature of 2°C. For air source heat pumps, frosting occurs at temperatures below 6°C (see section 4.1), which is the shutoff temperature for air source heat pumps without defrosting.

However, there are methods to defrost air source heat pumps and therefore operate them at lower temperature levels: The most common way is to reverse the heat pump cycle (see fig. 3.2) to heat and deice the evaporator periodically. This causes a severe decrease in heating capacity and efficiency during the defrosting period. In a recent study by Jia et al. (2024), an innovative approach especially for defrosting large-scale air source heat pumps called air heat absorption defrosting (AHAD) is proposed: It works by independently controlling the heat exchangers of the large-scale heat pump and only defrosting one heat exchanger at a time versus reversing the whole cycle. It was experimentally validated and compared to reverse cycle defrosting for a large-scale air source heat pump unit (710 kW). The findings were that, with an additional investment cost per unit of 6%, the average heating capacity in the defrosting phase only sank to 315,7 kW compared to -663,4 kW of a conventional reverse Carnot defrosting unit. The defrosting period lasts 5 min for reverse cycle defrosting and 15 min for AHAD, resulting in a decrease of average heating capacity of 21 % for reverse cycle defrosting and 14 % for AHAD compared to a case with no frost build-up. As the HotMaps (2024) dispatch model features hourly resolution, this time period is too short to capture accurately in the model. Instead, the maximum power of the heat pump is reduced linearly from 6 °C, where frost buildup starts, to -15°C, which is sufficiently low for the European climate (see fig. 3.13). This results in a conservative estimation of the benefits of defrosting strategies.

The following figure shows the comparison of shutoff temperatures:

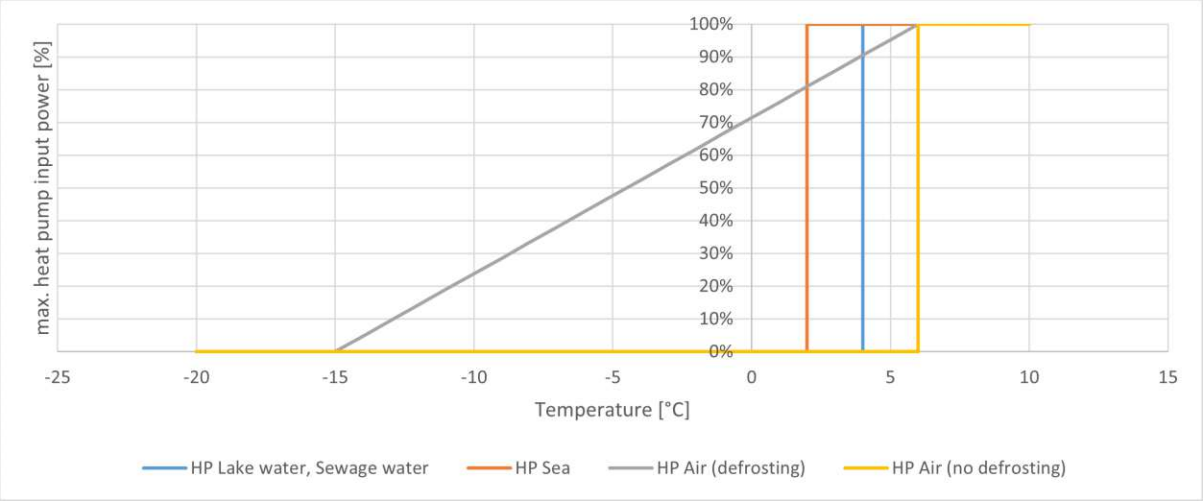

Figure 3.9: Maximum heat pump input power [%] and shutoff temperatures [°C] for LSHP using different heat sources

3.4.1 Sub-Scenario 1: Refrigerants

In the sub-scenario 1, the impact of different heat pump refrigerants is compared: R134a is the most commonly used, but problematic refrigerant due to its high global warming potential (see section 4.3) and it is compared to R600a (iso-butane) and R290 (propane), which both feature a low global warming potential. This leads to a variation of the investment cost as well as nominal COP and the sensitivities of COP to temperature change. The method of calculation is described in section 3.3.1. All heat pumps feature the respective refrigerant in each case.

3.4.2 Sub-Scenario 2: Economies of scale and city size

The goal of the second scenario is to determine how the value of LSHP changes based on the individual heat pump unit size and the city size. LSHP unit sizes start at 1 MW thermal capacity, which is implemented in the first case. However, the units can reach sizes up to 20 MW thermal capacity (Barco-Burgos et al., 2022), which is implemented in the second case. This maximal size is also confirmed by the projects collected for the database. The investment costs are scaled according to eq. (3.27). Two exceptions are ground water heat pumps and air source heat pumps, which are limited to 5 MW per unit for air source heat pumps and 6 MW per unit for groundwater heat pumps. The details of this limitation are described in section 4.1. For the CHP and Peak gas boiler, no economies of scale effects are assumed.

For example, the specific TCI per MW for the 3 refrigerants used for different heat pump unit sizes at a source temperature of 20°C and a flow temperature of 90°C is shown in the following fig. 3.10:

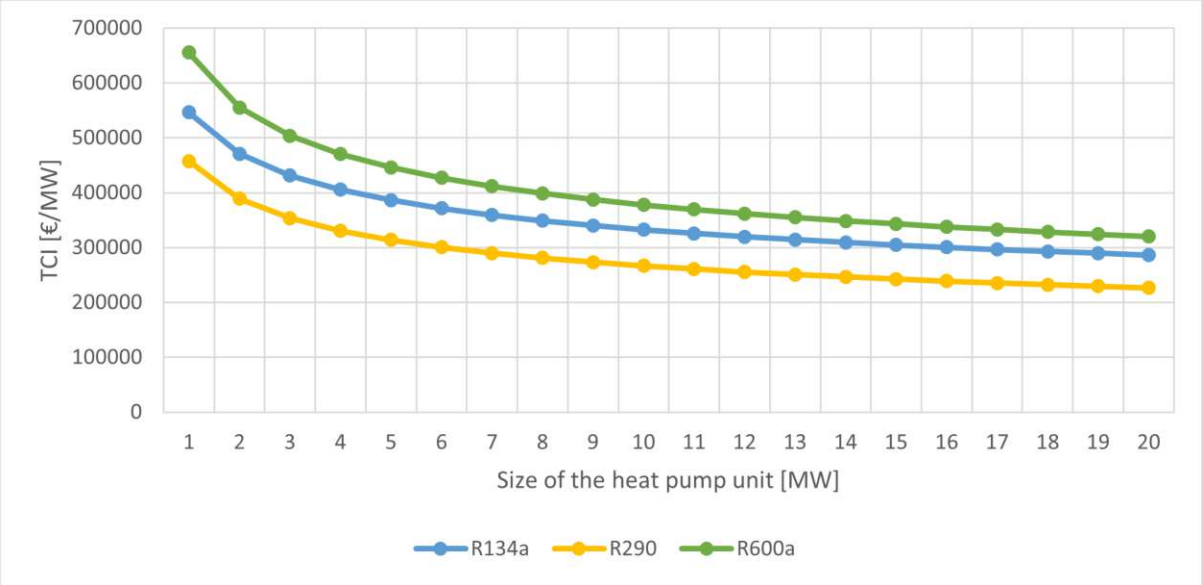

Figure 3.10: Specific TCI for heat pump units of different sizes using the refigerants R134a, R290 and R600a

This indicates that R290 is the cheapest in terms of total investment costs, while R600a is the most expensive.

The total heat demand is estimated based on Totschnig et al. (2018), in which typical cities and district heating systems in Austria are typologized. To take into account that the larger HP units are generally found in larger cities with a higher heating demand, 2 different total

heating demands are chosen. The total demand over the year is 1 780 000 MWh for a big city, which corresponds to a type 3 city in Totschnig et al. (2018).

For a small city, the total demand is changed to 420 000 MWh, corresponding to a type 5 city in Totschnig et al. (2018). It shows that the demand of the large city is around 4 times larger than the demand of the small city.

Additionally, the maximal possible heating capacity to install depends on the heat source. While the cost per MW of installed capacity is dependent on the unit size, it is possible to have multiple units in a city, leading to higher total installed capacities. While the heat sources peak boiler and seawater have a practically unlimited potential capacity, other heat sources are limited. For a big city, the LSHP sources geothermal, lake water and industrial process heat feature a high potential capacity of 200 MW, while sewage water is limited to 100 MW. Ground water is limited to 50 MW and air is limited to 80 MW due to the restrictions mentioned in section 4.1. Biomass CHP is limited to 250 MW according to EPA (2007). For the heat storage, a fixed charging and discharging capacity of 140 MW based on a large storage in the city of Helsinki is chosen (Pursiheimo et al., 2022). The potential for the large city is then scaled down by 1/4 according to the 2 total heat demands, as seen in the following table.

Table 3.13: Maximal possible heating capacity [MW] to install for a large and small city

Heat Source	**Large city (Heat pump unit size: max)**	**Small city (Heat pump unit size: 1MW)**
CHP Biomass	250	62.5
Peak Boiler	∞	∞
HP Air	80	20
HP Sewage water	100	25
HP Sea	∞	∞
HP Lake	200	50
HP Geothermal	200	50
HP Industrial process heat	200	50
HP Ground water	50	12.5
Heat storage	140	35

However, the resulting installed capacity of all heat generators will depend on the most cost-effective way to cover the demand over the year, as no capacity is installed initially for any heat generator.

3.4.3 Sub-Scenario 3: Climate conditions

To reflect the impact of different climate conditions, the heat demand profile and the heat source temperatures are changed for a northern, central, and southern European case. The following graphs show typical heat demand profiles for northern (Stockholm), central (Vienna), and southern (Andalusia) Europe. They are calculated based on the outside temperature, which is accurate for the heating season. For times that are not in the heating season, they are smoothed out, assuming there is only a hot water demand at this time, but no space heating demand. This is done by calculating the moving average over one week for the period with no space heating demand.

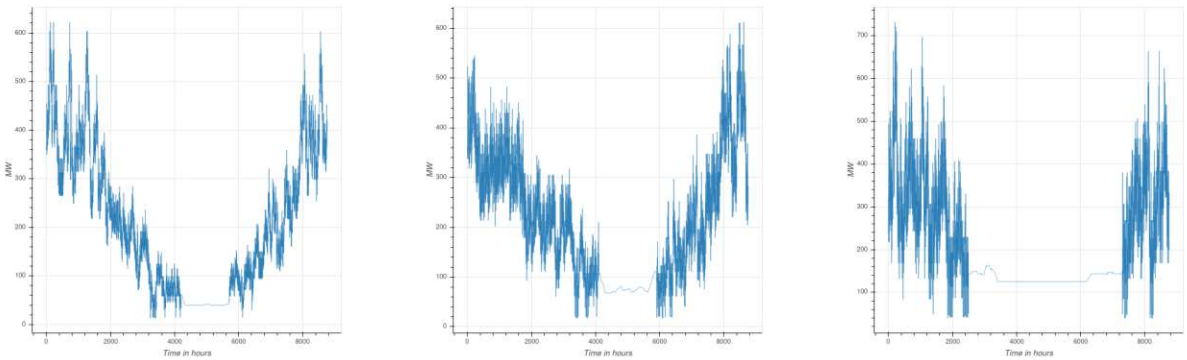

(a) Adapted heat demand profile Stockholm of the year 2010

(b) Adapted heat demand profile Vienna of the year 2010

(c) Adapted heat demand profile Andalusia of the year 2010

Figure 3.11: Exemplary heat demand profiles in Europe (HotMaps, 2024)

It is clear to see that the heating period takes considerably longer in a northern climate compared to the southern climate. Further, as the cities all cover the same total heating demand over the year (section 3.4.2), the southern city must be larger than the northern one.

For DH flow temperatures, a representative profile for the 3^{rd} generation of DH systems adapted from the city of Vienna is used for all model runs. It has a maximum temperature of 95 °C and a minimum temperature of 75 °C. This fits the design flow temperature of 90 °C for the LSHP used for almost all of the year. When the flow temperature is above 90°C, the additional peak boiler can provide the missing temperature lift. The return temperature is set to be constantly 50°C. The profile is shown in the following figure:

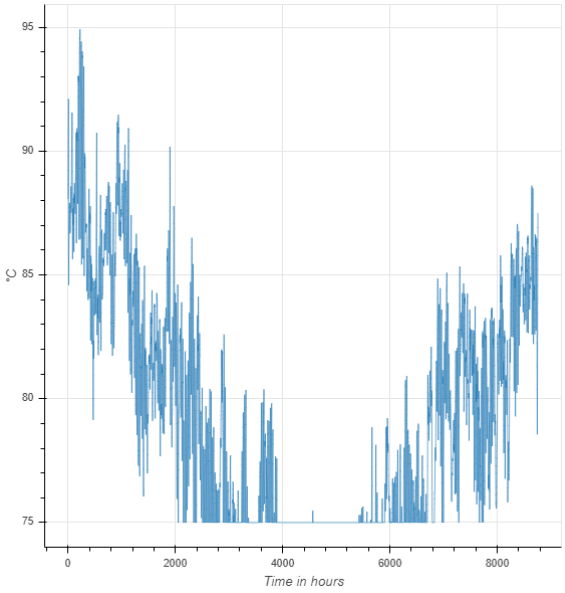

Figure 3.12: Adapted flow temperature profile Vienna of the year 2016 (HotMaps, 2024)

Hourly heat source temperature profiles

In the following section, the heat source profiles for different regions in Europe are presented. Due to the difficulty of data acquisition for certain heat sources, different years have to be taken for certain profiles and due to the fact that most cities do not have direct access to all heat sources, profiles from exemplary cities in northern, central and southern Europe are compared and used as model input data. This way, consistent portfolios can be compared and conclusions can be drawn about the competitiveness of heat sources under different climate conditions.

Hourly air temperature profiles are accessed from the National Centers for Environmental Information (NCEI, 2024) and can be seen in the following figure. Representative for a northern climate is Berga near Stockholm in Sweden, for a central European climate Vienna in Austria and for a southern European climate Rome in Italy. The high temperature fluctuations are characteristic of air compared to other heat sources.

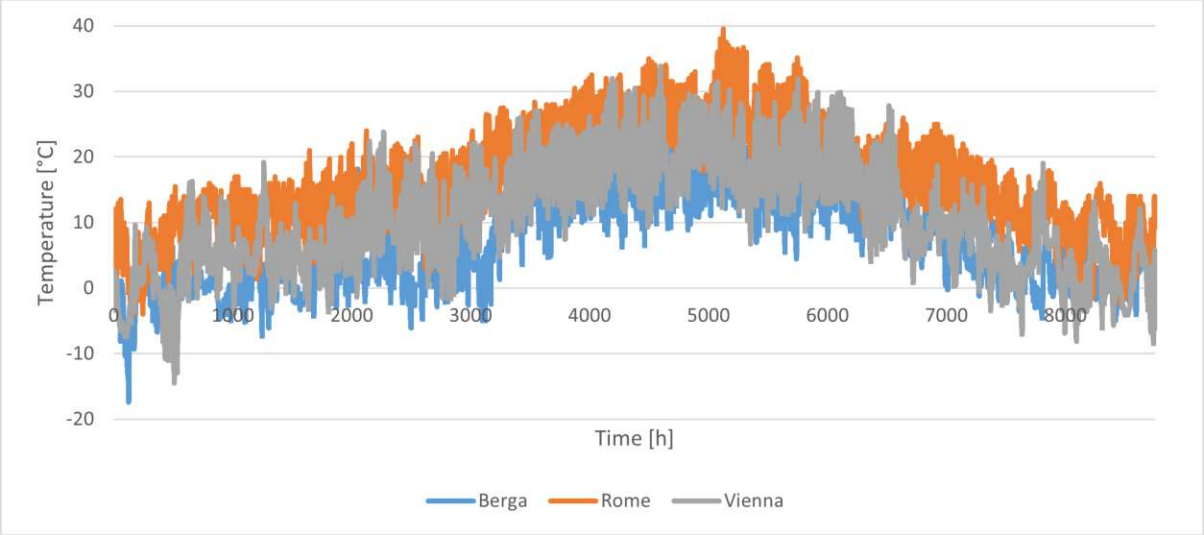

Figure 3.13: Ambient air temperatures of the year 2016 (NCEI, 2024)

Hourly sea water temperatures for Europe are accessed from the *Copernicus Marine Data Store* (2024). The following graph shows the sea water temperatures from 3 locations in northern (Stockholm), central (Den Haag) and southern (Valencia) Europe.

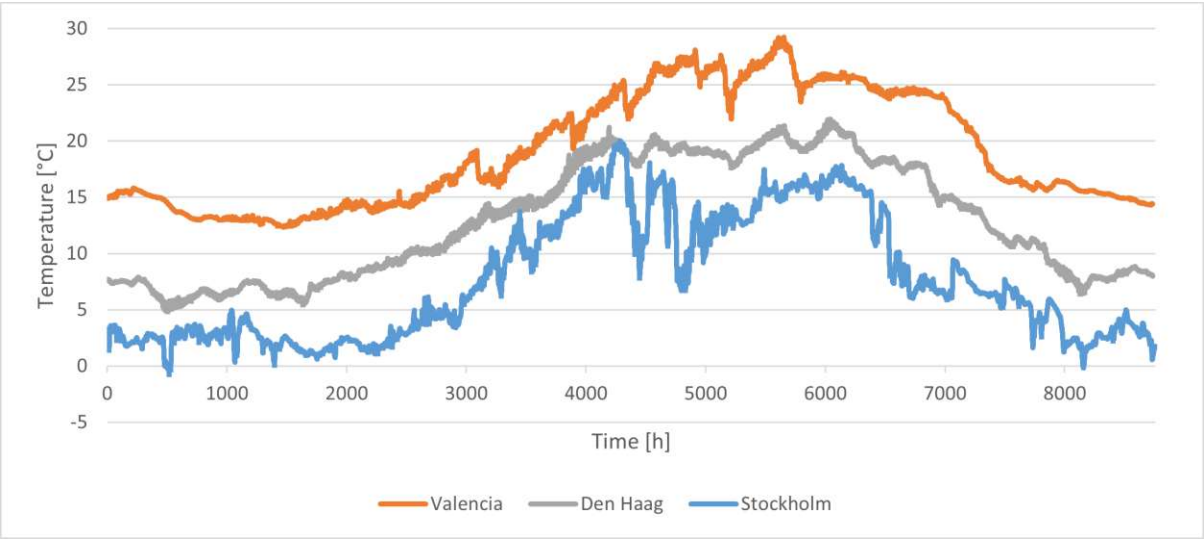

Figure 3.14: Sea water temperatures of the year 2023 (*Copernicus Marine Data Store* 2024)

Daily mean lake surface water temperatures are accessed from the database GloboLakes available at CEDA archive (Carrea and Merchant, 2019). For conversion into hourly resolution, a cubic spline interpolation is performed. It uses the given daily mean data points as midpoints and creates a smooth function that estimates the temperature at every hour of the year. Representative for the northern European climate is lake Vanern in Sweden, for the central European climate lake Constance in Austria and for the southern European climate lake Bolsena in Italy. In northern climate, the lake surface temperature reaches freezing temperature in winter, which makes lake water an unfavourable choice for heat extraction under these conditions. A possible solution for this is to extract water at a greater depth, as water with 4 °C is the most dense and sinks to the bottom of the lake, when the surface freezes. There are methods for predicting water temperatures at a certain depth, like using artificial neural

networks and 3D circulation models as described in Liu and W.-B. Chen (2012), but applying these methods to generate temperature profiles would exceed the scope of this work.

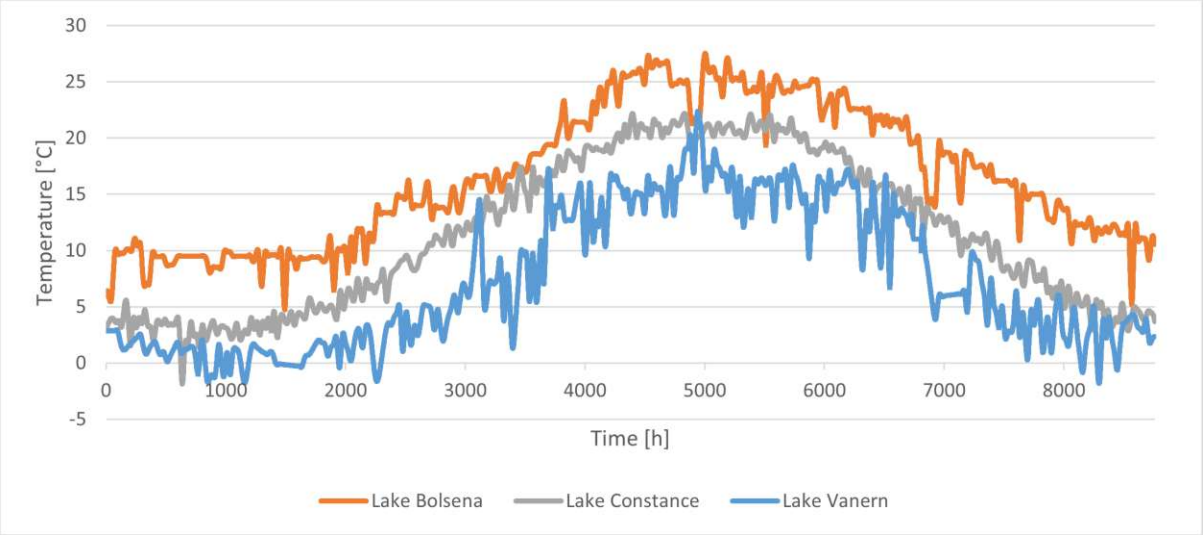

Figure 3.15: Lake water temperatures of the year 2016 (Carrea and Merchant, 2019)

For sewage water, there is hardly any data available on a detailed hourly base. However, in Golzar, Nilsson, and Martin (2020), an artificial neural network was developed to predict sewage water temperatures more accurately based on sample historical data from the Stockholm sewage water system from the years 2009 - 2019. The hourly sewage water temperatures of the year 2019 are used as input for the northern European case.

In Cipolla and Maglionico (2014), the sewage water of Bologna in Italy has been monitored over a period of 6 months and the flow and temperature variations have been analysed. Through this analysis, a temperature coefficient C_t is obtained. It accounts for the deviations in hourly mean temperature from the daily mean temperature. For different measuring stations, it ranges in average from 0.95 - 1.05, following a approximate sine shape with a drop in temperature of 5 % in the first half of the day and increased temperatures of 5 % in the second half of the day. The implementation of this method can be seen in fig. 3.17. Another finding is that the temperature in sewage water systems is relatively stable compared to outside air temperature, although influenced by it. This stability is beneficial for the use of heat pumps. In Hart and Halden (2020), a deterministic model using among others air and soil texture data is implemented to estimate the wastewater temperature on a global scale on a monthly basis. These are then compared with nearly 400 observations extracted from 20 studies to ensure accurate prediction of the seasonal dynamics of sewage water. Among those were also the results from Cipolla and Maglionico (2014). To generate realistic temperature curves for the north and central European case, the hourly temperatures were calculated based on the monthly mean temperatures from Hart and Halden (2020) using cubic spline interpolation together with the daily fluctuation obtained by Cipolla and Maglionico (2014). In fig. 3.16, these generated temperature curves for Bologna (south) and Wuppertal (central) are compared with the one for Stockholm (north) from Golzar, Nilsson, and Martin (2020). It shows a similar range of daily fluctuations, although the wastewater temperatures for Stockholm are higher in the heating season in comparison.

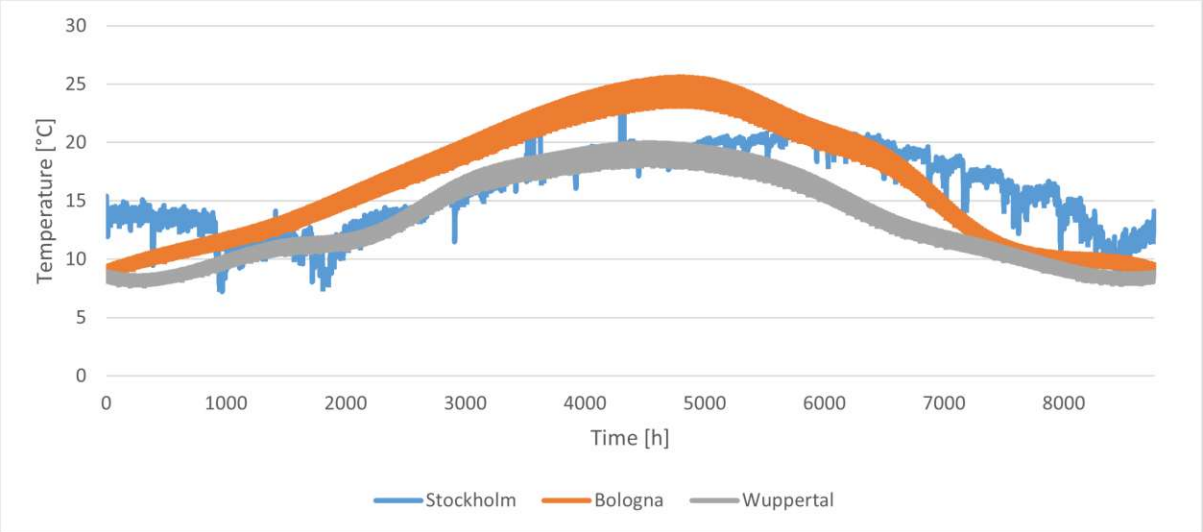

Figure 3.16: Sewage water temperatures (Stockholm (2019): Golzar, Nilsson, and Martin (2020), Bologna (2014) and Wuppertal (2009): own calculation based on Hart and Halden (2020)

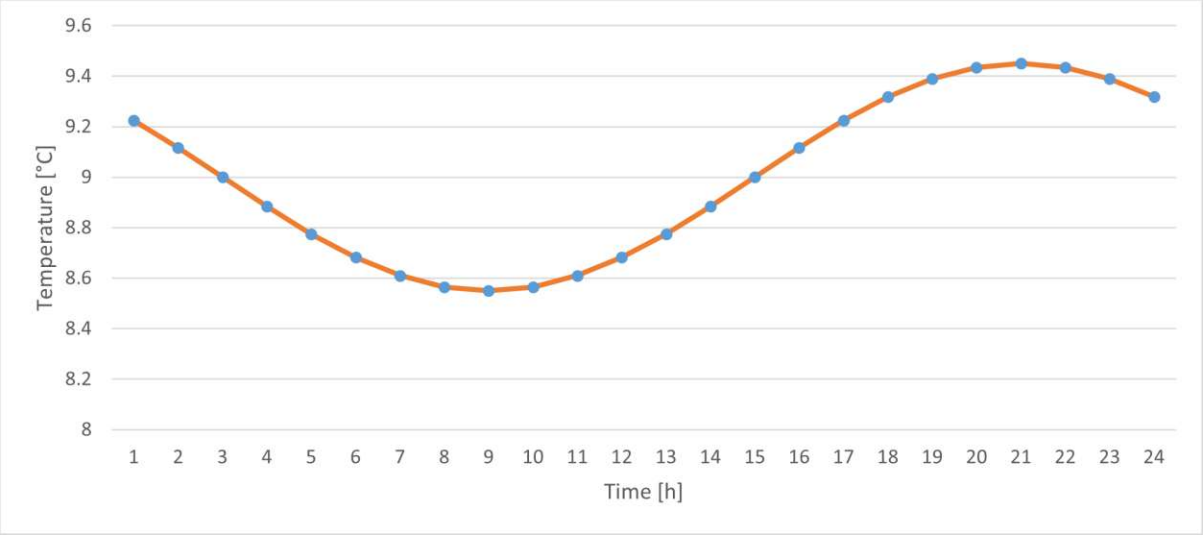

Figure 3.17: Daily sewage water temperature fluctuations for Bologna on the first of January based on own calculation

4 The current status of large-scale heat pumps in European district heating systems

To capture the spatial and temporal distribution of LSHP in Europe, a map and a timeline are generated: In the following fig. 4.1, the main heat source is indicated by the color and the installed heating capacity is displayed as the circle size, with the center being at the location of the LSHP. It features sizes from 1 MW in Madrid up to 300 MW in Stockholm and 500 MW in Helsinki for a future project and 22 different heat sources in total including 1 category for unknown sources.

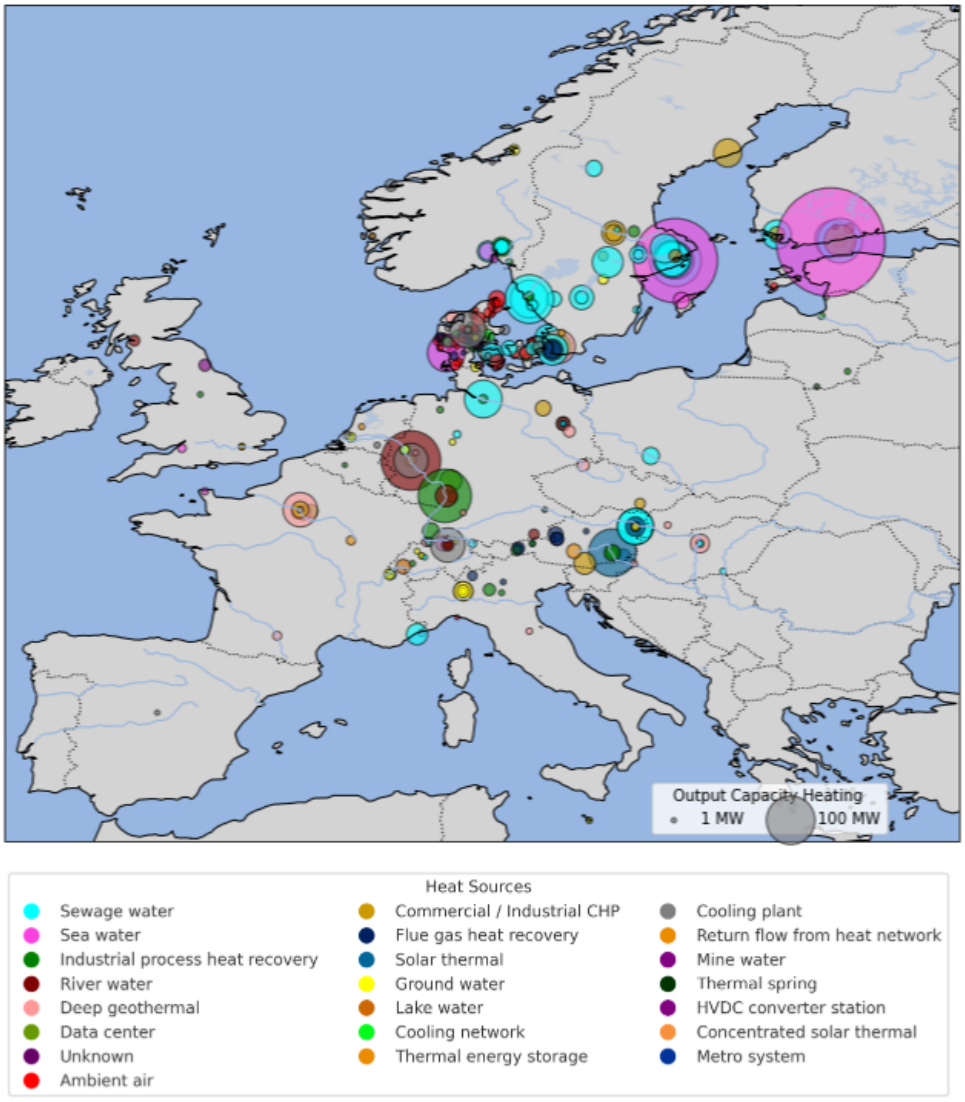

Figure 4.1: Large-scale heat pump installations in Europe

There is a high concentration of LSHP in the Nordic countries while they are only sparsely installed below 45° Latitude. Factors for this are among others the colder climate in Nordic countries, which necessitates a higher demand for heating solutions, as well as cheap electricity and government incentives.

In fig. 4.1, it can be seen that the majority of large-scale air source heat pumps are installed in Denmark. A possible reason for this is the Danish strategy for operating DH systems in conjunction with wind power and CHP plants (Averfalk et al., 2017):
Due to the very high proportionality of wind power,

> "CHP plants are operated to meet both electricity demand and wind power supply variations. But when the CHP electricity generation is reduced during windy days, CHP heat generation becomes more expensive. Hence, other heat supply is required for maintaining a low cost level. The demand part of a strategy can be to use power-to-heat installations in order to counteract temporary surpluses of electricity giving low electricity prices. Heat pumps and electric boilers can then supply low cost heat when the CHP plants are expensive. Heat storages can be used for storing this low cost heat for later use."

Because the heat source *ambient air* is available everywhere, and because modern air source heat pumps, like the model *Albatros* from Ochsner (2021) can supply 80°C flow temperature, even when the air temperature is -10°, large-scale air source heat pumps show potential to provide cost-effective flexibility to the power system.

In fig. 4.2 the installations are ordered by date, with the highest total installed capacity at the bottom of the graph.

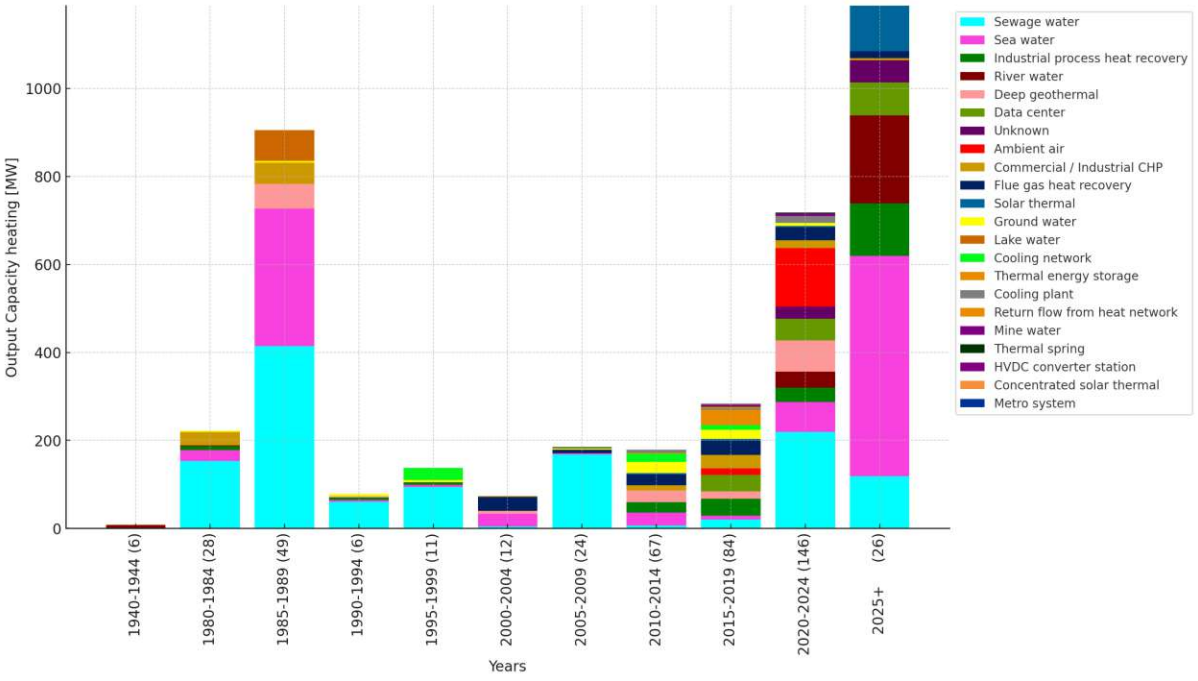

Figure 4.2: Timeline of large-scale heat pump installations in Europe

The fig. 4.2 shows that LSHP are not a novel technology, with some pioneering projects from Switzerland constructed in the 1940s, which are still operating today (Zogg, 2008). It can be seen that there was a boom in LSHP installations in the 1980s, while in the period from 1990 to 2010, there was little interest in installing LSHP and also research activity (see fig. 2.2).

A closer examination of the data shows that these LSHP were almost exclusively installed in Sweden in the 1980s and are still operating. According to Averfalk et al. (2017), this first wave of LSHP installations happened, because there was "a national electricity surplus from nuclear power for some years", which supplies the LSHP with cheap electricity. Looking even further back in history, the oil crisis in the 1970s contributed to an emergence of research and scientific publications in the field of LSHP in the following years, as mentioned in Jesper et al. (2021) and Sulzer et al. (2021) in fig. 2.2. This may also be a factor that the Swedish government made an early decision to be more independent from fossil fuels. A particularly interesting insight is that the number of accumulated installed units from 2010 onwards rapidly increases, as the number of different heat sources does as well. This suggests that, even when the technology of the heat pump per se is well-matured, the different application possibilities (heat sources) are just recently tested out and there is a possible learning curve ahead. Lower network temperatures in future DH systems also benefit the use of low-temperature heat sources for LSHP (Guelpa et al., 2023). For projects planned beyond 2025, there is only sparse information available, but the data indicates an exponential growth in LSHP installations from 2015 onward.

The following fig. 4.3 shows the total installed heating capacity. It can be seen that *Sewage water* and *Sea water* amount to over half of the installed capacity, whereas *River water* to *Lake water* (10 heat sources) amount to $\sim$ 40%, while other lesser used heat sources amount to the final 3.5% of the total installed capacity of 4032 MW_{th}. To avoid cluttering, the heat sources with the lowest installed capacity have been grouped to a rest category.

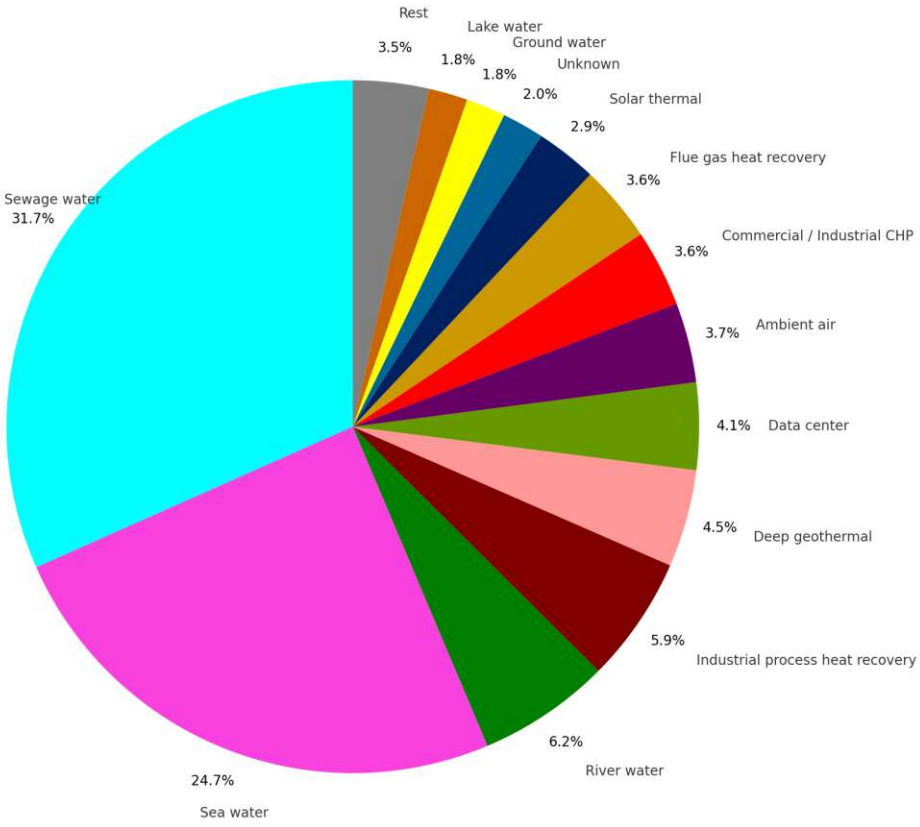

Figure 4.3: Total installed heating capacity [MW_{th}] of large-scale heat pump installations in Europe

4.1 Key Parameters of Heat Sources

4 Parameters for the heating season are identified as distinctive elements of the different heat sources and they are compared for each heat source in the following section.

1. Flow temperature T_F
2. Source temperature going into the heat exchanger T_{SI}
3. $\Delta T = T_F - T_{SI}$
4. $COP_{Heating}$

The smaller ΔT and the larger T_{SI} is, the larger is the $COP_{Heating}$.

In literature (Pieper, Krupenski, et al., 2021), there are many advanced techniques on how to model or approximate COP under various conditions, but the most fundamental one is the **Carnot efficiency** η_C (Carnot and Ostwald, 1892) for heat pumps, which can be interpreted as an idealized $COP_{Heating}$, and must be larger than the efficiency ϵ calculated by real values, where losses are included. It shows the important relationship between the temperatures, the amount of heat energy Q_H generated by the heat pump and the electrical energy W_{el} supplied to the heat pump compressor:

$$\eta_C = \frac{T_{hot}}{T_{hot} - T_{cold}} = \frac{T_F}{T_F - T_{SI}} = \frac{T_F}{\Delta T} > \epsilon = \frac{Q_H}{W_{el}} \tag{4.1}$$

The $COP_{Heating}$, which is obtained from technical data sheets, only contains the COP for one operating point under design conditions. Design conditions generally refer to the lowest expected temperatures in which the heat pump operates. To display the distribution of data, box plots are used. Here, the temperatures are plotted on the first y-axis, while the $COP_{Heating}$ is plotted on the second y-axis in green color to be better distinguishable. Entries with $\Delta T = 0$ due to missing data are sorted out for this evaluation.

Additional information on every heat source is mentioned here and the heat sources are sorted by installed heating capacity (see fig. 4.3).

Sewage water (1287 MW_{th}), 60 projects

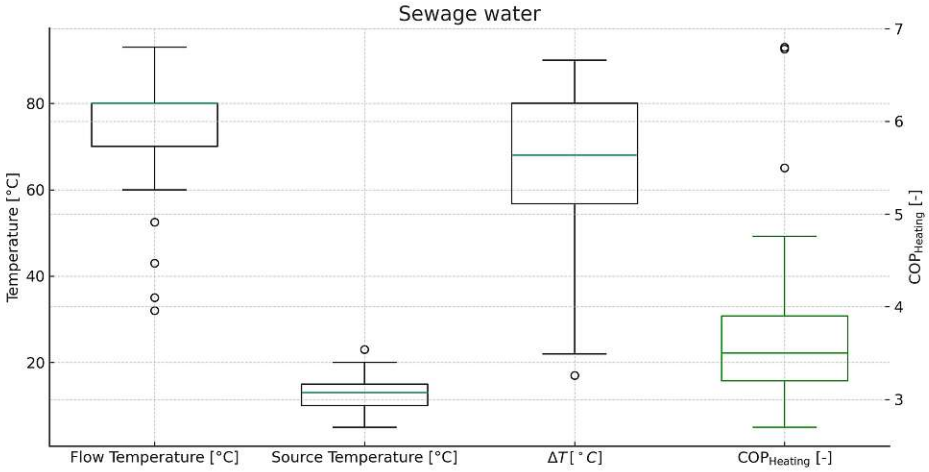

Figure 4.4: Sewage water temperatures and $COP_{Heating}$

The source temperature of sewage water ranges from 8°C - 23°C with a median $COP_{Heating}$ of 3.5 (fig. 4.4). Sewage water shows a low daily temperature variation of 3°C and can be extracted from sewage water treatment plants or directly from pipelines (W.-A. Chen et al., 2022), whereby for large-scale applications sewage water treatment plants are preferably used (Cipolla and Maglionico, 2014). In a study about modeling wastewater temperatures, Hart and Halden (2020) showed that wastewater in the European climate does show a seasonal variation from 9°C in the winter and 19°C in the summer. Any major city has a potential for using sewage water as a heat source which is a reason why it is the most prominent heat source. Kiss (2017) mentions a potential of 200 MW for a city like Paris for large-scale sewage water heat pumps. As the implemented cities in HotMaps (2024) are smaller than Paris, this limit is reduced.

Sea water (984 MW_{th}), 22 projects

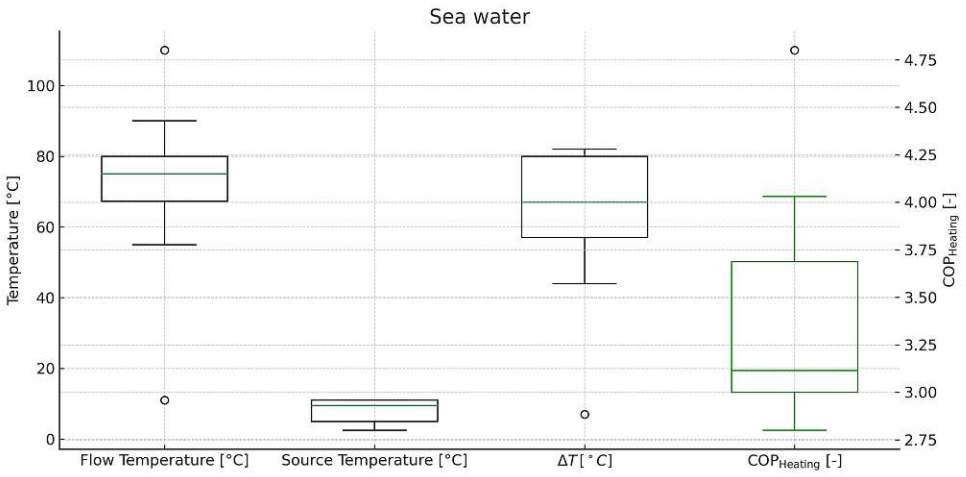

Figure 4.5: Sea water temperatures and $COP_{Heating}$

The source temperature of sea water ranges from 4°C - 11°C with a median $COP_{Heating}$ of 3.1 (fig. 4.5), which is considerably lower than sewage water. Large-scale sea water heat pumps are mainly installed in the Nordic countries, as seen in fig. 4.1. An advantage to other environmental water sources is the lower seasonal temperature fluctuations due to the large heat capacity of the sea (Yu et al., 2023).

River water (246 MW_{th}), 9 projects

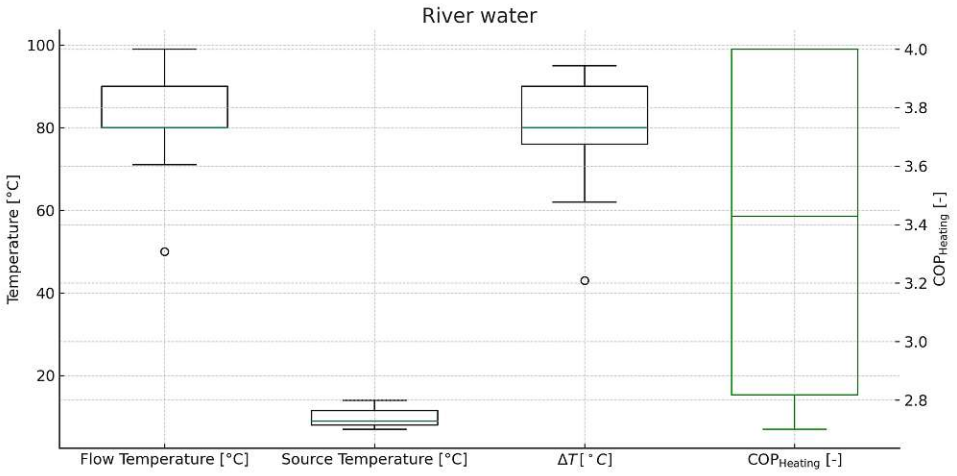

Figure 4.6: River water temperatures and $COP_{Heating}$

The source temperature of river water ranges from 7°C - 9°C with a median $COP_{Heating}$ of 3.42 (fig. 4.6). Compared to sea water, it shows stronger seasonal fluctuations. Large-scale river water heat pumps have not been built until recently, with 6 from 9 projects being built after 2022.

Industrial process heat recovery (234 MW_{th}), 35 projects

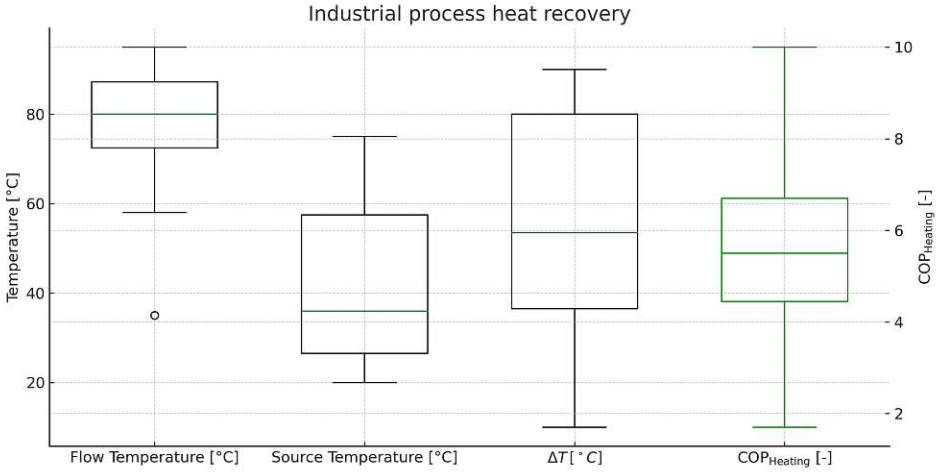

Figure 4.7: Industrial process heat recovery temperatures and $COP_{Heating}$

Industrial process heat provides a high temperature range from 20°C - 75°C and therefore also very high values for COP, with a median value of 5.3 (fig. 4.7). However, due to the high variety of industrial processes, it is not possible to estimate a general temperature profile, instead, the profile has to be case-specific. Dénarié et al. (2019) compares different methodologies to estimate industrial waste heat recovery and presents their own, using an MDCA (multi-criteria decisions analysis). It mentions, however, that for calculating the real technical heat recovery potential of an industrial process, the knowledge of excess heat potential becomes relevant, for which an analysis of each industrial process has to be performed. Manz et al. (2021) estimates the available industrial excess heat potential of Europe at sites that are in a 10km radius of DH areas by using LSHP (reduction of exhaust gas temperature to 25°C) to be 941 PJ/a, where the largest potential is attributed to refineries (331 PJ/a). This large capacity points to the promising potential of industrial process pumps.

Deep geothermal (184 MW_{th}), 19 projects

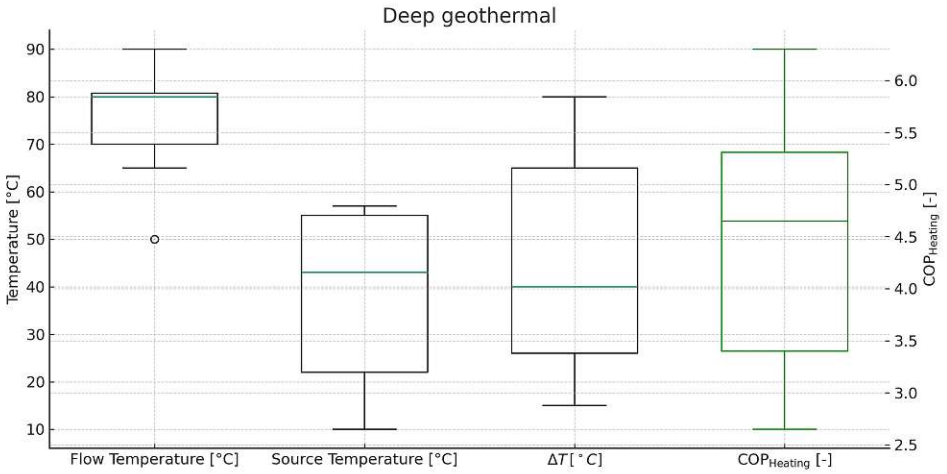

Figure 4.8: Deep geothermal temperatures and $COP_{Heating}$

The source temperature of deep geothermal ranges from 10°C - 57 °C with a median $COP_{Heating}$ of 4.7 and no seasonal variation (fig. 4.8).

For the use of deep geothermal heat, boreholes to an underground aquifer in a depth of 150m - 5000m have to be drilled (Goetzl, 2020). The geothermal gradient describes the temperature increase per km depth. Depending on the location, it lies between 27,8 K/km and 35,3 K/km with an average of 29,8 K/km (*geothermischer Gradient* 2024). A detailed analysis of the techno-economic potential of large-scale deep geothermal district heating systems can be found in Molar-Cruz et al. (2022).

Data center (162 MW_{th}), 12 projects

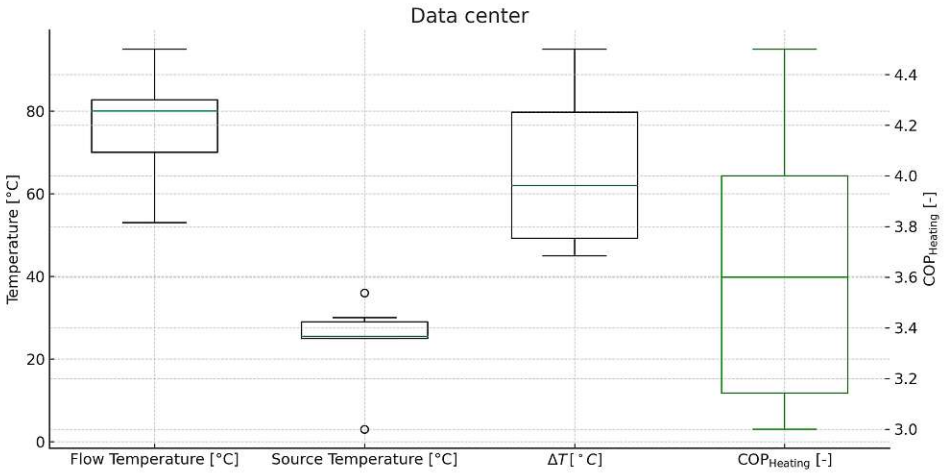

Figure 4.9: Data center temperatures and $COP_{Heating}$

The source temperature of data centers ranges mainly from 25°C - 43°C with a median $COP_{Heating}$ of 3.6 (fig. 4.9). The temperatures of this heat source are relatively consistent for the whole year. However, there is a low outlier with a source temperature of 3°C for data centers in the city of Akalla-Kista in Sweden. This is due to the combined heating and cooling operation of the heat pumps (Friotherm, 2023). The market for data centers in Europe is expected to grow by 7,4% from 2024 to 2028 (*Analyse der Marktgröße und des Anteils von Rechenzentren in Europa - Branchenforschungsbericht - Wachstumstrends* 2024), making this a promising heat source for future applications.

Ambient air (148 MW_{th}), 40 projects

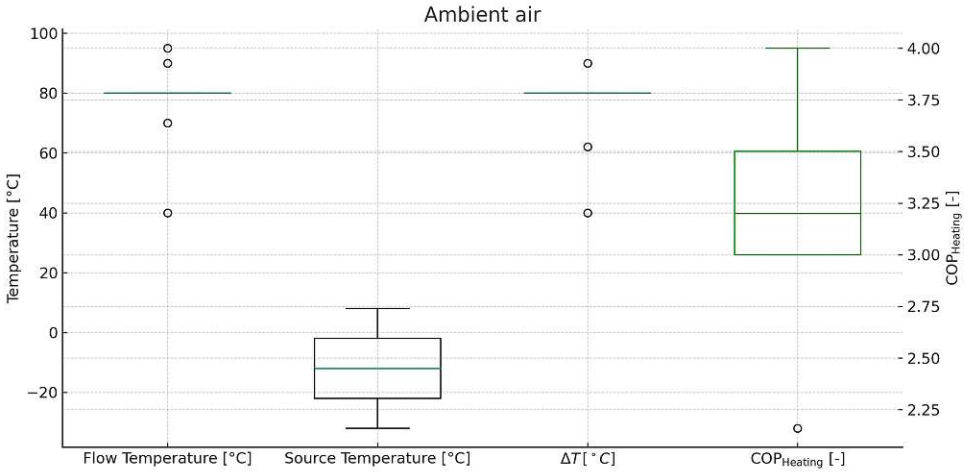

Figure 4.10: Ambient air temperatures and $COP_{Heating}$

The source temperature of ambient air ranges from -32°C - 8°C with a median $COP_{Heating}$ of 3.2 (fig. 4.10). This is the heat source with the lowest average source temperature, but also a high potential of expansion, since ambient air is available everywhere and no additional requirements have to be fulfilled. According to Nowak (2023), air source heat pumps of all sizes are the most common form of heat pump in Europe. They have a significantly lower land footprint than ground source heat pumps (Carroll, Chesser, and Lyons, 2020). A challenge to overcome for air-source heat pumps is the issue of frosting, especially in damp or cold climates (Carroll, Chesser, and Lyons, 2020), where a frost layer on the outdoor heat exchanger of an air source heat pump decreases the COP. Song et al. (2018) mentions that frosting occurs in an environment with a temperature ranging from -7°C - 5°C and a relative humidity above 65%.

A CFD-simulation of a large-scale air source heat pump (1.2 MW) in Brædstrup, Denmark is done in Rogié et al. (2020) to show the effects of air-recirculation and the micro-climate for different wind conditions. It shows a typical horse-shoe temperature profile for winds going lengthwise around the evaporator. Here, the cold air from the heat pump gets trapped by the horse-shoe-formed boundary layer around the heat exchanger, which has ambient temperature. For a heat exchanger with a length of 50m and width of 10m, this layer reaches a width of 20m at the end of the heat exchanger. Further, the model shows that depending on the wind direction, the re-circulation on the evaporator intakes ranges from 16.9% to 52.2 %, which lowers the efficiency. This effect is expected to be even larger for bigger units, leading to the

conclusion that it is more favorable to construct many smaller units instead of a few large ones.

Commercial / Industrial CHP (143 MW_{th}), 17 projects

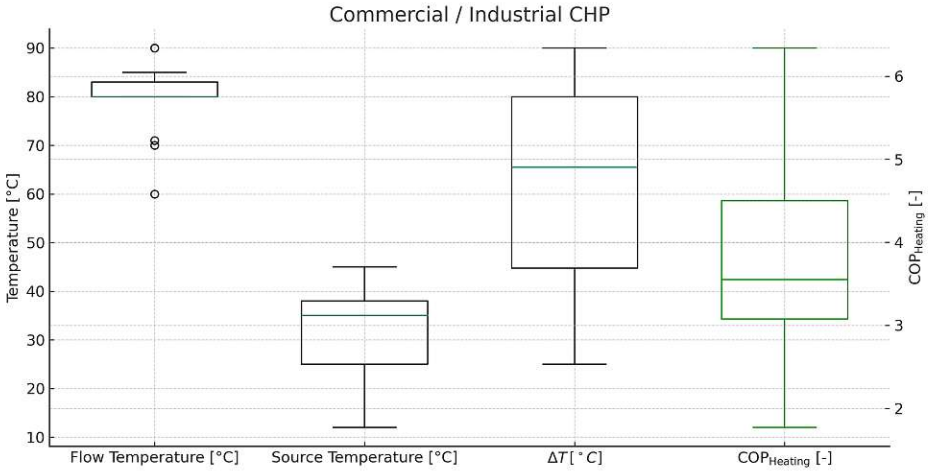

Figure 4.11: Commercial / Industrial CHP temperatures and $COP_{Heating}$

The source temperature of Commercial / Industrial CHP ranges from 12°C - 45°C with a median $COP_{Heating}$ of 3.5 (fig. 4.11). Here, LSHP fulfill the purpose of lifting low-temperature heat from CHP plants up to a level that is usable for DH networks. There are many benefits for the CHP plant when implementing LSHP. These include increased run-hours and electricity generation, reduced cost for heat rejection and less CO2 emissions due to greater electrical generation (O'Shea et al., 2019).

Flue gas heat recovery (143 MW_{th}), 27 projects

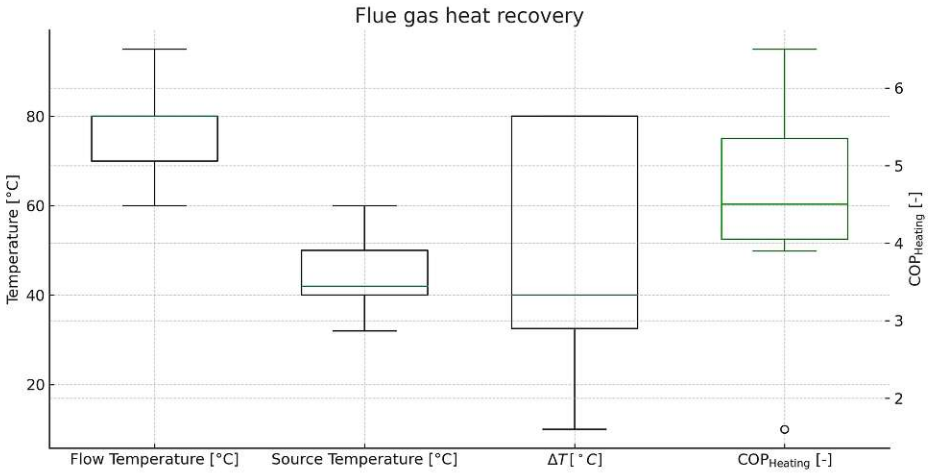

Figure 4.12: Flue gas heat recovery temperatures and $COP_{Heating}$

The source temperature of Flue gas heat recovery ranges from 34°C - 60°C with a median $COP_{Heating}$ of 4.5 (fig. 4.12). Due to their high source temperatures and low temperature lift, LSHP using this source are simpler and cheaper than LSHP using other sources (Pieper, Ommen, et al., 2018).

Solar thermal (114 MW_{th}), 8 projects

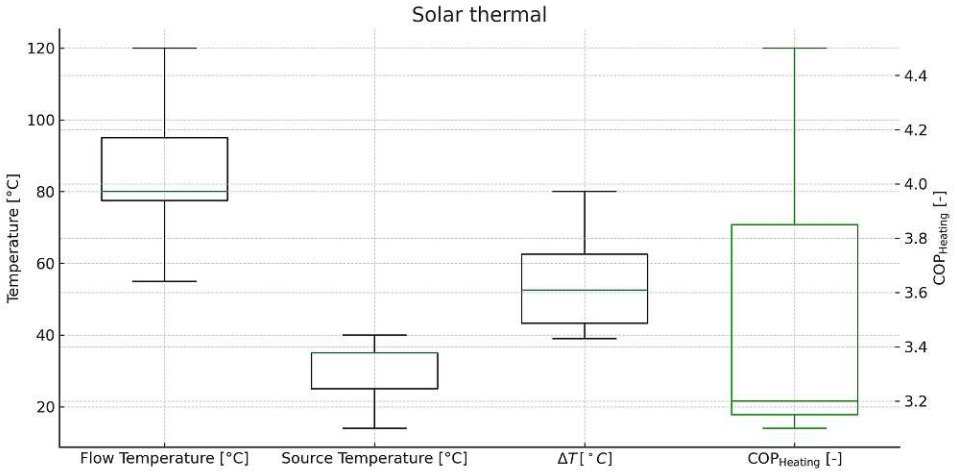

Figure 4.13: Solar thermal temperatures and $COP_{Heating}$

The source temperature of Solar thermal ranges from 14°C - 40°C with a median $COP_{Heating}$ of 3.2 (fig. 4.13). Solar thermal can be used in conjunction with a seasonal thermal energy storage and a LSHP to increase overall system efficiency, like for example in Berlin-Köpenick (*Großwärmepumpen in deutschen Fernwärmenetzen - energiewendebauen.de* 2024).

Ground water (78 MW_{th}), 23 projects

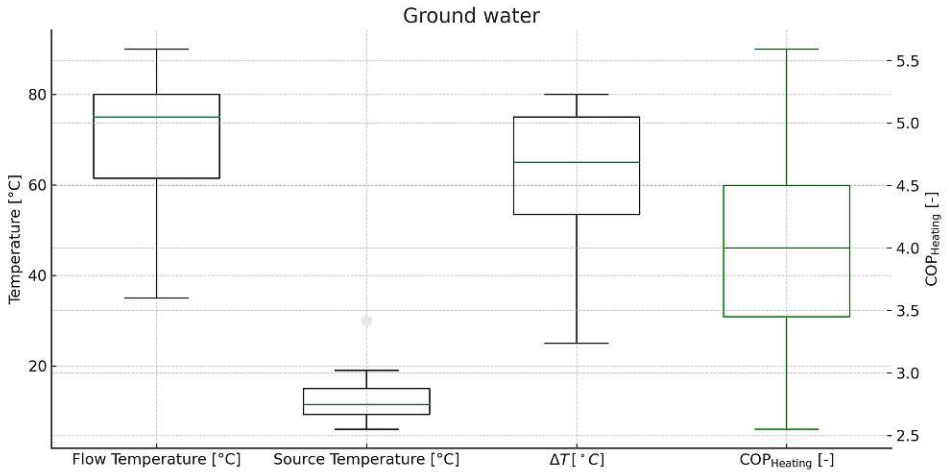

Figure 4.14: Ground water temperatures and $COP_{Heating}$

The source temperature of ground water ranges from 6°C - 19°C with a median $COP_{Heating}$ of 4 (fig. 4.14) and is like deep geothermal depending on the depth of extraction. According to Pieper, Mašatin, et al. (2019), the groundwater temperature at a depth of 25m to 75m is approximately 6°C-7°C in Estonia, and a constant value of 7°C can be assumed. Because the long-term stability of the groundwater reservoir should not be risked by extracting too much ground water, a practical limit of 6 MW per location is assumed in Pieper, Mašatin, et al. (2019) which is also considered in this thesis.

Lake water (72 MW_{th}), 9 projects

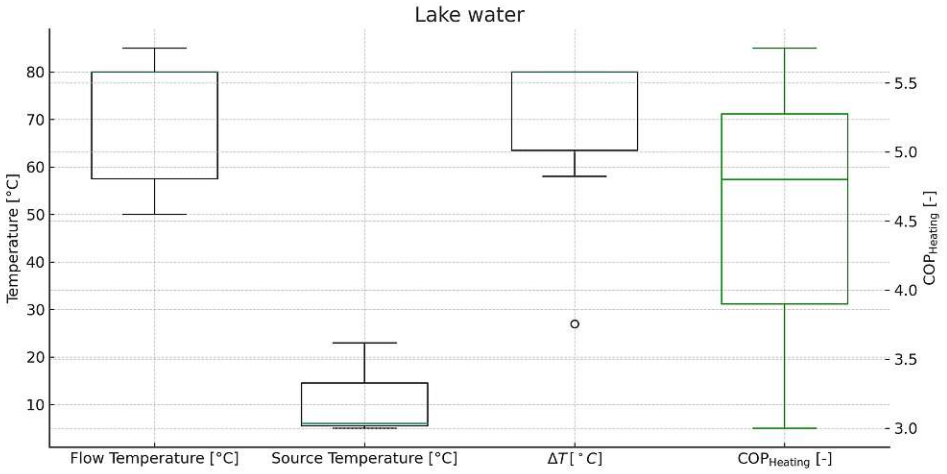

Figure 4.15: Lake water temperatures and $COP_{Heating}$

The source temperature of lake water ranges from 5°C - 23°C with a median $COP_{Heating}$ of 4.8 (fig. 4.15). The high outlier at 23°C originates from one of the first LSHP, built in 1941. It uses waste heat from the city swimming pool outlet combined with waste heat from a transformer station and lake water (Zogg, 2008).

Cooling network (62 MW_{th}), 7 projects

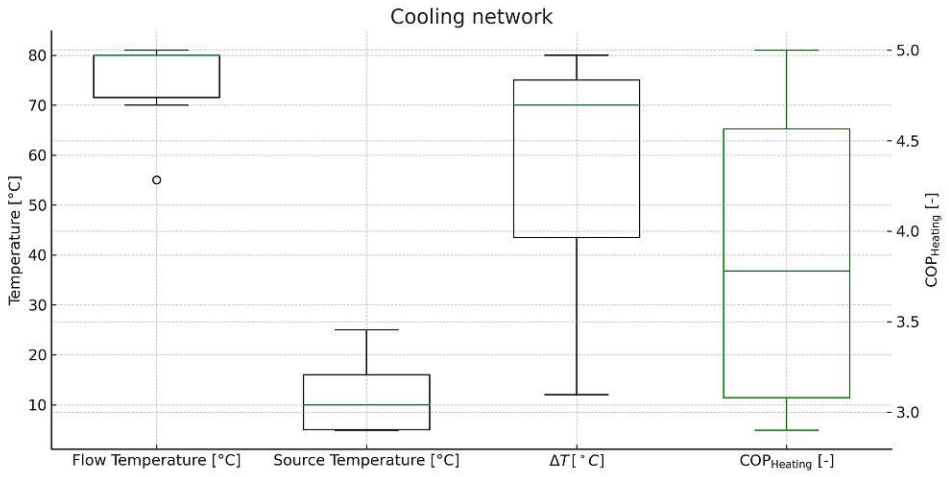

Figure 4.16: Cooling network temperatures and $COP_{Heating}$

The source temperature of cooling networks ranges from 5°C - 25°C with a median $COP_{Heating}$ of 3.8 (fig. 4.16). Here, the return water of district cooling networks in the summertime is used as a heat source (Averfalk et al., 2017). Currently, district cooling networks are located in larger cities with high cooling demand but due to global warming, the need for cooling networks will increase.

Cooling plant (29 MW_{th}), 11 projects

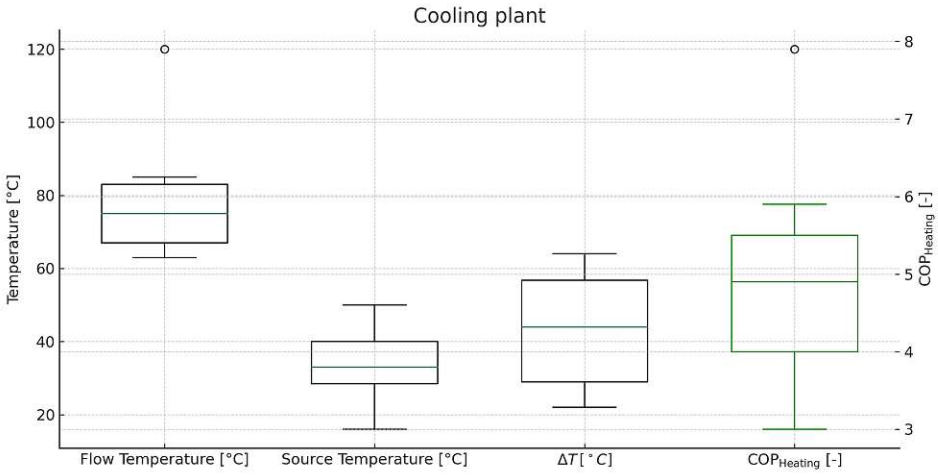

Figure 4.17: Cooling plant temperatures and $COP_{Heating}$

The source temperature of cooling plants ranges from 10°C - 44°C with a median $COP_{Heating}$ of 4.9 (fig. 4.17). Apart from the use in DH systems, LSHP can also be implemented for use in industrial processes that require heating and cooling at the same time, for example in dairy production (Ahrens et al., 2021).

Other heat sources (141 MW_{th}), 18 projects

Due to the small sample size, the following heat sources have been grouped into a single category (fig. 4.18). They are included in the database, but will not be investigated further in this work.

- Return flow from heat network (12 MW_{th}, 2 projects)
- Thermal spring (4 MW_{th}, 3 projects)
- HVDC converter station (3 MW_{th}, 1 project)
- Concentrated solar thermal (1 MW_{th}, 1 project)
- Metro system (1 MW_{th}, 1 project)
- Thermal energy storage (37 MW_{th}, 4 projects)
- Unknown (78 MW_{th}, 6 projects)

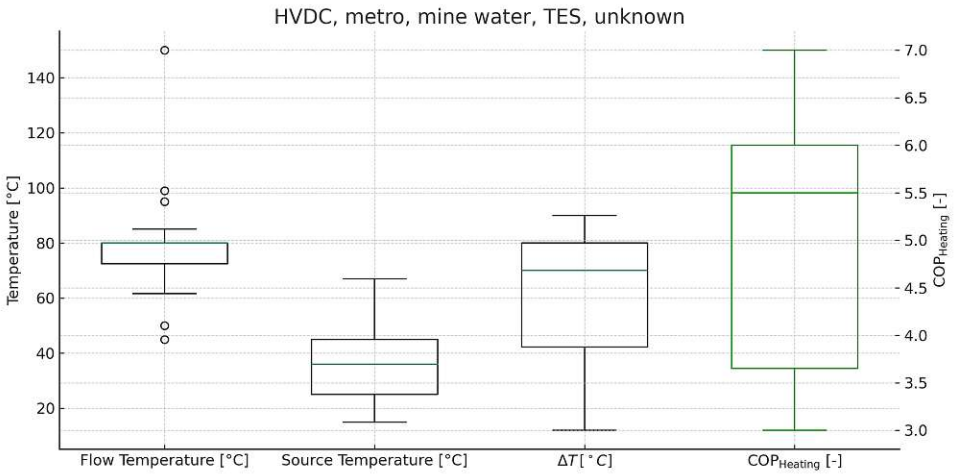

Figure 4.18: Other heat source temperatures and $COP_{Heating}$

4.2 Technical and economic data

As a summary of the previous chapter, the most relevant average technical (table 1) and economic information (table 2) is presented here. The tables are found in the appendix. The following fig. 4.19 shows the most important average technical data for each heat source, featuring the average temperatures, COP and the average heating capacity per project. It shows average heating capacities ranging from 3 MW (Cooling plant) to 28 MW (River water) and average COP ranging from 3.2 (Ambient air) to 5.5 (Industrial process heat recovery).

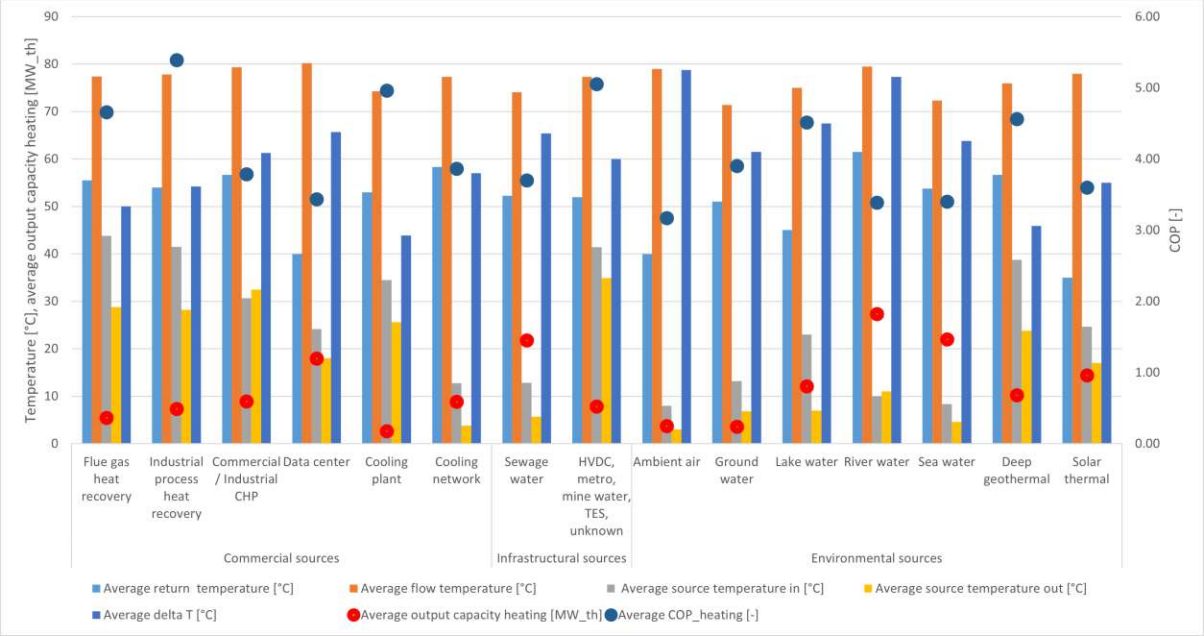

Figure 4.19: Average technical data of large-scale heat pumps

In the following fig. 4.20, the average capital cost, the annual operation hours and the average annual energy savings are shown for each heat source. Even though there is not much data available for these categories, it can be seen that LSHP feature high full load hours over 5000h/year and considerable annual energy savings of up to 101 GWh. Additionally, the high difference in capital cost of deep geothermal compared to the other heat sources is also present here (compare fig. 3.5).

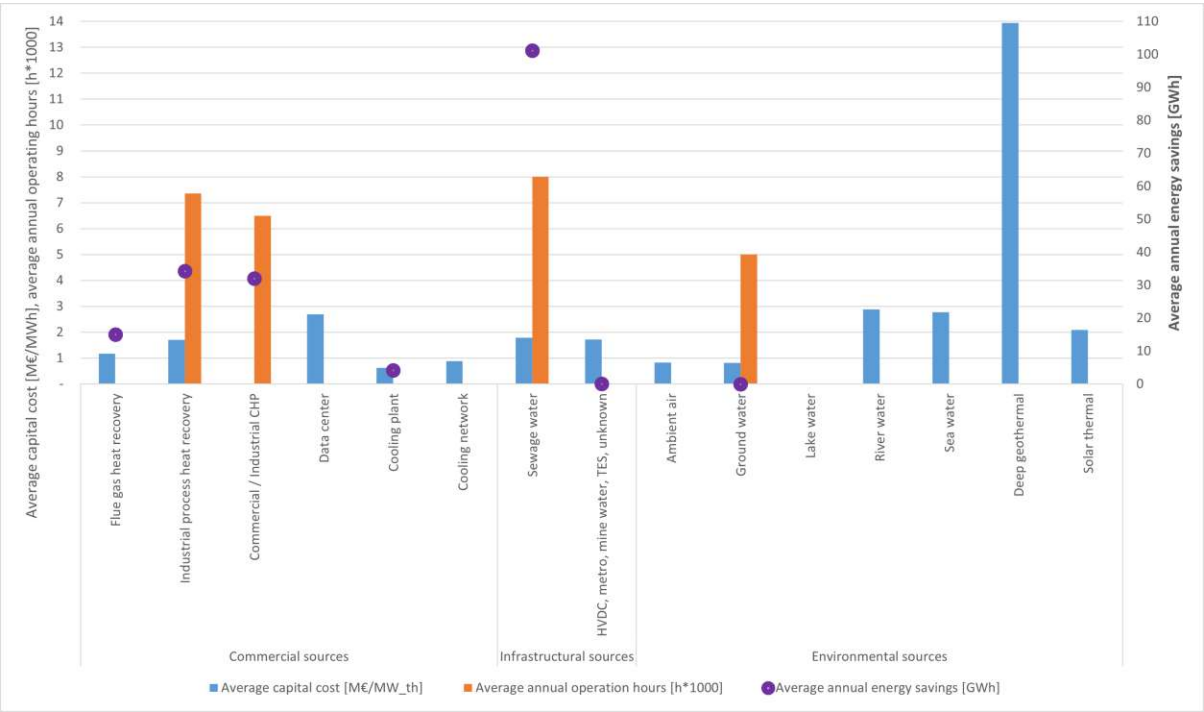

Figure 4.20: Average economic data of large-scale heat pumps

4.3 Other visualizations

In this section, other useful background information from the database is presented. The number of projects, which is 315 (see section 3.1.1) is used in the following graphs as a reference.

Active large-scale heat pump installations

Over 90% (291 projects) of the heat pumps investigated are still operating today, while 24 projects are decommissioned (fig. 4.21).

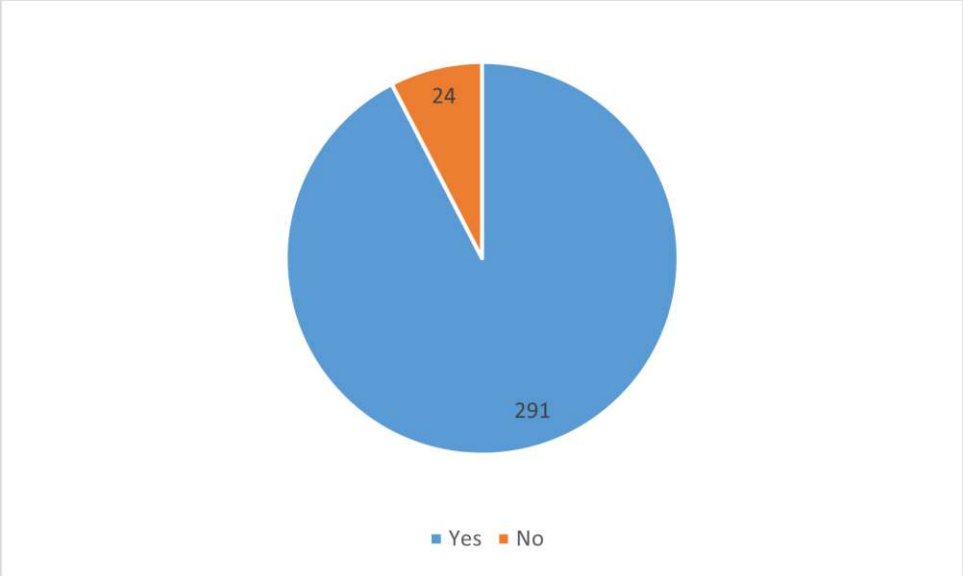

Figure 4.21: Active large-scale heat pump installations

Technology type

Compression heat pumps make up the majority of all LSHP, while absorption or hybrid systems are not well established yet (fig. 4.22).

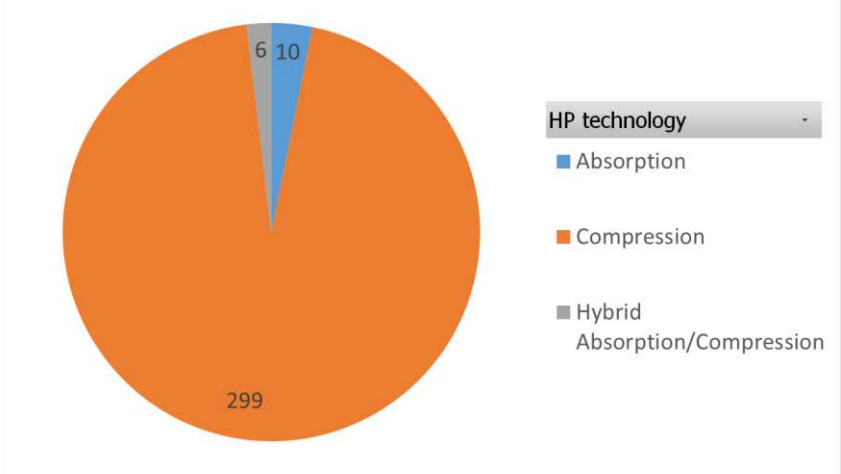

Figure 4.22: Large-scale heat pump technology

Refrigerants

Refrigerants are classified into natural, hydrofluorolefin and hydrofluorocarbon (Nielsen et al., 2018), where each refrigerant has an individual R-number. According to Nielsen et al. (2018), the optimal refrigerant relies on the following factors: the thermophysical properties, toxicity, flammability, compatibility with materials, price, impact on the environment and legal restrictions. Certain hydrofluorocarbon refrigerants such as R-134a and R-12 have a high **G**lobal **W**arming **P**otential (GWP) of over 150, meaning that they contribute over 150 times as much as CO_2 to global warming. For this reason, they are gradually phased out. In normal operation, the GWP of the refrigerant is no issue, but Aguilera et al. (2022) shows that refrigerant leakage is the second most common fault in LSHP after fouling. These are also among the most widely used refrigerants for LSHP, as seen in fig. 4.23. Therefore, there is a need to replace them and compare the economic viability of R-134a to other refrigerants with low GWP, which is done in section 3.4.1.

Newly emerging refrigerants, such as R-744 (CO_2) for example have an annual COP that is 27,5% higher than R-134a, while having a 34,8% lower lifetime carbon footprint (Fabris et al., 2024). The majority of LSHP use 5 different refrigerants, with the most prominent natural refrigerant being ammonia (R-717), while $H_2O/LiBr$ is used only in absorption heat pumps. The most prominent recent hydrofluorolefin refrigerant is R1234ze, which has a GWP of less than 1 and good thermodynamic properties. In 148 projects, the used refrigerant could not be identified.

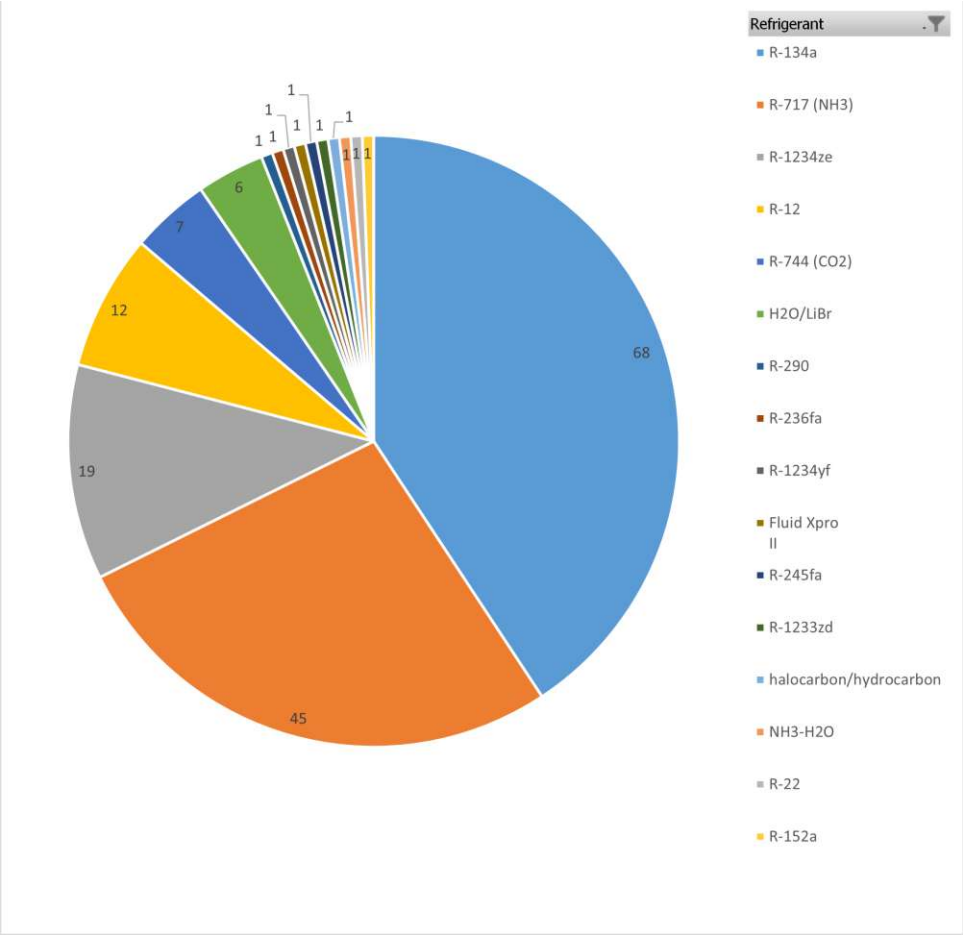

Figure 4.23: Refrigerants used for large-scale heat pumps

Cooling capability

The fig. 4.24 shows that 62 projects have cooling capability while 91 do not, and for 162 projects it is unknown.

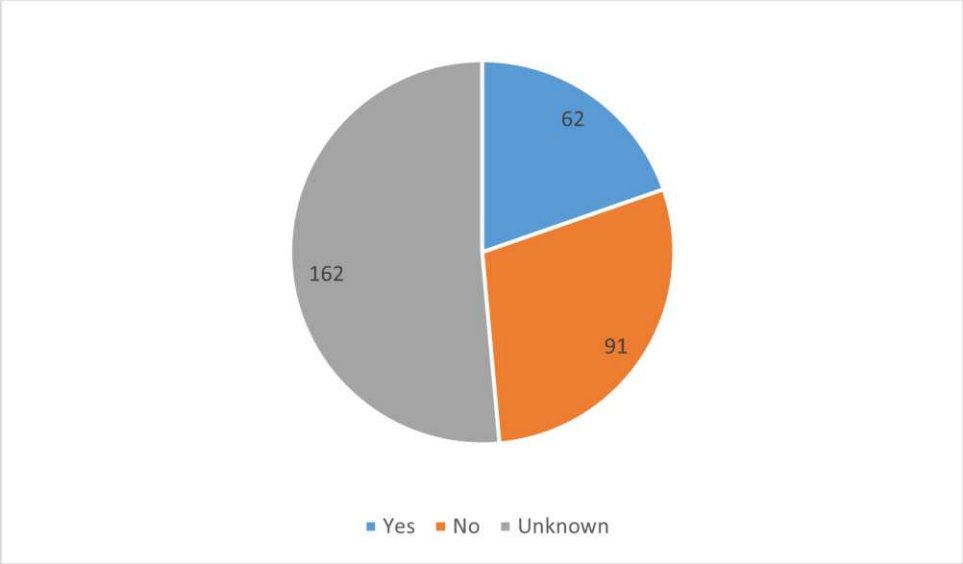

Figure 4.24: Cooling capability of large-scale heat pumps

Connection to district heating

The fig. 4.25 shows that 270 LSHP are connected to district heating, while the remaining 44 are used for other large-scale local heat production, which is shown in fig. 4.26.

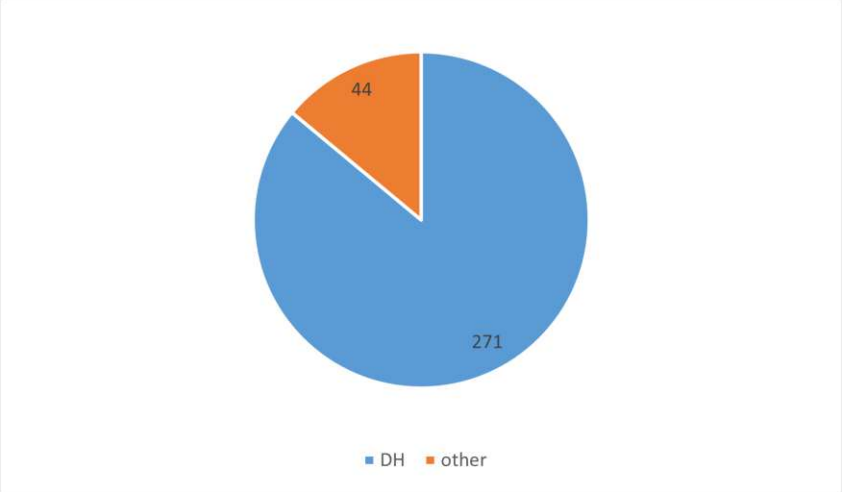

Figure 4.25: Large-scale heat pump connection to district heating

Other forms of utilization

The following fig. 4.26 shows the various forms of local utilization for LSHP, ranging from heating large buildings to various forms of industrial processes.

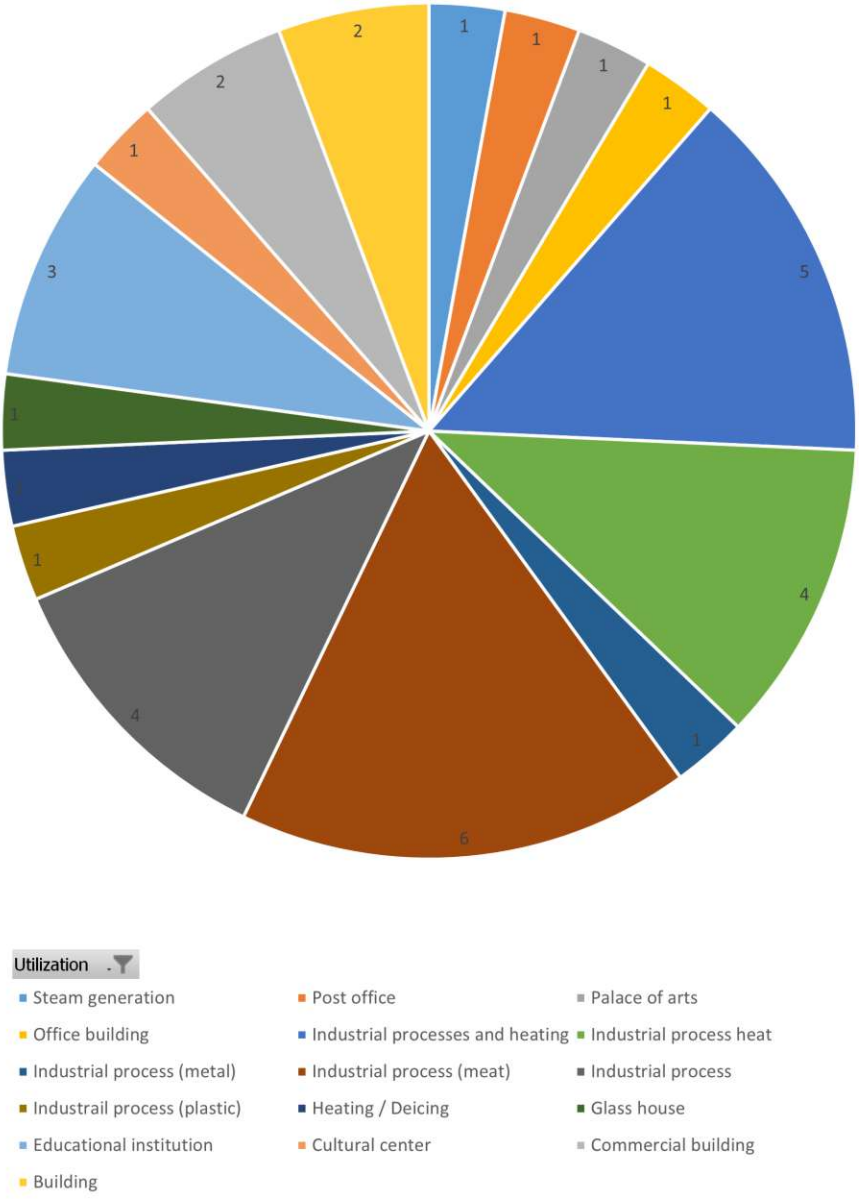

Figure 4.26: Other forms of large-scale heat pump utilization

Large-scale heat pump manufacturers

The market for LSHP has a high level of competitiveness, with 18 heat pump manufacturers identified. Out of these, the manufacturers Friotherm and Trane are the most prominent ones, making up nearly half of all manufacturers identified, as seen in fig. 4.27.

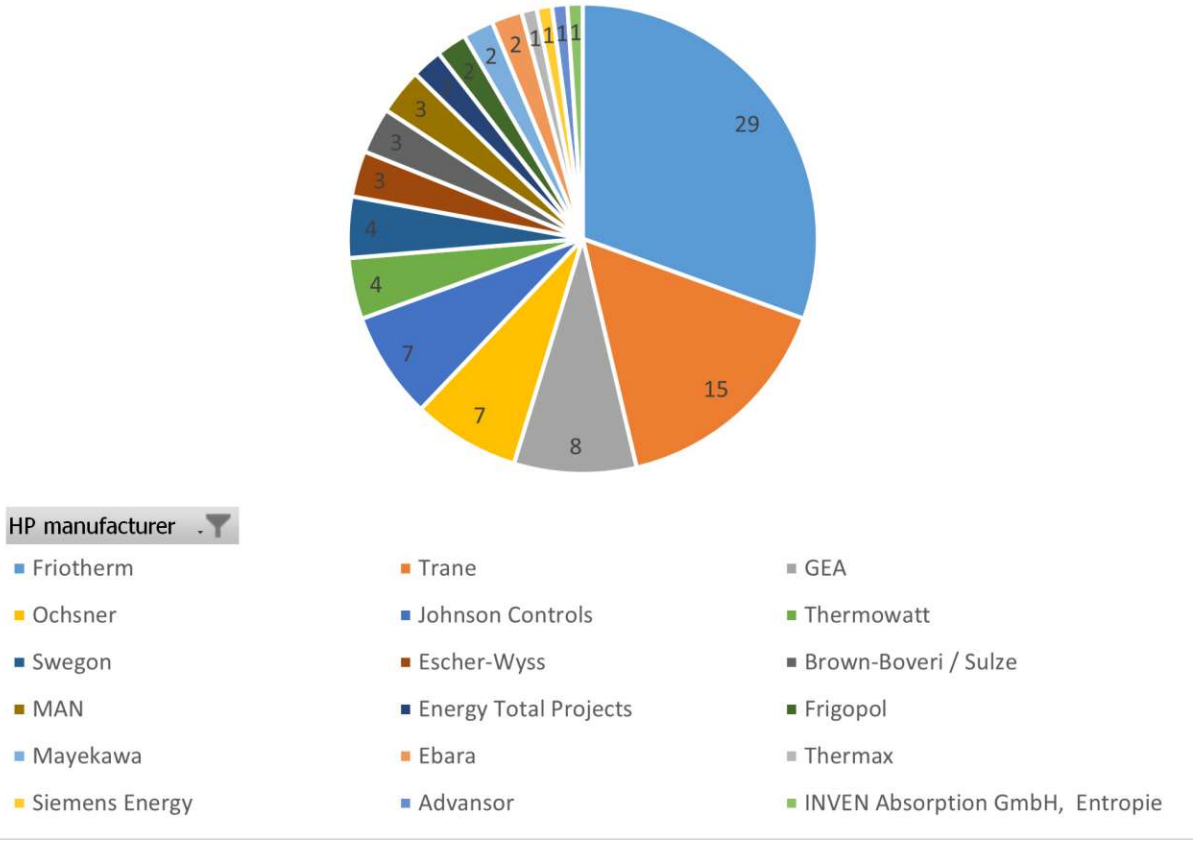

Figure 4.27: Large-scale heat pump manufacturers

5 Modeling results

In this section, the modeling results are presented. First, key parameters like levelized cost of heat, full load hours and installed capacities are compared across all scenarios. The resulting total heat generation is then compared over all scenarios section 5.4, then by climate condition in section 5.5 and portfolio in section 5.6. Here, the thermal generation mix over the year for selected cases is also presented. The efficiencies of LSHP are compared in section 5.7. Finally, the results are reviewed critically based on the assumptions made in chapter 3.

The following graphs give an overview of the resulting data points of all 54 simulation runs. The 3 portfolios are arranged from top to bottom, while the 3 refrigerants (sub-scenario 1, section 3.4.1) are arranged from left to right. This results in 9 diagrams in total. The size of the city and heat pump units (sub-scenario 2, section 3.4.2) is marked by different colors: Blue is used for a heat pump unit size of 1 MW with a small total heat demand. This case is called "1 MW". Orange is used for the case with the maximal heat pump unit size, utilizing economies of scale effects and a large total heat demand. This case is called "max". The climate condition (sub-scenario 3, section 3.4.3) is marked by different shapes of the data point, with a circle for the central European climate, a square for the northern European climate, and a triangle for the southern European climate. When referring to a specific case, it is done in the order portfolio,refrigerant,size,climate. For better visibility, the data is also presented with box plots in addition to the data point visualization.

5.1 Levelized cost of heat

First, the average levelized cost of heat (LCOH) are discussed. LCOH are a measure of how much one unit of heat costs over the lifetime of the heating system. In fig. 5.1, it is shown that there is a decrease in LCOH in the max case compared to the 1 MW case. This is expected, as the specific costs per MW decrease with larger heat pump sizes (see fig. 3.10). The case with the lowest overall LCOH is portfolio2,R134a,max,south with 44.3 €/MWh. The highest overall LCOH are found at the worst-case scenario for LSHP in portfolio3,R600a,1MW,north with 59.6 €/MWh. This is the only case where no LSHP are installed in the 1MW and max case, meaning also no economies of scale effects for LSHP that would make the max portfolio cheaper. Another interesting result is that the south case is always the cheapest. Reasons for this are the higher efficiencies of LSHP in a southern climate as well as the high share of total demand covered in the summer (see fig. 3.11). Likewise, the northern profile is the most expensive due to the low efficiencies and temperatures. Additionally, it can be seen that portfolio 2 has the lowest overall spread in LCOH concerning the climate. This may be due to the high amount of industrial process heat installed, which temperature is independent of the climate.

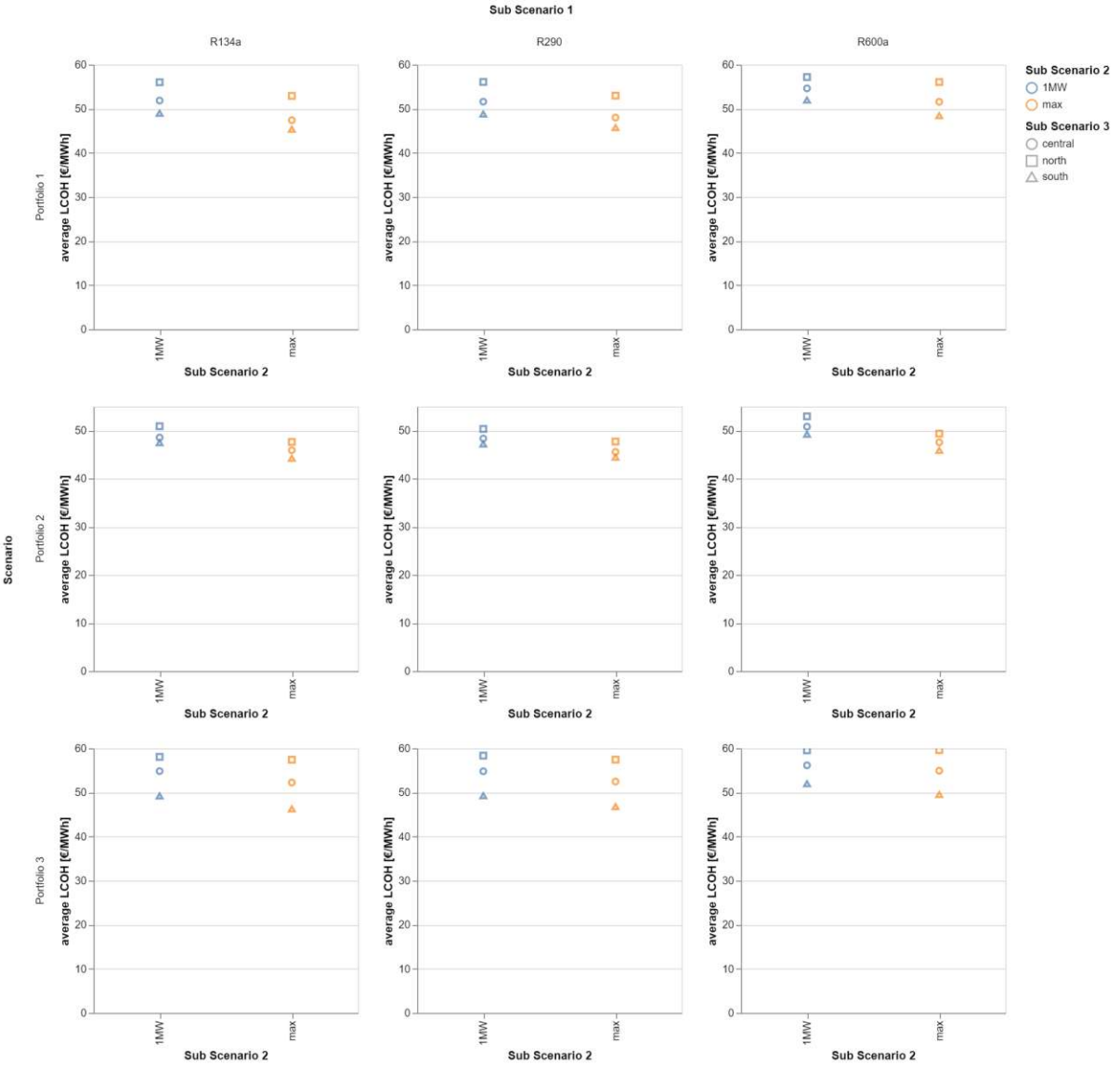

Figure 5.1: Average levelized cost of heat of the portfolios [€/MWh]

The portfolios using the refrigerants R134a and R290 have the lowest LCOH, while R600a has a significantly higher cost. R290 is competitive to R134a due to its lower specific TCI (see fig. 3.10). However, R134a has better thermodynamic properties, such as a higher nominal COP (see table 3.8), although having the lowest source temperature sensitivity. In contrast, R600a has the highest source temperature sensitivity (see table 3.10), meaning R600a would be more economical for higher source temperatures. The lower maximum COP per refrigerant can be seen in fig. 5.26. In the following fig. 5.2, the LCOH are broken down to the specific heat technology level.

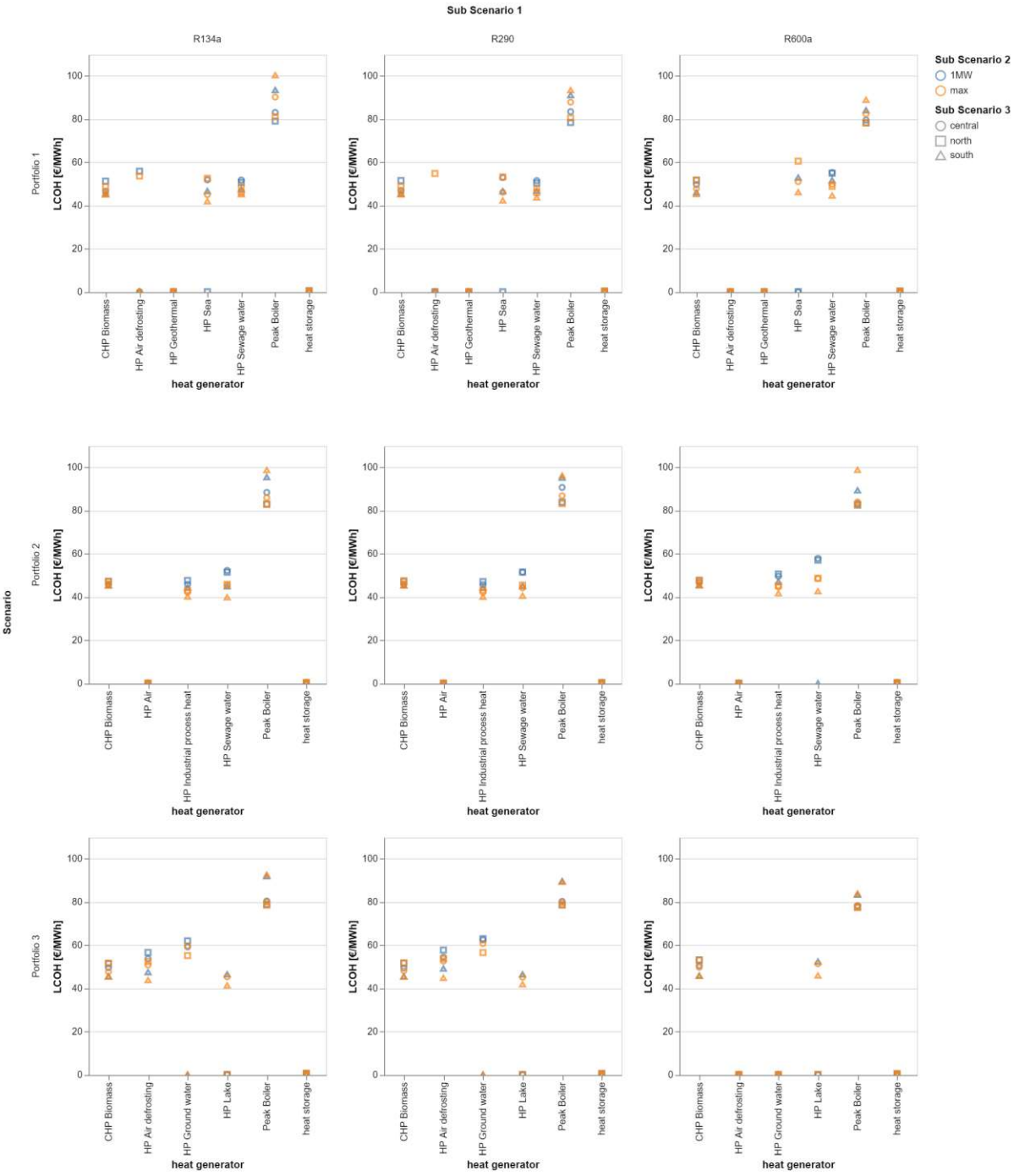

Figure 5.2: Levelized cost of heat [€/MWh] of each heat generator

For technologies with no installed capacity, LCOH are displayed as 0. The heat storage features very low LCOH ranging from 0.20 €/MWh (portfolio1,R600a,max,central) to 0.64 €/MWh (portfolio3,R134a,max,north). This is because the total annualized costs of the heat storage consist of just the annualized investment and operational cost, but the cost for actual heat generation is accounted to the heat generator that provides the energy. As it is designed as a daily heat storage, it has a loading and unloading pattern with a high frequency (see section 5.5), leading to a large amount of heat unloaded. These two factors lead to low LCOH of heat, which is annual cost divided by annual heat generation. For LSHP, the LCOH are reduced by 2 - 5 €/MWh in the case with maximal unit size compared to 1MW unit size, depending on

the heat source, refrigerant and portfolio. Further, the heat pump options are always cheaper than the peak boiler: LCOH for LSHP are in a range of 39.75 €/MWh (Sewage water: portfolio2,R134a,max,south) to 62.91 €/MWh (Ground water: portfolio3,R290,1MW,north), while the LCOH of the peak boiler are in a range of 77.4 €/MWh (portfolio3,R600a,max,north) to 100.24 €/MWh (portfolio1,R134a,max,south). The biomass CHP ranges from 44.99 €/MWh (portfolio1,R134a,max,south) to 53.05 €/MWh (portfolio3,R600a,max,north), making it competitive with LSHP.

For a clearer visualization, the LCOH of all heat generators over all portfolios together with the number of installations n are displayed in the following fig. 5.3:

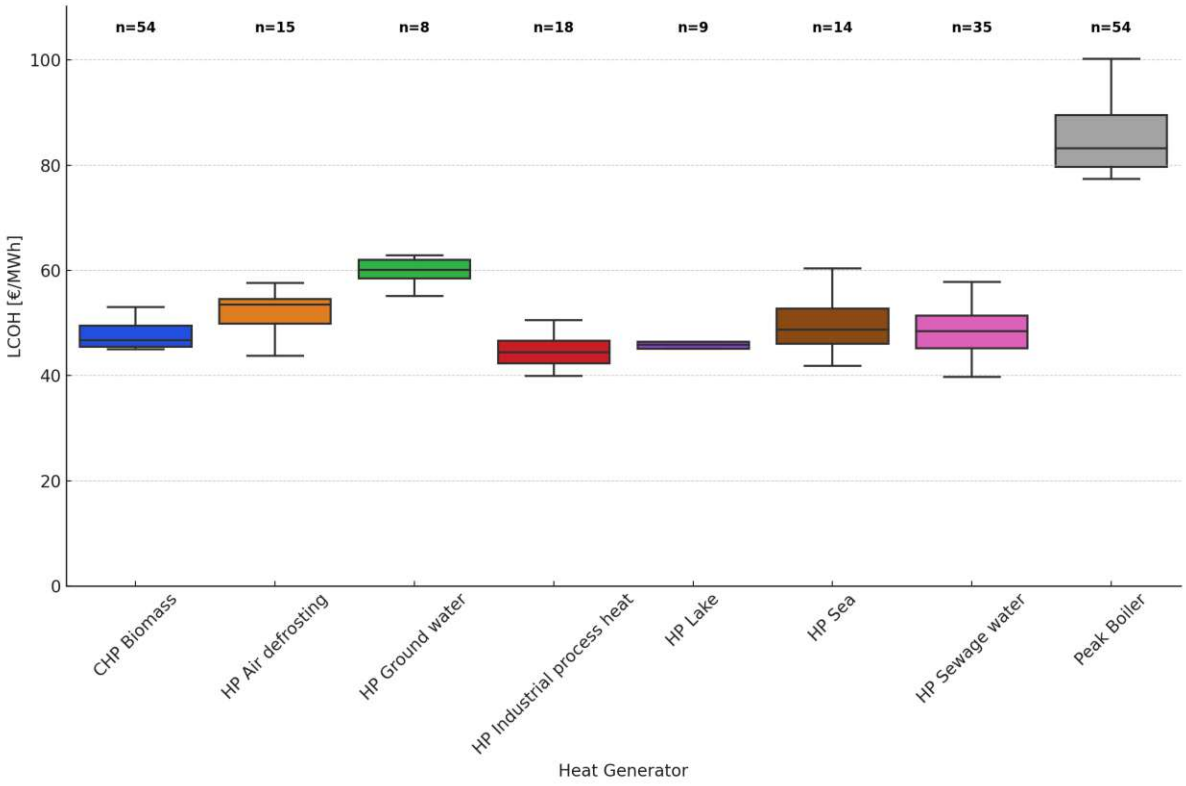

Figure 5.3: Levelized cost of heat [€/MWh] for LSHP using different heat sources

It shows that LSHP using industrial process heat have the lowest median LCOH with 44 €/MWh and the ones using groundwater have the highest median LCOH with 60 €/MWh. The range of LCOH of the peak boiler is noticeable higher than the other generators. This can be explained by the large spread in installed capacities, seen in fig. 5.7 and fig. 5.8.

5.2 Full load hours

A reason for the high LCOH of the peak boiler lies in the low full load hours, as it is most beneficial to be only used for heat demand peaks in wintertime. Especially in the southern climate, the full load hours of the peak boiler are in a range of 240h to 625h across all portfolios.

LSHP feature full load hours ranging from 2121h (Lake Water: portfolio3,R600a,north) to 5356h (Sea water: portfolio1,R600a,south) making them optimal intermediate load generators.

Ambient heat sources like sea and lake water heat pumps feature higher full load hours in southern climate, as they can be utilized more often in these conditions. In portfolio 1, the sewage water heat pump is favored in the northern climate, as its temperatures are higher in winter compared to sea water, whereas sea water is favored in a southern climate. This can be seen in more detail in section 5.5. In all portfolios, the biomass CHP is used as a baseload generator with high full load hours ranging from 5816h (portfolio1,R134a,1MW,north) to 6724h (portfolio1,R600a,1MW,south).

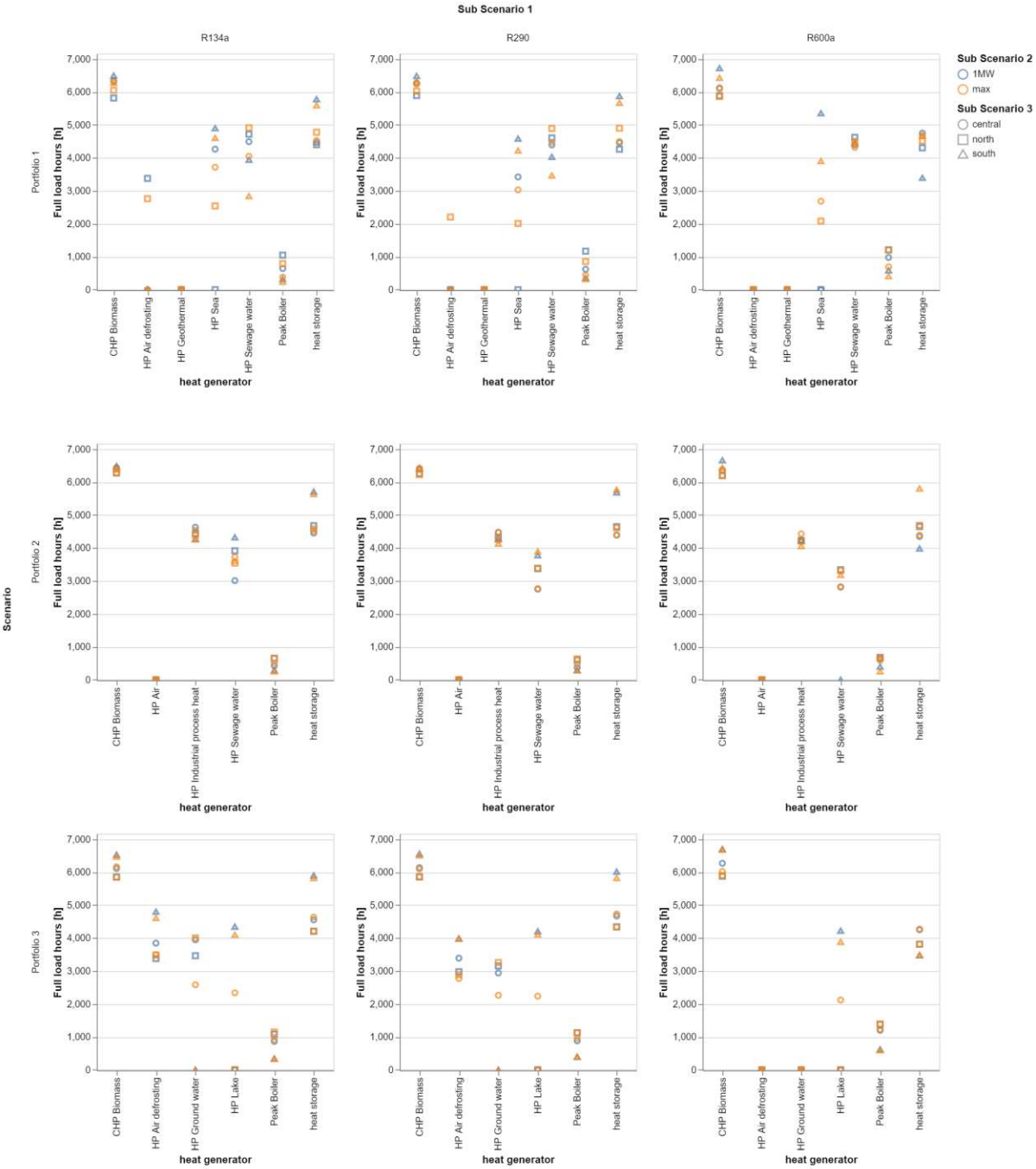

Figure 5.4: Full load hours [h]

In fig. 5.5, it is clear to see that kinds of LSHP are all in the same range of full load hours of 2000h to 5500h and that they have a higher spread in full load hours with the exception of

industrial process heat. This is because heat generation is independent from climate and also because the installed capacities are the same in every scenario.

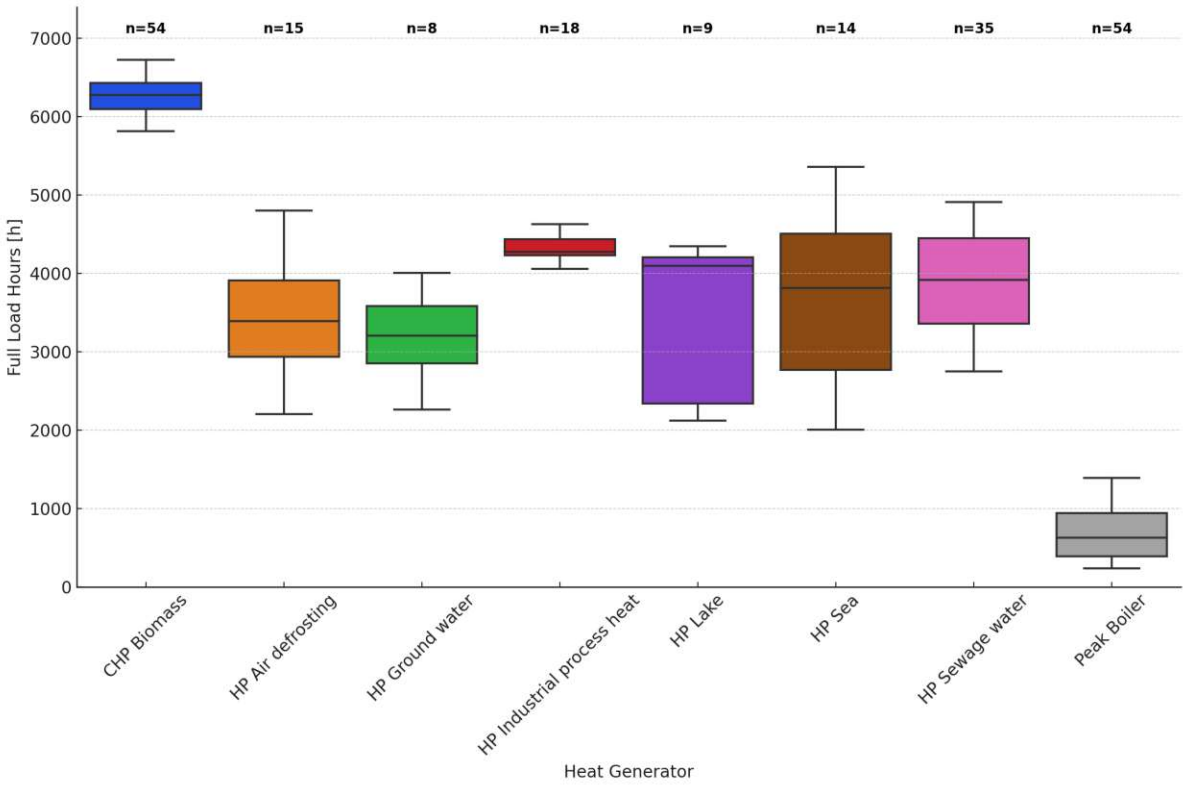

Figure 5.5: Full load hours [h]

5.3 Installed capacities

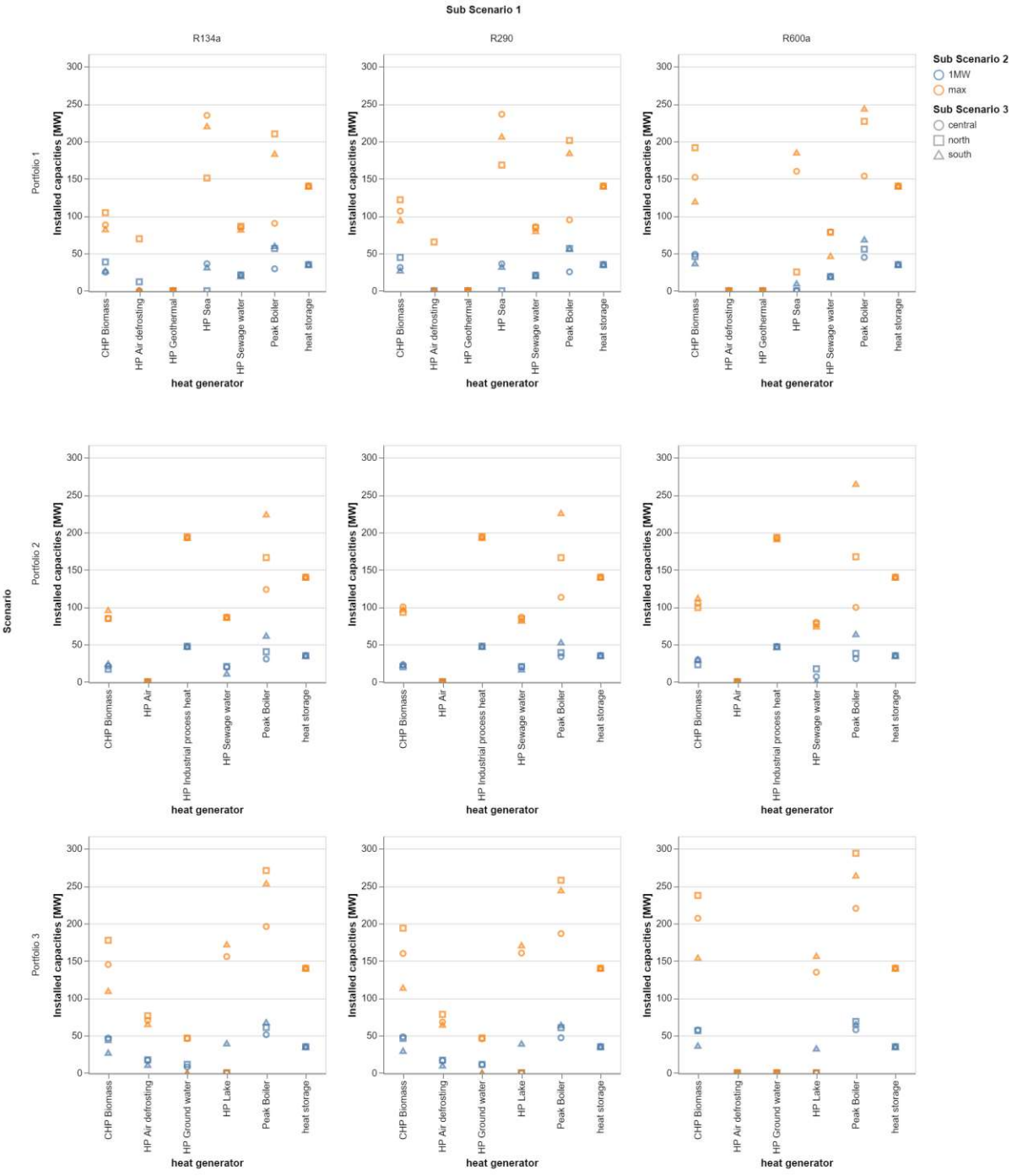

Figure 5.6: Installed capacities [MW]

For all portfolios, it can be seen that deep geothermal and air source heat pumps without defrosting are the only heat sources that are not installed in any case. This does not necessarily mean they are not economic at all, but rather not cost-optimal in the specific case. Reasons for this are the high TCI of deep geothermal heat pumps as well as the missing ability to provide heat in the wintertime when heat demand is highest for air-source heat pumps without defrosting. This also hinders lake and sea water heat pumps from being installed in northern climate, which can be seen in more detail in section 5.5.

When air-source heat pumps have defrosting, they are most viable in a northern climate, as seen in portfolios 1 and 3. This is due to their ability to heat at lower temperatures compared to LSHP using other heat sources (see fig. 3.9). This comparison also shows that whether the same heat pump is installed or not, depends on the competition form other heat generators. Because industrial process heat has a very high competitiveness due to its low TCI and a constantly high source temperature of 35 °C, the maximal possible capacity of 200 MW is always installed in portfolio 2. An apparent difference between the portfolios is that the peak boiler has the highest installed capacity in portfolios 2 and 3, while for portfolio 1, the sea water heat pump is favored more. This is, however highly dependent on the refrigerant. As stated before, R600a has the overall worst economic case, leading to a reduced or no installed capacity compared to the other refrigerants.

For the box plot visualisation the max and 1MW case are displayed separately because the maximal installed capacity differs by a factor of 4 (compare table 3.13) between the sub-scenarios 1MW and max, leading to $n = 27$ cases in total.

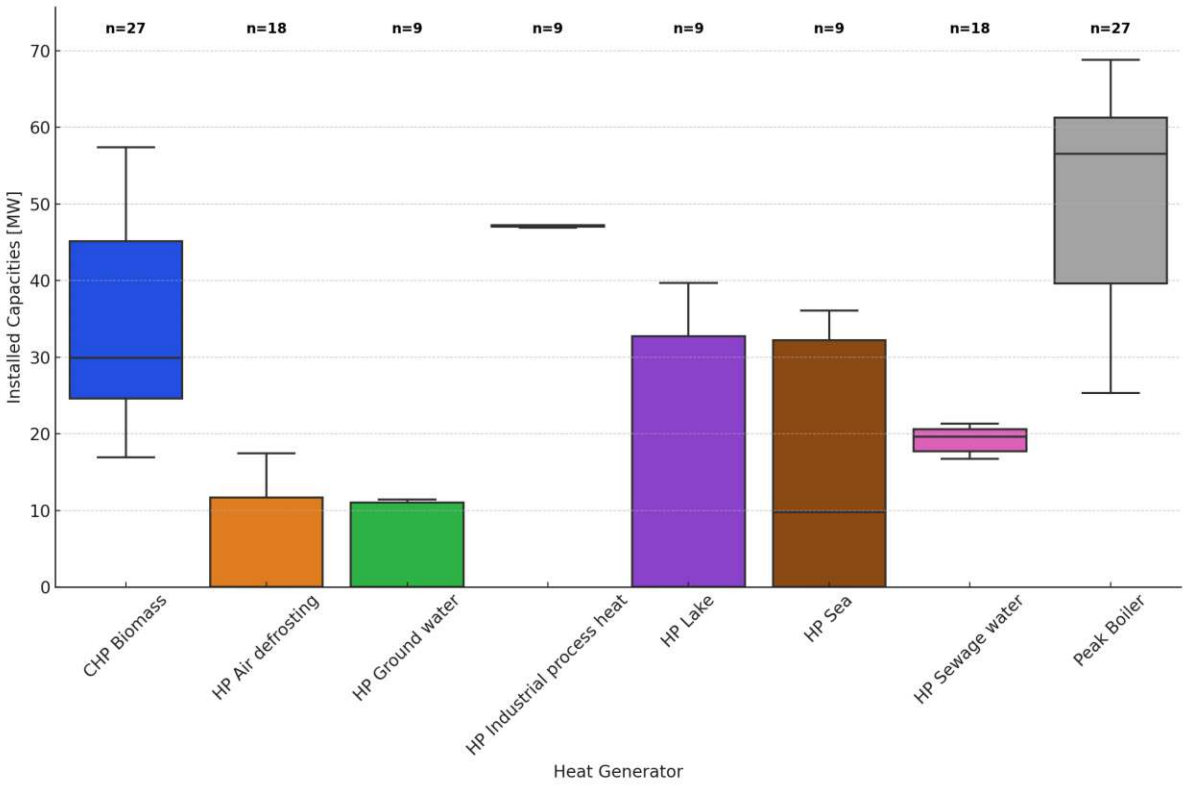

Figure 5.7: Installed capacities (sub-scenario: 1MW)

When comparing fig. 5.7 to fig. 5.8, the sea water heat pump is installed in all scenarios in fig. 5.8 and not consistently installed in fig. 5.7. It shows that either a large or no sea water heat pump capacity is optimally installed, depending on economies of scale. Other than that, a different size of the heat pump units does not change the installed capacity significantly relative to the demand.

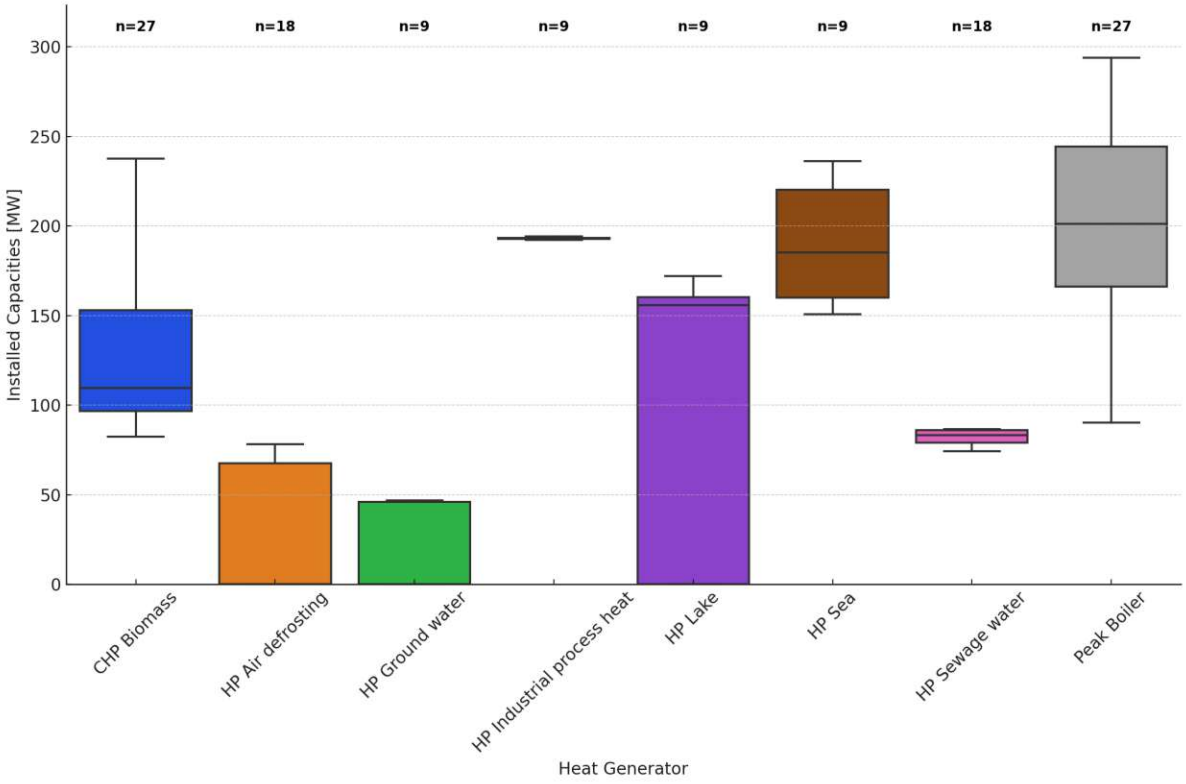

Figure 5.8: Installed capacities (sub-scenario: max)

5.4 Total Heat Generation

The total heat generation over the year results from full load hours and installed capacity and is therefore a key parameter for evaluating the performance of LSHP. The detailed results of total heat generation are presented in fig. 5.9. It highlights the before mentioned high total heat generation of LSHP using industrial process heat in portfolio 2. For ambient heat sources like sea and lake water heat pumps, it largely depends on the climate (section 5.5) and refrigerant (section 5.6). Due to their limited maximal installed capacity, air and groundwater heat pumps feature a lower share in the total heat generation.

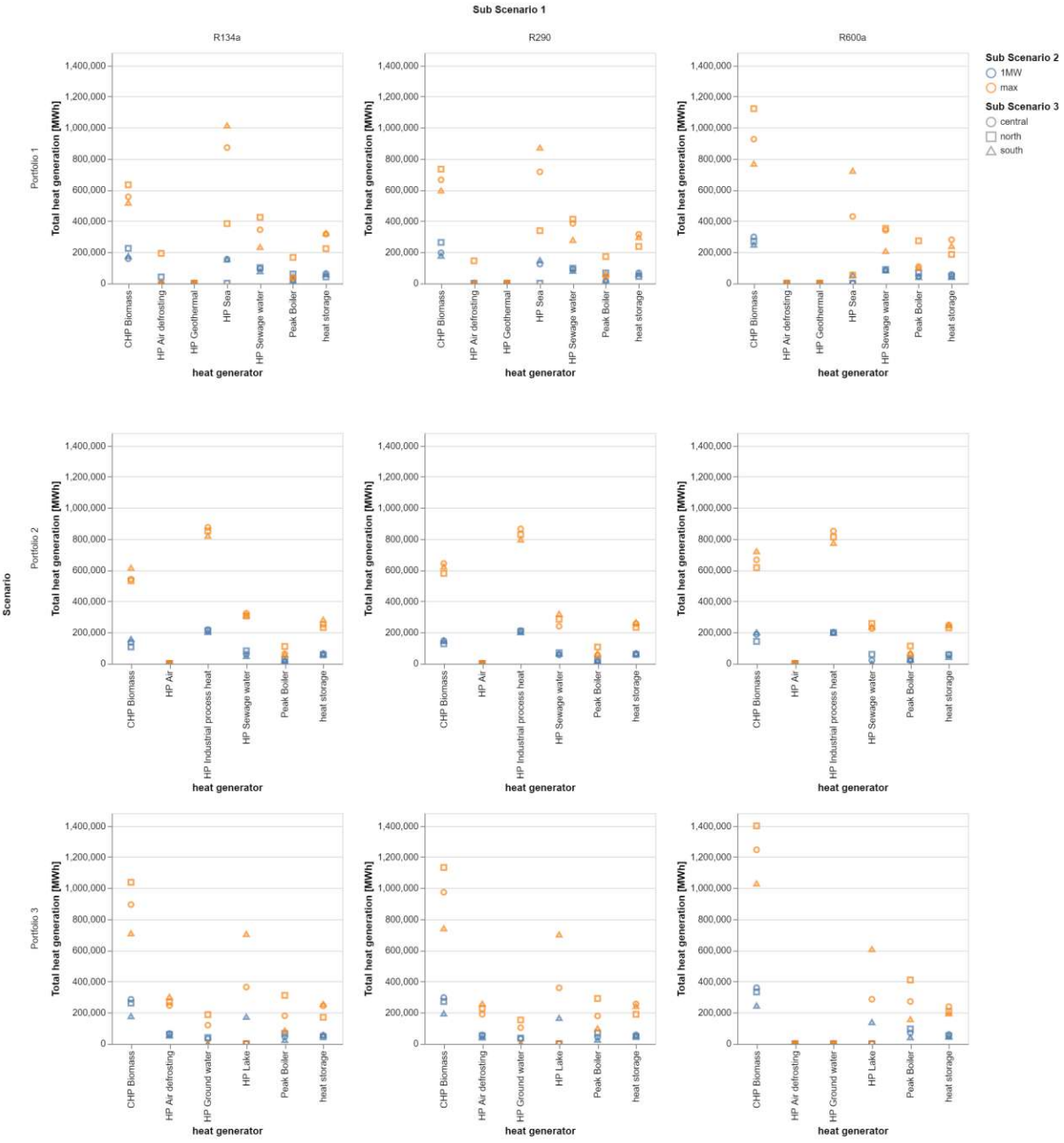

Figure 5.9: Total heat generation [MWh]

As it is a crucial parameter, the total heat generation is investigated further, specifically the share of each heat generator on the total heat generation and the thermal energy mix over the year for the refrigerant R290 in the max case. This is done because R290 is the most viable refrigerant option together with R134a (compare fig. 5.1), which is not allowed to be installed in the future. The max case is also more beneficial for LSHP due to lower investment costs.

In the following section 5.5, the influence of climate conditions on the total heat generation of all portfolios is compared first, together with the thermal energy mix over the year. Then, the variations on refrigerant, size and climate condition are compared for the individual portfolios in section 5.6.

5.5 Total Heat Generation by Climate

5.5.1 Northern Climate

In the northern climate (fig. 5.10), the heat demand can be covered by over 60% only in portfolio 2, where a large amount of industrial excess heat is available. For portfolio 1, there is a large difference in heat generation between the sub-scenario max for R290 and R600a, where over 50% is covered, and the sub-scenario 1MW, where only 20% of demand is covered by LSHP. For portfolio 3, demand can be covered by around 20% by air source heat pumps with defrosting and ground water heat pumps, except for the sub-scenario using R600a.

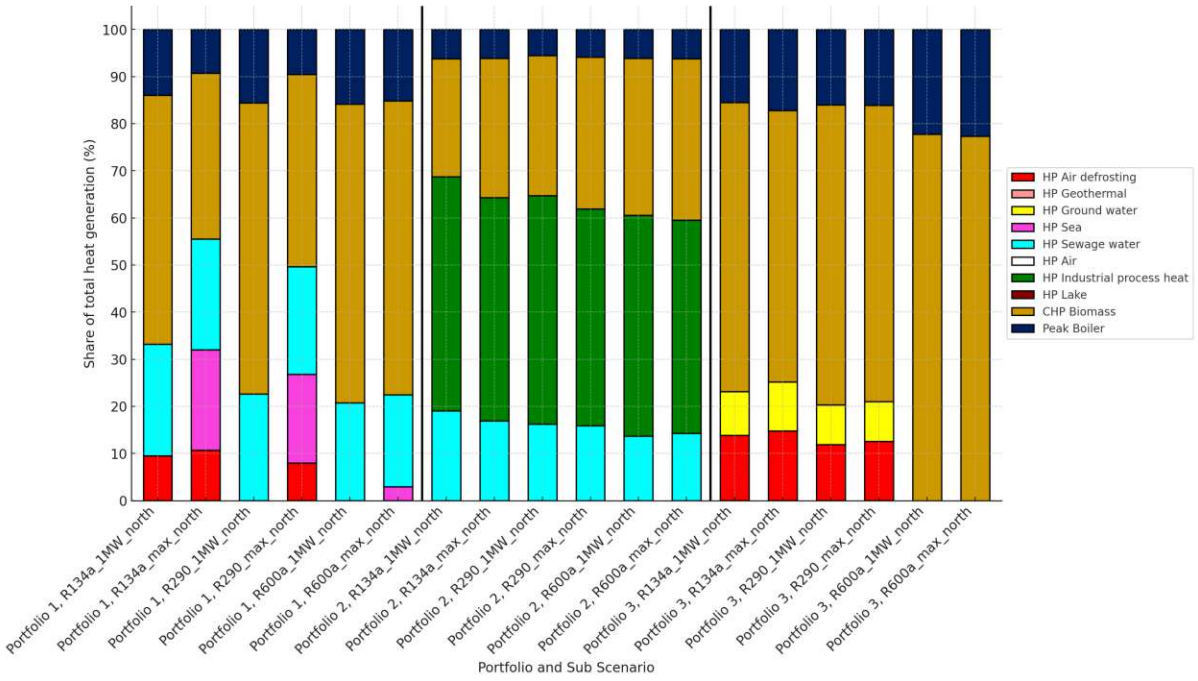

Figure 5.10: Northern climate condition

5.5.2 Thermal energy mix: Northern Climate

In portfolio 1 (fig. 5.11), the northern case is the only one where air source heat pumps are installed. This is due to their superior defrosting capabilities compared to other heat sources (see fig. 3.9). In summer, the heat storage is loaded with heat from CHP when electricity prices are high and it is unloaded in periods of low electricity prices. This is done on a daily basis, leading to a high number of cycles over the year. In winter, the heat storage is used to cover peak demands on a daily basis. Additionally, for a cost-optimal outcome, LSHP have to have a high number of cold-starts to make use of the varying electricity prices. This leads to an average number of cold-starts for LSHP over all scenarios of 687, meaning around 2 cold-starts per day. LSHP account for half of the total heat generation in this scenario.

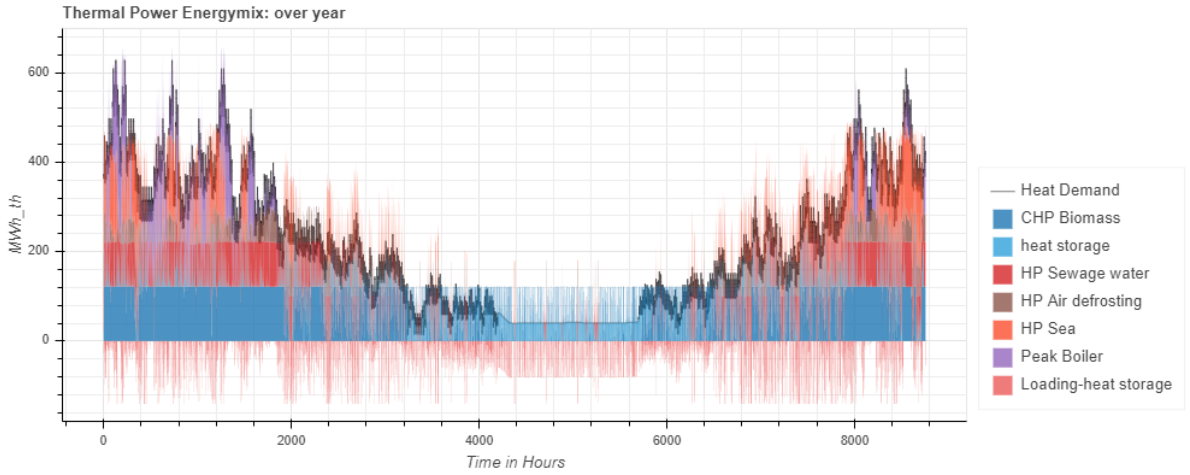

Figure 5.11: Thermal energy mix, portfolio 1,R290,max,north

In fig. 5.12, it can be clearly seen how LSHP using industrial process heat together with sewage water are able to cover most of the heat demand, leaving only peaks above 400 MW for the peak boiler and having less installed CHP capacity than portfolio 1.

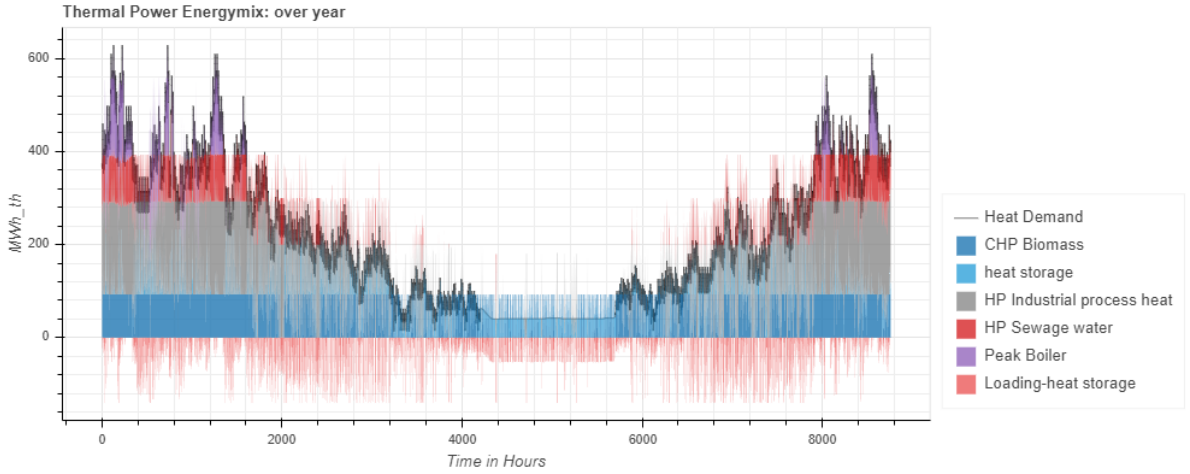

Figure 5.12: Thermal energy mix, portfolio 2,R290,max,north

Compared to the other portfolios, portfolio 3 (fig. 5.13) is the case with the least amount of LSHP capacity installed and a total heat demand covered of 20% (compare fig. 5.10). This is due to the limited maximal capacities for ground and air source heat pumps and the inability for lake water to be used in winter due to frosting issues in the northern climate (see fig. 3.15). This also leads to higher installed capacities for CHP biomass and peak boiler in comparison.

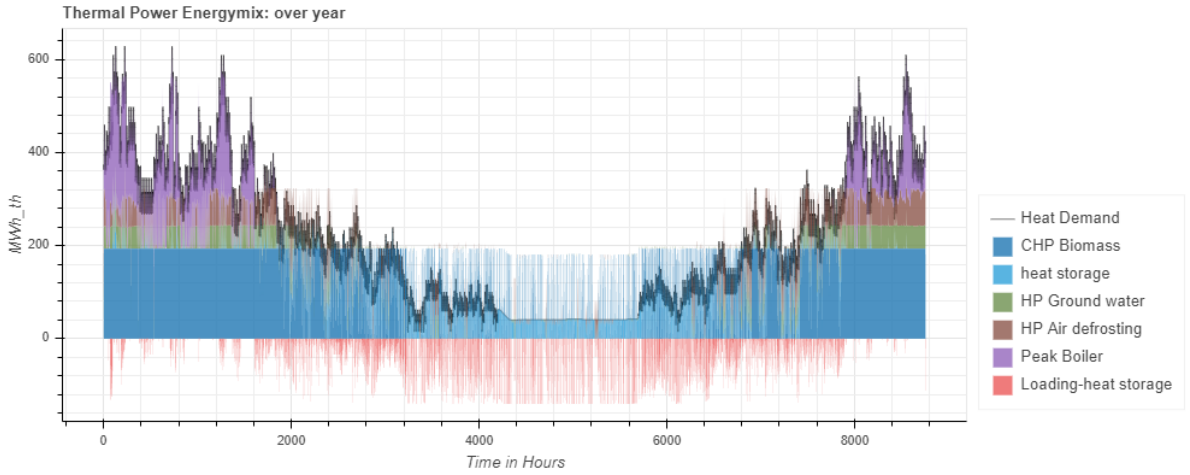

Figure 5.13: Thermal energy mix, portfolio 3,R290,max,north

5.5.3 Central Climate

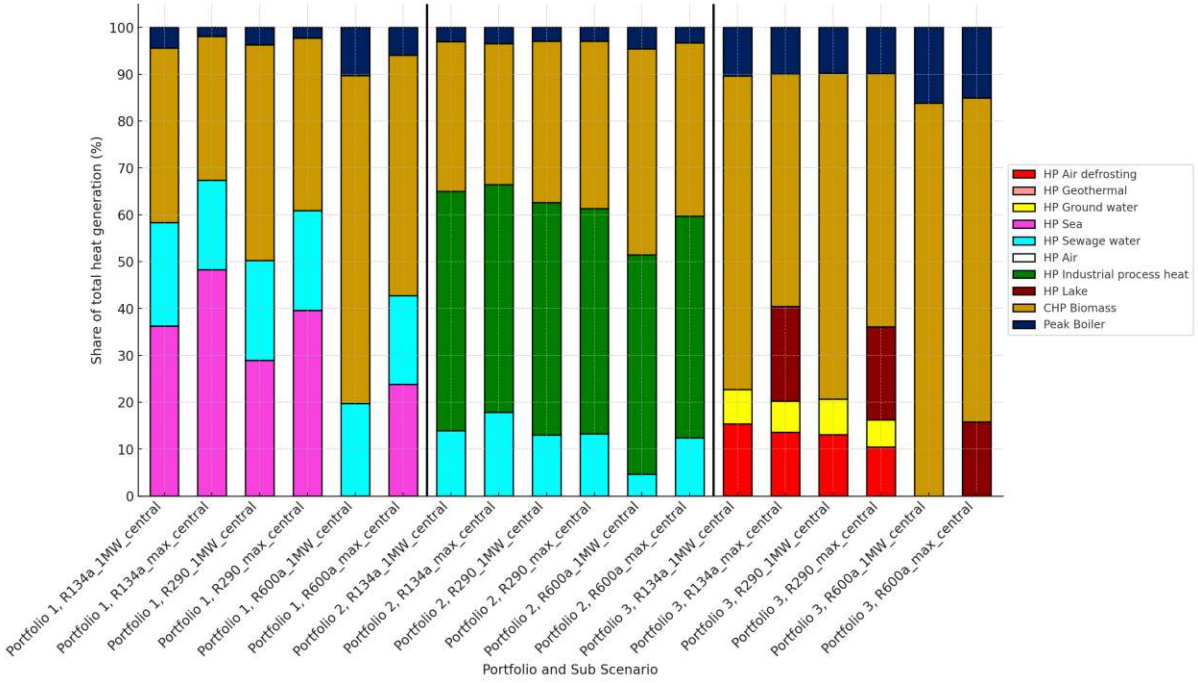

Figure 5.14: Central climate condition

In central climate (fig. 5.14), the ideal sea water capacities are increased significantly in portfolio 1, leading to the majority of the demand being covered by sea and sewage water heat pumps for R290 and R600a. While portfolio 2 stays in a similar range, the lake water heat pumps in portfolio 3 are a viable option to install for maximal heat pump size.

5.5.4 Thermal energy mix: Central Climate

The fig. 5.15 shows that the sea water heat pumps are now able to cover more peak demands, resulting in higher full load hours and a higher overall share of the demand covered. They are installed here instead of air source heat pumps, which are only installed in northern climate.

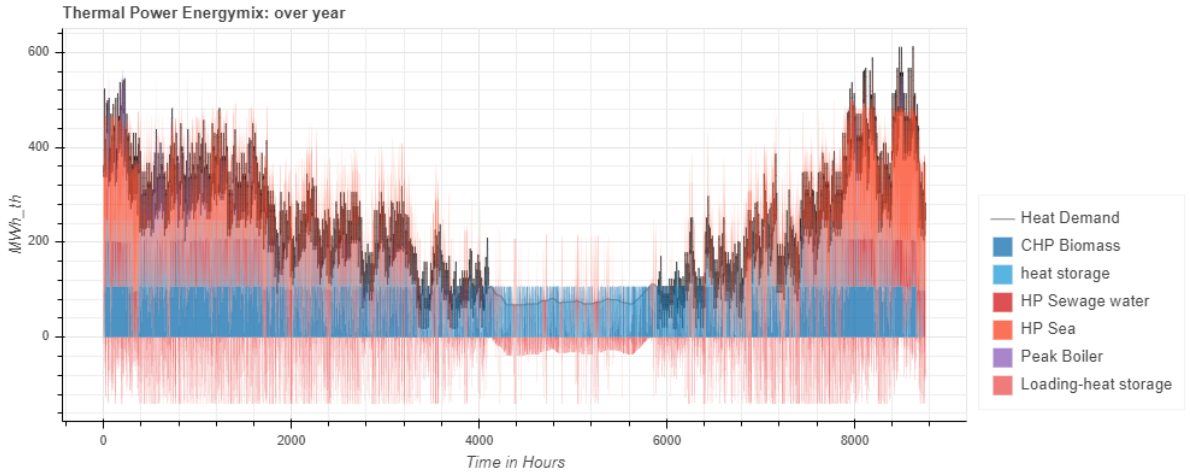

Figure 5.15: Thermal energy mix, portfolio 1,R290,max,central

While the share in total heat generation stays the same over all climate conditions for portfolio 2, fig. 5.16 shows that sewage water is above industrial process heat in the merit order, while it is below sea water in portfolio 1. This suggests that it is more viable than sea water but not as viable as industrial process heat.

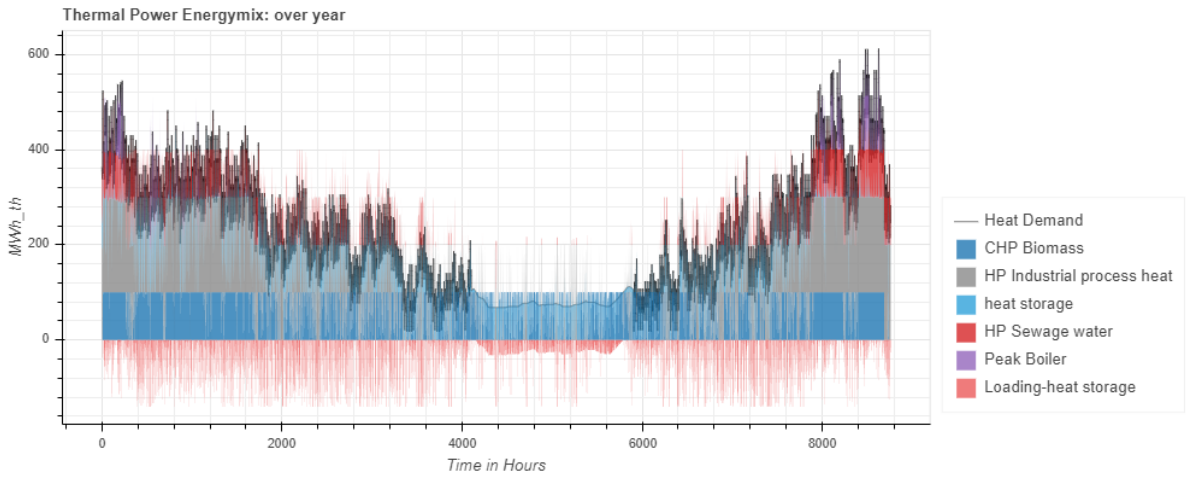

Figure 5.16: Thermal energy mix, portfolio 2,R290,max,central

For the central climate in portfolio 3 (fig. 5.17), lake water LSHP can now be used in winter time, which is not possible in the northern climate. While LSHP using air and ground water are used as mid-load generators, lake water can also cover demand peaks now, although there is still a need to install a peak boiler.

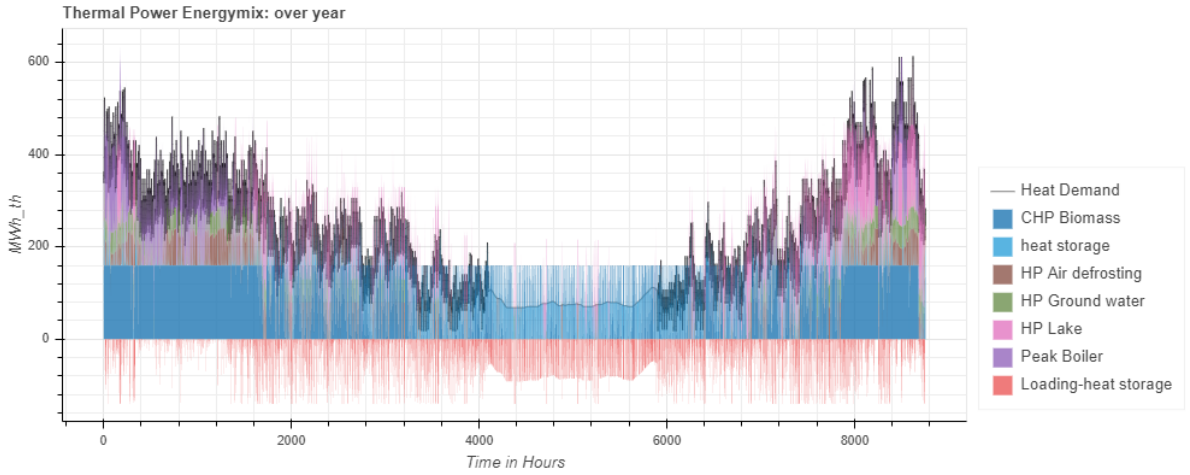

Figure 5.17: Thermal energy mix, portfolio 3,R290,max,central

5.5.5 Southern Climate

In southern climate (fig. 5.18), the share of LSHP on the total heat generation is much more balanced over all portfolios. When not using R600a, the total heat demand can be covered by more than 50% in all 3 portfolios, highlighting the importance of refrigerant choice.

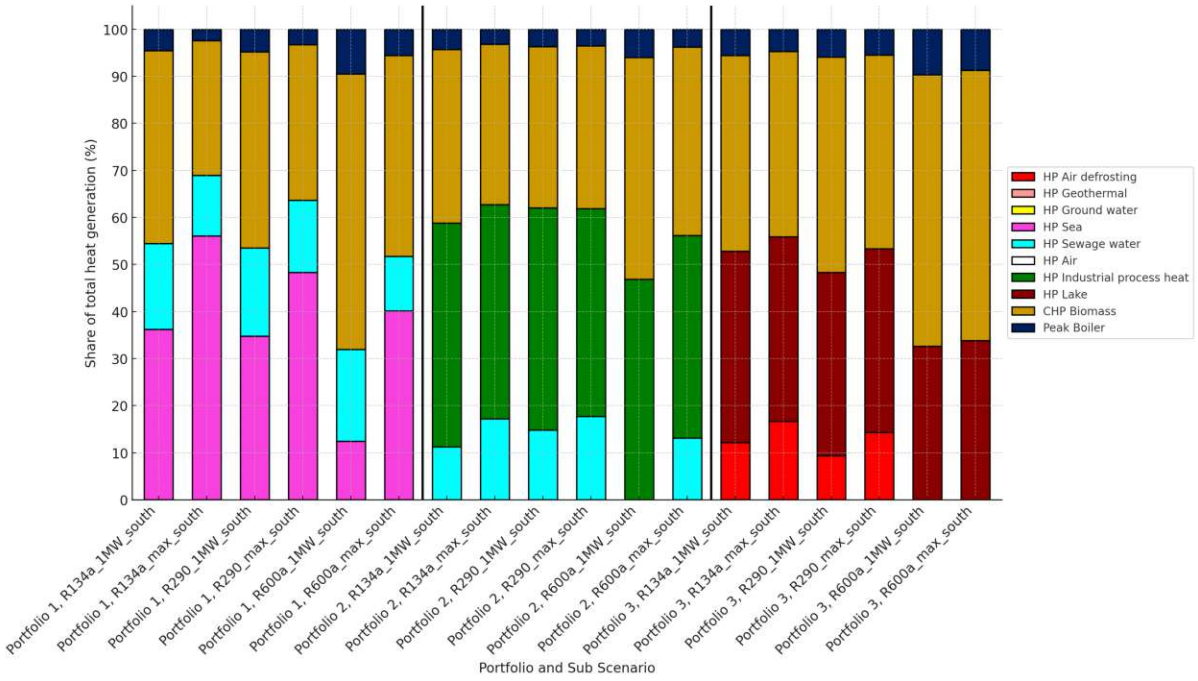

Figure 5.18: Southern climate condition

5.5.6 Thermal energy mix: Southern Climate

Whereas sewage water is the best heat source for LSHP in terms of merit order for northern and central climates, for southern climates it is sea water instead (fig. 5.19). However, the total thermal generation and full load hours in the central and southern scenarios are similar.

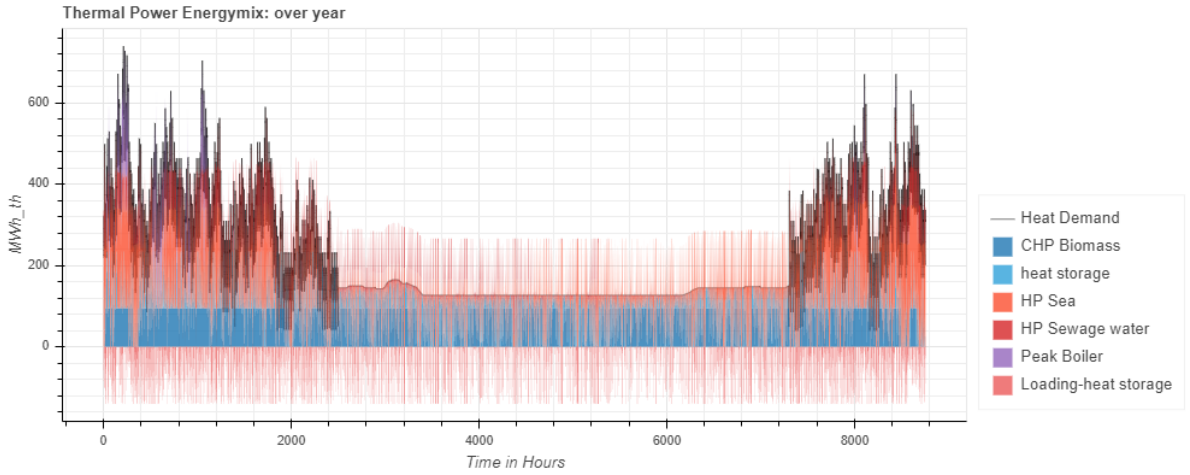

Figure 5.19: Thermal energy mix, portfolio 1, south

While the installed LSHP capacity stays the same for portfolio 2 in southern climate as well, it can be seen in fig. 5.20 that in this climate, the heat generation during summer is much more diverse than in the northern climate, where it only consists of biomass CHP and the heat storage. Here, all heat generators except for the peak boiler are used together with the heat storage for optimal dispatch.

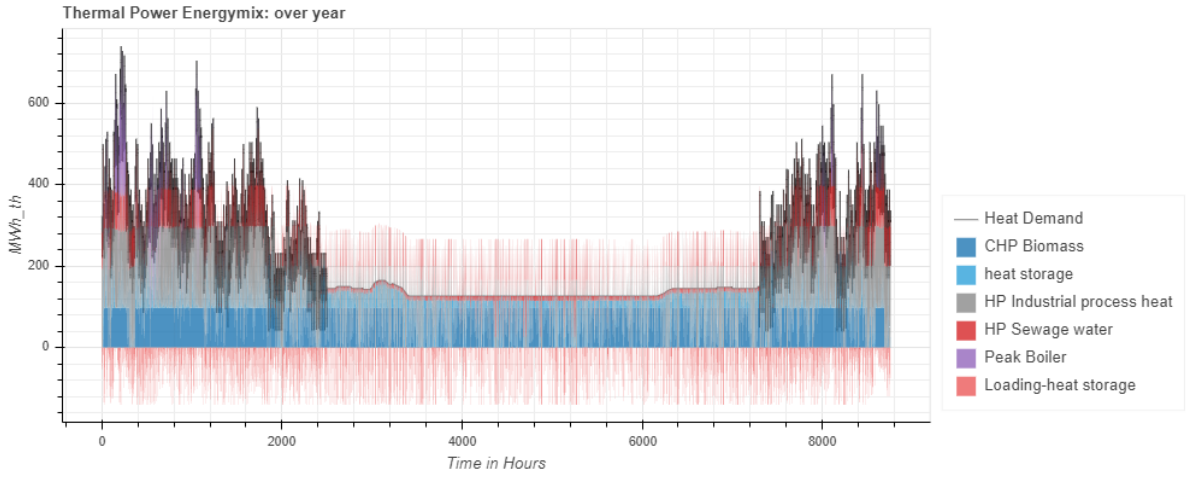

Figure 5.20: Thermal energy mix, portfolio 2, south

For southern climate (fig. 5.21), lake water and air become more viable, resulting in increased full load hours and total thermal generation, but also in no installed capacity for ground water. This is reasonable, as the source temperature of ground water is constantly 8°C and does not benefit from the warmer environment.

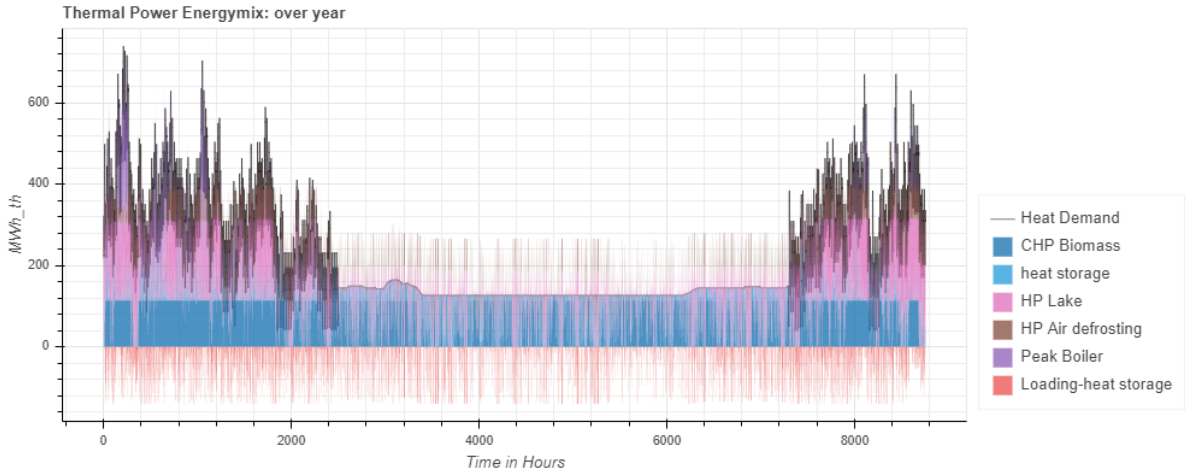

Figure 5.21: Thermal energy mix, portfolio 3, south

5.6 Total Heat Generation by Portfolio

To highlight the difference of the portfolios, the data is rearranged and grouped by portfolio in this section.

5.6.1 Portfolio 1

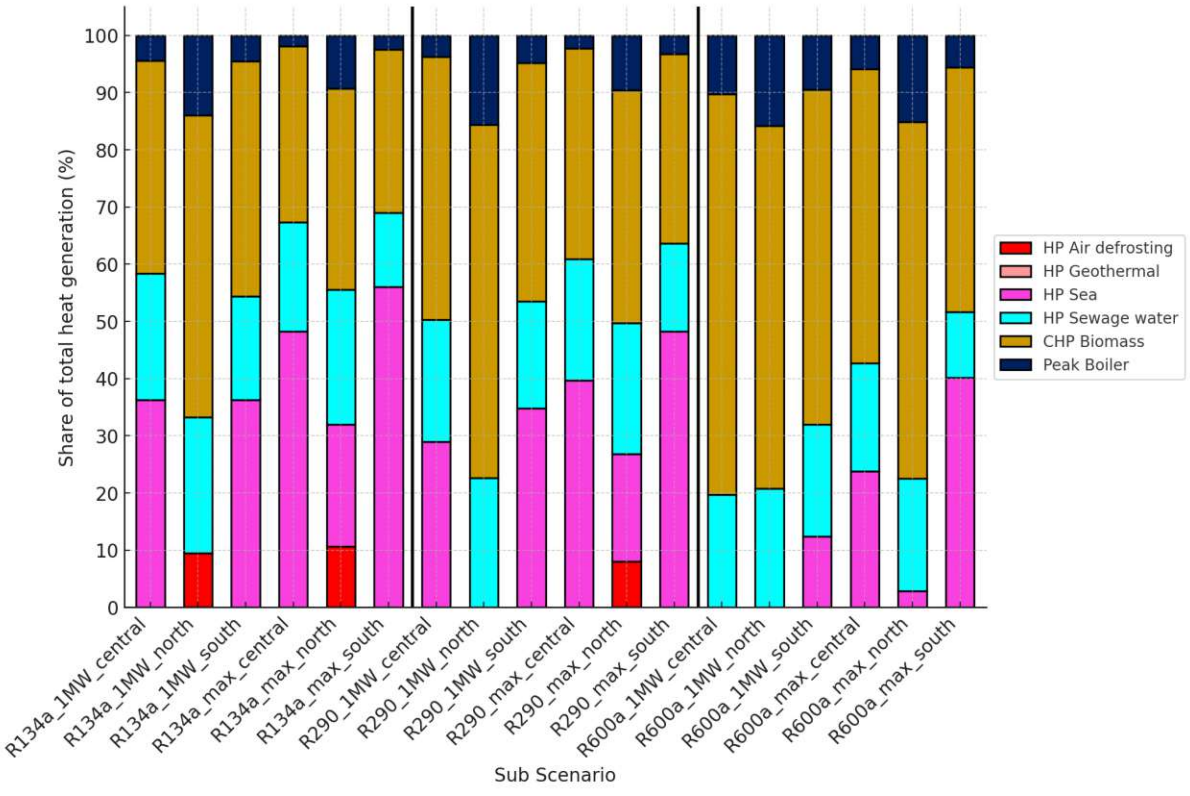

Figure 5.22: Portfolio 1

For portfolio 1 (fig. 5.22), the economic value of using different refrigerants is clearly visible, as there is less heat generated by LSHP using R600a than by using R134a or R290.

5.6.2 Portfolio 2

For portfolio 2 (fig. 5.23), the share of LSHP is much more steady because of the use of industrial process heat, which has the lowest investment costs of LSHP and high heat source temperatures of 35°C across the year, making it independent from climate. The heat demand is covered by LSHP from 60% to 68% in most cases, with R600a,1MW,south being the case with the least coverage of 47%.

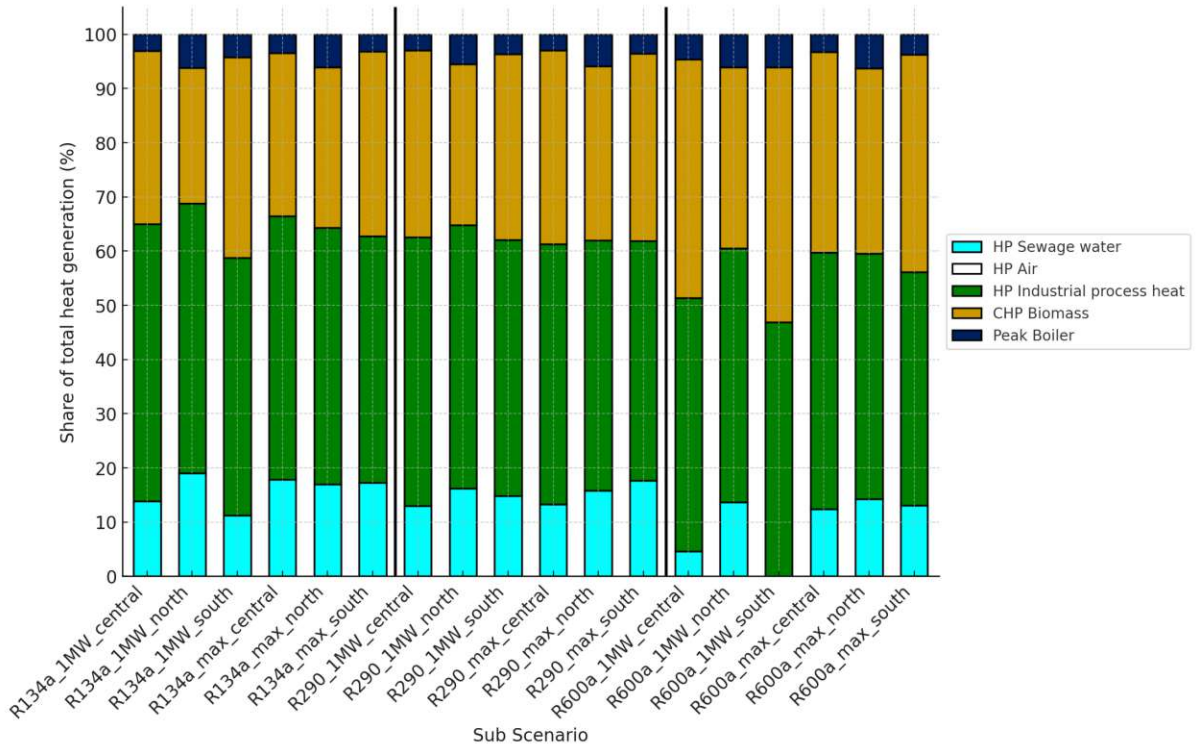

Figure 5.23: Portfolio 2

5.6.3 Portfolio 3

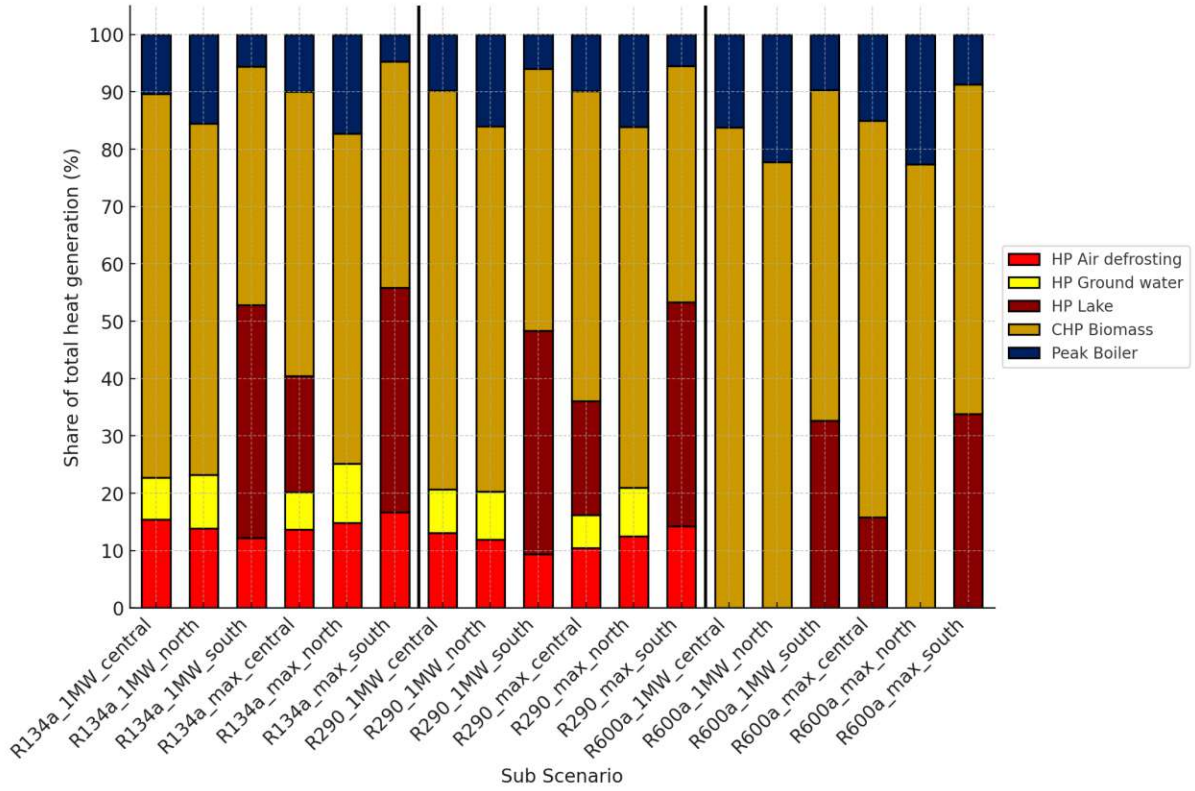

Figure 5.24: Portfolio 3

Of all portfolios, the least amount of heat is generated by LSHP in portfolio 3 (fig. 5.24). While heat pumps using the sources air, ground water and lake water are able to cover over 20% and up to to 56% of the total demand using R134a or R290, for R600a only lake water heat pumps are a viable option in southern and central climate, while there are 3 cases with R600a, where no heat is generated by LSHP. This shows the large impact of an unfavorable refrigerant on the share of total heat generation.

5.7 Coefficient of performance (COP)

The following fig. 5.26 shows the maximal COP over the year. It ranges from 3 (Ground water: P3,R290,north/central) to 4.44 (Air: portfolio3,R134a, south).

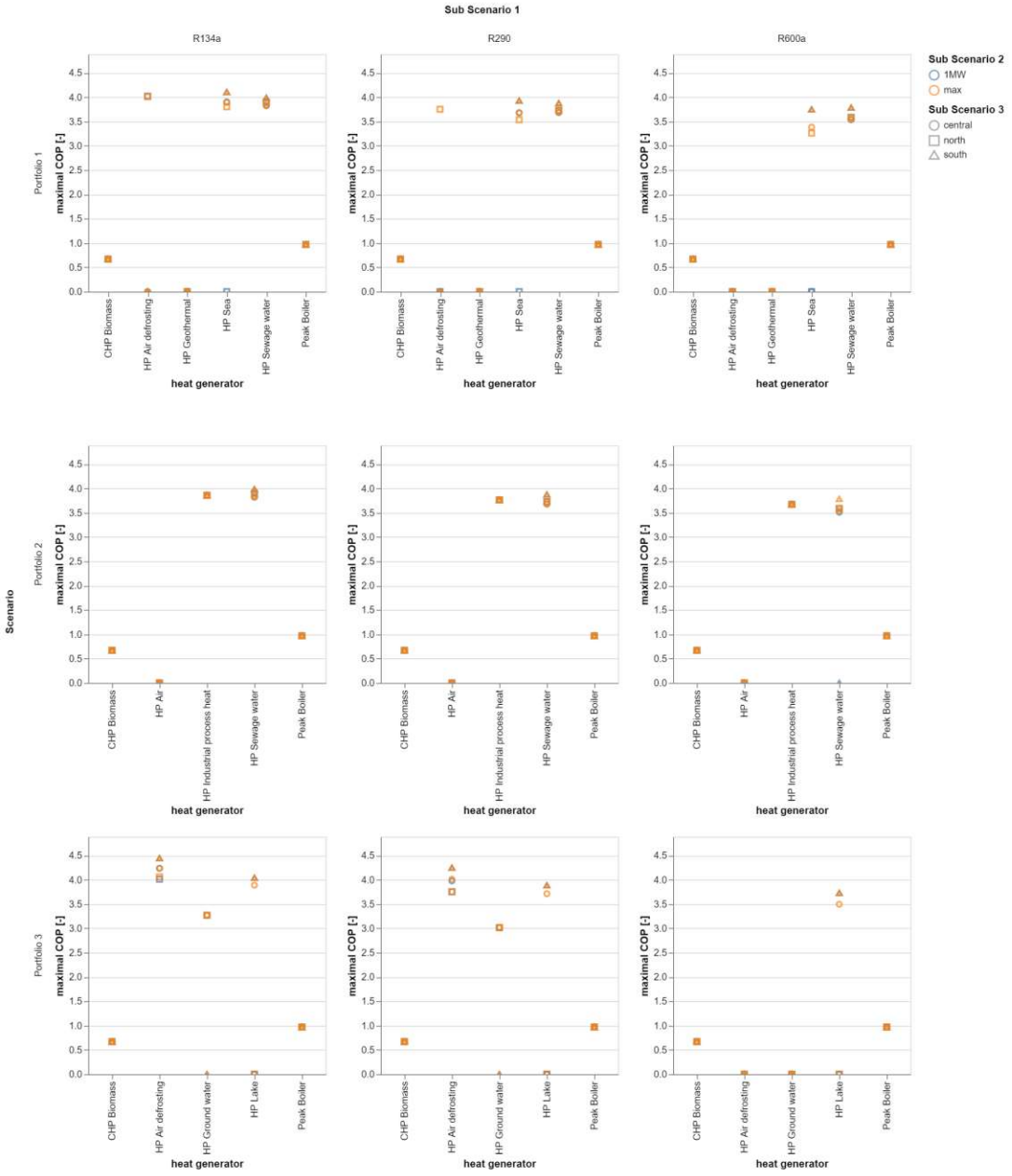

Figure 5.25: Maximal COP

As an example of the yearly COP, the profile of a seawater heat pump in portfolio 1,max,south can be seen in the following fig. 5.26. It is similar in range to the seawater COP collected for the database found in fig. 4.5.

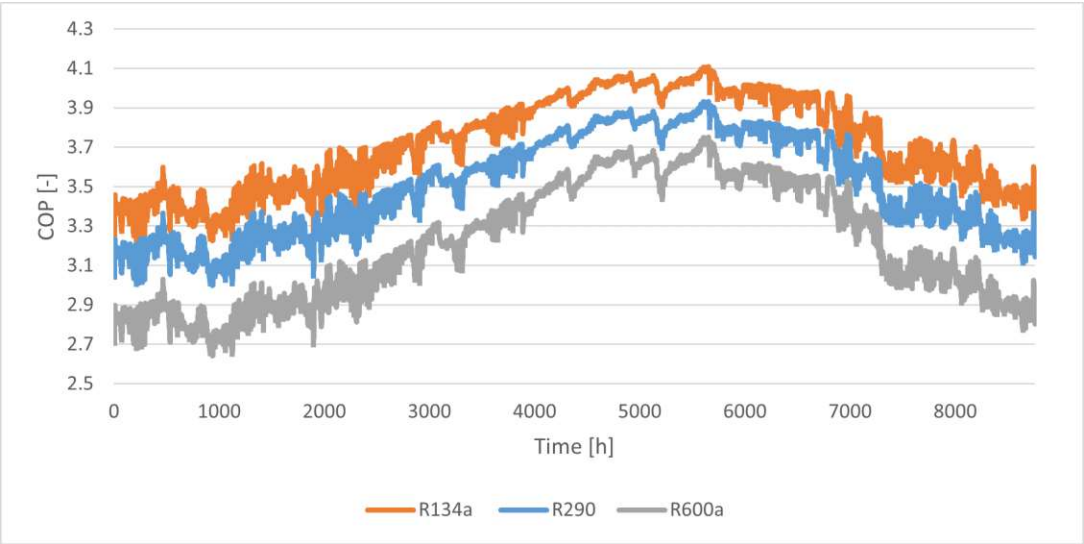

Figure 5.26: Yearly COP for a seawater heat pump in southern climate for R134a, R290 and R600a

The seasonal performance factor (SPF) is the heat energy produced over a year divided by the electricity used by the heat pump, or in other words the average of the yearly COP seen in fig. 5.26. For the heat sources used in the model runs, SPF is shown across all runs in fig. 5.27. It is relatively consistent for all LSHP using ambient heat sources, while the median is higher for LSHP using industrial process heat and lower for the ones using ground water. This corresponds to the LCOH of heat pumps presented in fig. 5.3, where LSHP using industrial process heat have the lowest median LCOH and LSHP using ground water have the highest median LCOH.

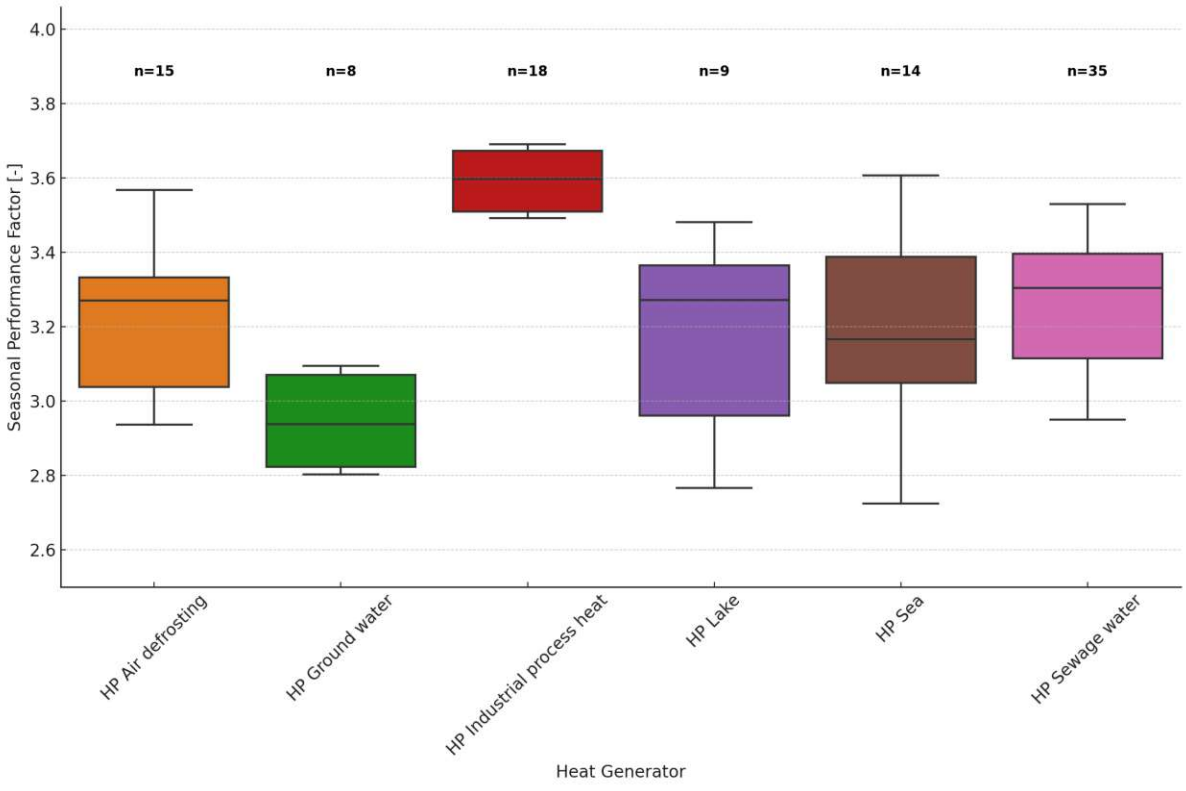

Figure 5.27: Seasonal performance factor for LSHP

5.8 Heat storage sizes

For the heat storage, the installed capacity gets optimized. The following figure fig. 5.28 shows the installed capacity for the 1 MW and max case. It is proportional to the heat demand of the small and large city, and it is optimized for the use on a daily basis. This may be the more economic variant compared to a seasonal energy storage due to the electricity prices, which have high fluctuation (fig. 3.7) and to avoid very large storage losses when storing heat over long periods of time. The behavior of the storage over the year can be seen in more detail in section 5.5.

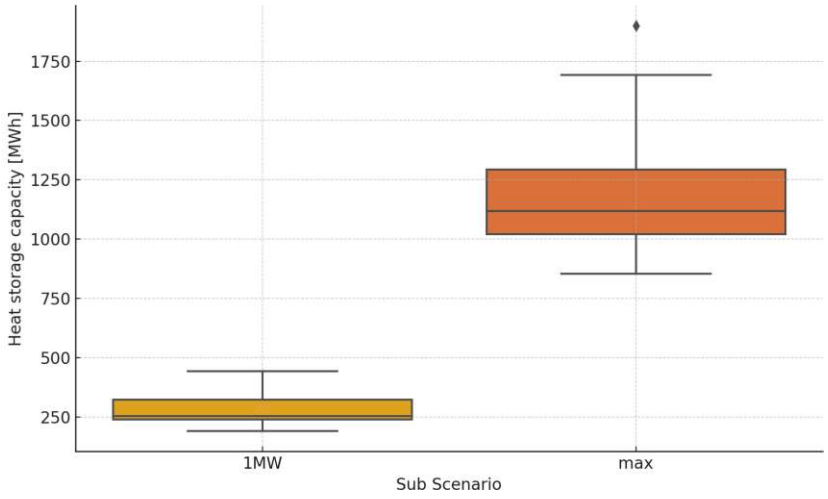

Figure 5.28: Installed heat storage capacity [MWh] for small and large cities

5.9 Discussion of the results and limitations of this study

In the following section, the modeling results are discussed and potential limitations of this study are pointed out.

5.9.1 Economic input data and LCOH

Although assessing current economic information is challenging to find and to generalize, the application of cost functions (section 3.3.1) provides a viable solution for estimating the cost of LSHP. However, there is a price uncertainty in the investment cost of the biomass CHP and peak boiler, as these are highly case-specific. For example, the specific investment cost of biomass CHP range from 2.39 M€/MWh (chosen input) to 3.75 M€/MWh for a large-scale CHP plant of a similar size (DEA, 2023). The electricity price for LSHP is expected to stay relatively stable in the future as seen in fig. 3.8 and is similar to the input price (Schmitt, 2022). Additionally, implementing biomass CHP as a base load generator across Europe would increase the demand for wood pellets and subsequently their price. Schmitt (2022) also mentions a much higher increase in gas prices for 2050 ranging from 72 €/MWh to 110 €/MWh depending on the scenario compared to 53 €/MWh currently, which is used as input. This will make the peak gas boiler less economical in the future. In Popovski et al. (2019), the LCOH of LSHP in Germany are higher initially (252 €/MWh) but are reduced to match the

LCOH for coal-fired CHP (40 €/MWh) through subsequent measures like reducing supply temperatures, lowering electricity prices and reducing CAPEX (see section 2.3) . Under the assumptions of this thesis,this value can already be reached by LSHP, which are in a similar range as biomass CHP in this study (see fig. 5.3). Pieper, Mašatin, et al. (2019) also shows that low LCOH for LSHP of 37 €/MWh can be achieved under current conditions, closely matching the lowest LCOH of LSHP in this work with 40 €/MWh.

5.9.2 Full Load Hours

LSHP showed full load hours ranging from 2121 to 5356 hours, making them ideal for intermediate load operations. Compared to the findings from the database in fig. 4.20, where the full load hours range in average from 5000 to 8000 hours, this is rather low. A reason for this is that LSHP are not currently expanded to their maximum potential, which is done in the model. When their installed capacity is not high compared to the total capacity of the heat generators in the DH system, it is easier to operate them at full load all of the time. However, in future scenarios, where LSHP cover up to 70% of DH heat generation, Energiewende (2023) estimates only 1300 full load hours per year for LSHP to meet high flexibility requirements. Peak boilers, in contrast, have significantly lower full load hours, ranging from 240 to 625 hours, because they are only used during the highest demand periods. Biomass CHP plants are ideally used as baseload generators with full load hours ranging from 5816 to 6724 hours.

5.9.3 Installed Capacities

The installed capacities of different heat sources vary significantly, depending on the climate, the portfolio, and the used refrigerant. Deep geothermal and air source heat pumps without defrosting capabilities were not installed due to high total capital investment (TCI) and operational constraints in winter. Industrial process heat pumps, with a constant source temperature of 35°C and low TCI, were consistently favored across all portfolios, demonstrating their economic viability. However, the potential available capacity as well as the temperatures for industrial process heat for example are highly case specific, as shown in fig. 4.7.

5.9.4 Total Heat Generation

The analysis of total heat generation showed that LSHP could optimally cover between 50% and 70% of the total heat demand. This is highly dependent on the heat source and climatic conditions, with industrial process heat pumps achieving the highest shares due to their steady temperature profiles, whereas in a southern climate, the share of total heat generation is much more balanced. It must be noted that the share of LSHP on the total heat generation in concrete cities is also depending on pre-installed heat generators and the relation of the city size to the potential heat sources available, which varies for every city. However, through the generalized approach used in this work, it is possible to highlight the impact of certain parameters like climate conditions.

5.9.5 Coefficient of Performance (COP)

The maximal COP of LSHP varied between 3.0 and 4.44, depending on the refrigerant and climate conditions. The highest COP values were achieved in southern climates with air-source heat pumps, highlighting the importance of climate and refrigerant choice on system efficiency.

Regarding the seasonal performance factor, the LSHP using industrial process heat showed the highest median with 3.6 and the lowest spread with 0.2, showing the advantages of a heat source with a constantly high source temperature. The COPs in the model (section 5.7) closely match the ones found in the database (section 4.1), showing the robustness of the method of calculation.

6 Conclusion

The method applied in this thesis has proven effective in answering the research question: "What is the current status and the potential contribution of large-scale heat pumps in European district heating systems under different conditions in terms of heat source availability and technology portfolio?". It consists firstly in the creation of a database, which results in an up-to-date assessment of various technical parameters like size, location, year of installation, and operating temperatures of LSHP across Europe, with over 2000 MW of additional LSHP capacity discovered compared to David et al. (2017). It also offers valuable insights into model input temperatures and the selection of the most common heat sources for further analysis. The use of a district heat supply model provided a valid method for assessing the cost-optimal installed capacity and dispatch of LSHP in various heat generation portfolios, sizes and climate conditions using different heat sources and refrigerants.

To answer the research question, the 3 sub-questions are subsequently addressed and answered:
Sub-question 1:"What are the potentials of heat sources currently in terms of size, temperature levels, fluctuations, and regulatory aspects?"
The database shows that there has been rapid growth in the installed capacities of LSHP in recent years from 2015 onward, alongside a diversification of heat sources used, indicating that this trend will continue in the future. This leads to the conclusion that LSHP are playing an increasingly important role in DH systems in Europe. This diversity shows not only in the heat sources used, but also in size, and temperature, where sea water heat pumps show the largest installed size. The modeling results also show that this increasing diversification makes sense, as some heat sources like lake water are not suitable for the use in winter in cold climates due to frosting issues, whereas others like ground water are restricted in their maximal capacity. The 2 heat sources for which LSHP are never installed are deep geothermal, having around 5 times the investment cost as other heat sources due to drilling and air source heat pumps without defrosting, which showed that they cannot be used effectively during the heating season. On the other side, the ideal heat source for LSHP is available all year around and has low investment costs, like industrial process heat. A mix of LSHP using different heat sources is therefore recommended for a more steady heat generation in various conditions and to reduce the capacity of individual sources for a higher share of the total demand covered by LSHP.

Sub-question 2: "Which technologies and framework conditions provide synergies with LSHP, and which are competing?"
Firstly, LSHP benefit from high source temperatures and low flow temperatures not only in having higher efficiency, but also lower investment costs, as it is shown in section 3.3.1. This should be kept in mind for future scenarios, which are not covered in this work. On the other side, it is shown that LSHP significantly benefit from economies of scale effects in all simulated cases, thus lowering the levelized cost of heat of the whole heat generation portfolio and increasing the share of LSHP on the total heat generation. This also implicates that a high share LSHP will reduce the overall cost of heat generation. Another consequence from this is that heat sources, that are not economical on a small scale, can become economical to be installed on a large scale, thus diversifying the portfolio. Nevertheless, LSHP fulfill the role of a medium load generator in all simulated cases, implicating that there is still a need for base-

and peak-load generators for them to be cost-optimal. These roles are fulfilled by biomass CHP plants and a gas boiler in this study, for which the discussion on prices in section 5.9 showed that the energy prices for these 2 competing technologies are expected to rise when deployed on a large scale across Europe, whereas LSHP costs are expected to drop because of the aforementioned reasons, suggesting that their significance will increase. In future scenarios, peak boilers could also be powered by hydrogen, resulting in a completely decarbonized heat energy system.

Sub-question 3: "How to improve the modeling (e.g. the COP) of LSHP in a DH supply optimization model?"
In contrast to studies like Popovski et al. (2019) or Pieper, Mašatin, et al. (2019), the investment cost, as well as the COP and temperature sensitivities of the COP are modeled depending on the refrigerant with the use of cost functions from Vannoni et al. (2023). Apart from the cost functions for LSHP themselves, the share of the heat source on the cost is considered as well. While LSHP using R134a have superior thermodynamic properties, such as higher COP, R290 has the lowest investment cost, resulting in a high viability for both refrigerants and and showing that there are economic alternatives for replacing refrigerants with a high global warming potential such as R134a, while R600a is performing consistently worse in this study. This dependency on the refrigerant showed a large impact on the share of LSHP on the total heat generation, as the refrigerant can even determine, if LSHP are an economic option to install or not. Because of this large difference in outcome, the distinction by refrigerant should be considered in future works. Another novelty of this study is the comparison of LSHP under different climate conditions, showing the large impact of the climate on their optimal share in total heat generation when ambient heat sources are used.

To wrap it all up, LSHP show significant growth in installed capacities in the recent years, using many novel heat sources. This is confirmed by the modeling implementation, which showed that it is cost-optimal to have a high share of LSHP in district heating systems, where only 3 out of 54 cases showed no LSHP installation. This leads to the final conclusion, that LSHP are already a viable option to be used in current DH systems, while there is still a need for additional peak- and baseload generators. At the same time, future trends for LSHP with sinking system temperatures are looking beneficial for their implementation. Therefore, this study affirms the estimation of Energiewende (2023), that LSHP will be able to cover 70% of the district heating supply in Germany by 2045. It exceeds the estimation of Paardekooper et al. (2018), that 25-30% of the heat demand in district heating systems can be supplied by LSHP in 2050.

For further research, the effect of having a larger amount of heat generators or a seasonal energy storage per portfolio can be studied, as there are 7 heat sources implemented for modeling LSHP in this study, while there are 21 heat sources identified for the database. Further, high flexibility with around 2 cold starts per day is required for a cost-optimal operation of LSHP (section 5.5). The effects on the lifetime of LSHP of such a high number of cold-starts could be investigated further in future works. The calculation of temperature sensitivities and COP could also be further refined, as the COP is nonlinear and its temperature sensitivity is just a linear approximation, depending on the chosen temperatures (fig. 3.6).

Appendix

Table 1: Average Technical Data

Heat source		Technical Data					
		Avg. inlet temp. condenser [°C]	**Avg. flow temp. [°C]**	**Avg. source temp. [°C]**	**Avg. outlet temp. evaporator [°C]**	**Avg. ΔT [°C]**	**Avg. output cap. heating [MW_{th}]**
Commercial sources	Flue gas heat recovery	56	77	44	29	50	5.50
	Industrial process heat recovery	54	78	42	28	54	7.32
	Commercial / Industrial CHP	57	79	31	33	61	8.95
	Data center	40	80	24	18	66	17.98
	Cooling plant	53	74	35	26	44	2.66
	Cooling network	58	77	13	4	57	8.86
Infrastructural sources	Sewage water	52	74	13	6	65	21.82
	HVDC, metro, mine water, TES, unknown	52	77	41	35	60	7.86
Environmental sources	Ambient air	40	79	8	3	79	3.70
	Ground water	51	71	13	7	61	3.56
	Lake water	45	75	23	7	68	12.08
	River water	62	80	10	11	77	27.36
	Sea water	54	72	8	5	64	21.99
	Deep geothermal	57	76	39	24	46	10.21
	Solar thermal	35	78	25	17	55	14.43

Table 2: Average Economic Data

Heat source		Economic Data			
		Avg. capital cost [M€/MW_{th}]	Avg. annual operation hours [h]	Avg. annual energy savings [GWh]	Avg. annual energy savings [M€]
Commercial sources	Flue gas heat recovery	1.166		15	220
	Industrial process heat recovery	1.701	7354	34	193
	Commercial / Industrial CHP		6500	32	
	Data center	2.685			
	Cooling plant	0.621		4	
	Cooling network	0.878			
Infrastructural sources	Sewage water	1.785	8000	101	340
	HVDC, metro, mine water, TES, unknown	1.716		0.05	
Environmental sources	Ambient air	0.831			400
	Ground water	0.810	5000	0.001	
	Lake water				
	River water	2.884			
	Sea water	2.777			
	Deep geothermal	13.944			
	Solar thermal	2.083			

Bibliography

AGFW (2024). *AGFW*. URL: https://www.agfw.de/ (visited on 03/26/2024) (cit. on p. 30).

Aguilera, José Joaquín et al. (Oct. 1, 2022). "A review of common faults in large-scale heat pumps." In: *Renewable and Sustainable Energy Reviews* 168, p. 112826. ISSN: 1364-0321. DOI: 10.1016/j.rser.2022.112826. URL: https://www.sciencedirect.com/science/article/pii/S1364032122007092 (visited on 05/24/2023) (cit. on pp. 10, 57).

Ahrens, Marcel Ulrich et al. (May 5, 2021). "Integrated high temperature heat pumps and thermal storage tanks for combined heating and cooling in the industry." In: *Applied Thermal Engineering* 189, p. 116731. ISSN: 1359-4311. DOI: 10.1016/j.applthermaleng.2021.116731. URL: https://www.sciencedirect.com/science/article/pii/S1359431121001861 (visited on 04/21/2024) (cit. on p. 53).

Analyse der Marktgröße und des Anteils von Rechenzentren in Europa - Branchenforschungsbericht - Wachstumstrends (2024). URL: https://www.mordorintelligence.com/de/industry-reports/europe-data-center-power-market (visited on 01/30/2024) (cit. on p. 49).

Argus Biomass Markets (2023-04-26).pdf (2024). URL: https://view.argusmedia.com/rs/584-BUW-606/images/Argus%20Biomass%20Markets%20%282023-04-26%29.pdf (visited on 05/02/2024) (cit. on p. 29).

Arpagaus et al., Cordin (June 1, 2018). "High temperature heat pumps: Market overview, state of the art, research status, refrigerants, and application potentials." In: *Energy* 152. Publisher: Pergamon, pp. 985–1010. ISSN: 0360-5442. DOI: 10.1016/j.energy.2018.03.166. URL: https://www.sciencedirect.com/science/article/pii/S0360544218305759 (visited on 05/29/2023) (cit. on p. 2).

Averfalk, Helge et al. (Nov. 1, 2017). "Large heat pumps in Swedish district heating systems." In: *Renewable and Sustainable Energy Reviews* 79, pp. 1275–1284. ISSN: 1364-0321. DOI: 10.1016/j.rser.2017.05.135. URL: https://www.sciencedirect.com/science/article/pii/S1364032117307839 (visited on 04/21/2024) (cit. on pp. 42, 43, 53).

Barco-Burgos, J. et al. (Jan. 15, 2022). "Review on the integration of high-temperature heat pumps in district heating and cooling networks." In: *Energy* 239, p. 122378. ISSN: 0360-5442. DOI: 10.1016/j.energy.2021.122378. URL: https://www.sciencedirect.com/science/article/pii/S036054422102627X (visited on 02/06/2024) (cit. on p. 33).

Bejan, Adrian, George Tsatsaronis, and Michael J. Moran (Dec. 12, 1995). *Thermal Design and Optimization*. Google-Books-ID: sTi2crXeZYgC. John Wiley & Sons. 562 pp. ISBN: 978-0-471-58467-4 (cit. on p. 24).

Bundestag, Deutscher (2007). *CO2-Bilanzen verschiedener Energieträger im Vergleich*. URL: https://www.bundestag.de/resource/blob/406432/70f77c4c170d9048d88dcc3071b7721c/wd-8-056-07-pdf-data.pdf (visited on 05/15/2024) (cit. on p. 28).

Carbon Price Tracker (2024). Ember. URL: https://ember-climate.org/data/data-tools/carbon-price-viewer/ (visited on 04/16/2024) (cit. on p. 28).

Carnot, Sadi and Wilhelm Ostwald (1892). *Betrachtungen über die bewegende kraft des feuers und die zur entwickelung dieser kraft geeigneten maschinen*. In collab. with unknown library. Leipzig, W. Engelmann. 98 pp. URL: http://archive.org/details/betrachtungenbe00carngoog (visited on 10/28/2023) (cit. on p. 44).

Carrea, Laura and Christopher J. Merchant (2019). *GloboLakes: Lake Surface Water Temperature (LSWT) v4.0 (1995-2016)*. In collab. with Centre For Environmental Data Analysis (CEDA) et al. Version 3.1. DOI: 10.5285/76A29C5B55204B66A40308FC2BA9CDB3. URL: https://catalogue.ceda.ac.uk/uuid/76a29c5b55204b66a40308fc2ba9cdb3 (visited on 04/03/2024) (cit. on pp. 37, 38).

Carroll, P., M. Chesser, and P. Lyons (Dec. 1, 2020). "Air Source Heat Pumps field studies: A systematic literature review." In: *Renewable and Sustainable Energy Reviews* 134, p. 110275. ISSN: 1364-0321. DOI: 10.1016/j.rser.2020.110275. URL: https://www.sciencedirect.com/science/article/pii/S1364032120305621 (visited on 07/10/2023) (cit. on p. 49).

Chen, Wei-An et al. (May 1, 2022). "Methodology of evaluating the sewage heat utilization potential by modelling the urban sewage state prediction model." In: *Sustainable Cities and Society* 80, p. 103751. ISSN: 2210-6707. DOI: 10.1016/j.scs.2022.103751. URL: https://www.sciencedirect.com/science/article/pii/S2210670722000828 (visited on 01/27/2024) (cit. on p. 45).

Cipolla, Sara Simona and Marco Maglionico (Feb. 1, 2014). "Heat recovery from urban wastewater: Analysis of the variability of flow rate and temperature." In: *Energy and Buildings* 69, pp. 122–130. ISSN: 0378-7788. DOI: 10.1016/j.enbuild.2013.10.017. URL: https://www.sciencedirect.com/science/article/pii/S0378778813006634 (visited on 02/29/2024) (cit. on pp. 38, 45).

Commission, European (2023). *Quarterly_Report_on_European_Gas_markets_Q1_2023.pdf*. URL: https://energy.ec.europa.eu/system/files/2023-10/Quarterly_Report_on_European_Gas_markets_Q1_2023.pdf (visited on 03/15/2024) (cit. on p. 29).

Copernicus Marine Data Store (2024). URL: https://data.marine.copernicus.eu/products (visited on 02/29/2024) (cit. on p. 37).

David, Andrei et al. (Apr. 2017). "Heat Roadmap Europe: Large-Scale Electric Heat Pumps in District Heating Systems." In: *Energies* 10.4. Number: 4 Publisher: Multidisciplinary Digital Publishing Institute, p. 578. ISSN: 1996-1073. DOI: 10.3390/en10040578. URL: https://www.mdpi.com/1996-1073/10/4/578 (visited on 05/24/2023) (cit. on pp. 2, 7, 10, 11, 24, 85).

DEA (Feb. 2023). *technology_data_catalogue_for_el_and_dh.pdf*. URL: https://ens.dk/sites/ens.dk/files/Analyser/technology_data_catalogue_for_el_and_dh.pdf (visited on 01/23/2024) (cit. on pp. 23, 24, 26, 27, 30, 82).

DECC (Mar. 2015). *National Heat Map: Water source heat map layer*. URL: https://assets.publishing.service.gov.uk/government/uploads/system/uploads/attachment_data/file/416660/water_source_heat_map.PDF (visited on 04/12/2024) (cit. on p. 32).

Dénarié, A. et al. (Jan. 1, 2019). "Industrial excess heat recovery in district heating: Data assessment methodology and application to a real case study in Milano, Italy." In: *Energy* 166, pp. 170–182. ISSN: 0360-5442. DOI: 10.1016/j.energy.2018.09.153. URL: https://www.sciencedirect.com/science/article/pii/S036054421831925X (visited on 07/03/2023) (cit. on p. 47).

District heating generations explained (2024). URL: https://www.danfoss.com/en/about-danfoss/articles/dhs/district-energy-generations-explained/ (visited on 04/23/2024) (cit. on p. 5).

Dolphin, Geoffroy et al. (Oct. 2023). "A net-zero target compels a backward induction approach to climate policy." In: *Nature Climate Change* 13.10. Number: 10 Publisher: Nature Publishing Group, pp. 1033–1041. ISSN: 1758-6798. DOI: 10.1038/s41558-023-01798-y. URL: https://www.nature.com/articles/s41558-023-01798-y (visited on 11/07/2023) (cit. on p. 1).

Durchschnittliche Börsenstrompreise — Energy-Charts (2024). URL: https://energy-charts.info/charts/price_average/chart.htm?l=de&c=DE&interval=year&year=-1 (visited on 05/19/2024) (cit. on p. 29).

Energiewende, Agora (2023). *Roll-out von Großwärmepumpen in Deutschland*. DOI: 10.24406/publica-1440. URL: https://www.agora-energiewende.de/publikationen/roll-out-von-grosswaermepumpen-in-deutschland (visited on 01/23/2024) (cit. on pp. 6, 83, 86).

EPA (2007). "Biomass Combined Heat and Power Catalog of Technologies." In: (cit. on p. 34).

Ewen, Matt (Jan. 23, 2024). *European wholesale electricity price data*. Ember. URL: https://ember-climate.org/data-catalogue/european-wholesale-electricity-price-data/ (visited on 02/20/2024) (cit. on pp. 29, 30).

Fabris, Francesco et al. (Mar. 1, 2024). "Evaluation of the carbon footprint of HFC and natural refrigerant transport refrigeration units from a life-cycle perspective." In: *International Journal of Refrigeration* 159, pp. 17–27. ISSN: 0140-7007. DOI: 10.1016/j.ijrefrig.2023.12.018. URL: https://www.sciencedirect.com/science/article/pii/S0140700723004747 (visited on 01/27/2024) (cit. on p. 57).

Fischer, David and Hatef Madani (Apr. 1, 2017). "On heat pumps in smart grids: A review." In: *Renewable and Sustainable Energy Reviews* 70, pp. 342–357. ISSN: 1364-0321. DOI: 10.1016/j.rser.2016.11.182. URL: https://www.sciencedirect.com/science/article/pii/S1364032116309418 (visited on 04/16/2024) (cit. on p. 6).

Friotherm (2023). *District heating / heat pumps — Welcome to Friotherm*. URL: https://www.friotherm.com/applications/district-heating-heat-pumps/ (visited on 08/25/2023) (cit. on pp. 10, 49).

Gaur, Ankita Singh, Desta Z. Fitiwi, and John Curtis (Jan. 1, 2021). "Heat pumps and our low-carbon future: A comprehensive review." In: *Energy Research & Social Science* 71, p. 101764. ISSN: 2214-6296. DOI: 10.1016/j.erss.2020.101764. URL: https://www.sciencedirect.com/science/article/pii/S221462962030339X (visited on 04/02/2024) (cit. on pp. 6, 7).

geothermischer Gradient (2024). URL: https://www.spektrum.de/lexikon/geowissenschaften/geothermischer-gradient/5754 (visited on 01/27/2024) (cit. on p. 48).

Gerhardt, Norman (June 2021). "Transformationspfade der Fernwärme in Rückkopplung mit dem Energiesystem und notwendige Rahmenbedingungen." In: (cit. on p. 31).

Geyer et al., Roman (Jan. 2019). *task-2-summary-report.pdf*. URL: https://heatpumpingtechnologies.org/annex47/wp-content/uploads/sites/54/2019/07/task-2-summary-report.pdf (visited on 08/25/2023) (cit. on p. 10).

Gilbert, Tristan et al. (Jan. 18, 2023). "Heat source and application-dependent levelized cost of decarbonized heat." In: *Joule* 7.1, pp. 128–149. ISSN: 2542-4351. DOI: 10.1016/j.joule.2022.11.006. URL: https://www.sciencedirect.com/science/article/pii/S2542435122005645 (visited on 08/02/2023) (cit. on p. 1).

Goetzl, Gregor (July 22, 2020). *MUSE – Differences between deep and shallow geothermal energy*. GeoERA. URL: https://geoera.eu/blog/muse-differences-between-deep-and-shallow-geothermal-energy/ (visited on 01/27/2024) (cit. on p. 48).

Golzar, Farzin, David Nilsson, and Viktoria Martin (Jan. 2020). "Forecasting Wastewater Temperature Based on Artificial Neural Network (ANN) Technique and Monte Carlo Sensitivity Analysis." In: *Sustainability* 12.16. Number: 16 Publisher: Multidisciplinary Digital Publishing Institute, p. 6386. ISSN: 2071-1050. DOI: 10.3390/su12166386. URL: https://www.mdpi.com/2071-1050/12/16/6386 (visited on 03/03/2024) (cit. on pp. 38, 39).

Großwärmepumpen in deutschen Fernwärmenetzen - energiewendebauen.de (2024). URL: https://www.energiewendebauen.de/projekt/neu-grosswaermepumpen-in-deutschen-fernwaermenetzen/ (visited on 04/21/2024) (cit. on p. 51).

Guelpa, E. et al. (Jan. 1, 2023). "Reduction of supply temperature in existing district heating: A review of strategies and implementations." In: *Energy* 262, p. 125363. ISSN: 0360-5442. DOI: 10.1016/j.energy.2022.125363. URL: https://www.sciencedirect.com/science/article/pii/S0360544222022459 (visited on 05/29/2023) (cit. on p. 43).

Hart, Olga E. and Rolf U. Halden (Apr. 1, 2020). "Modeling wastewater temperature and attenuation of sewage-borne biomarkers globally." In: *Water Research* 172, p. 115473. ISSN: 0043-1354. DOI: 10.1016/j.watres.2020.115473. URL: https://www.sciencedirect.com/science/article/pii/S0043135420300099 (visited on 01/27/2024) (cit. on pp. 38, 39, 45).

Havlicek, Daniela and Jeton Hasani (2020). *HotmapsDispatch - Model Description*. URL: https://tuw-eeg.github.io/hotmapsDispatch/Hotmaps%20Dispatch%20-%20Description.html (visited on 10/27/2023) (cit. on p. 17).

Heat Pump (Jan. 28, 2013). Saving Energy - Empowering Informed Decisions. URL: https://savingenergy.co.za/heat-pump/ (visited on 11/28/2023) (cit. on p. 11).

HotMaps, Dispatch (2024). *GitHub - alikoek/hotmapsDispatch at OpenGIS4ET*. GitHub. URL: https://github.com/alikoek/hotmapsDispatch (visited on 04/11/2024) (cit. on pp. 2, 3, 9, 17, 20, 23, 26–28, 30–32, 35, 36, 45).

Jesper, Mateo et al. (Mar. 1, 2021). "Large-scale heat pumps: Uptake and performance modelling of market-available devices." In: *Renewable and Sustainable Energy Reviews* 137, p. 110646. ISSN: 1364-0321. DOI: 10.1016/j.rser.2020.110646. URL: https://www.sciencedirect.com/science/article/pii/S1364032120309308 (visited on 05/24/2023) (cit. on pp. 2, 6, 7, 43).

Jia, Jikang et al. (Mar. 15, 2024). "Experimental investigation on a screw-type air source heat pump system with air heat absorption defrosting." In: *Applied Thermal Engineering* 241, p. 122412. ISSN: 1359-4311. DOI: 10.1016/j.applthermaleng.2024.122412. URL: https://www.sciencedirect.com/science/article/pii/S1359431124000802 (visited on 01/30/2024) (cit. on p. 32).

Juhrich, Kristina (2022). "CO2-Emissionsfaktoren für fossile Brennstoffe." In: (cit. on p. 28).

Kiss, Pal (2017). *P.3.7.1 Efficient solution for large heat pumps: wastewater heat recovery - HPT - Heat Pumping Technologies*. URL: https://heatpumpingtechnologies.org/publications/p-3-7-1-efficient-solution-for-large-heat-pumps-wastewater-heat-recovery/ (visited on 03/01/2024) (cit. on p. 45).

Liu, Wen-Cheng and Wei-Bo Chen (Aug. 1, 2012). "Prediction of water temperature in a subtropical subalpine lake using an artificial neural network and three-dimensional circulation models." In: *Computers & Geosciences* 45, pp. 13–25. ISSN: 0098-3004. DOI: 10.1016/j.cageo.2012.03.010. URL: https://www.sciencedirect.com/science/article/pii/S0098300412000982 (visited on 04/04/2024) (cit. on p. 38).

Lok, Wei Jen, Lik Yin Ng, and Viknesh Andiappan (May 1, 2020). "Optimal decision-making for combined heat and power operations: A fuzzy optimisation approach considering system flexibility, environmental emissions, start-up and shutdown costs." In: *Process Safety and Environmental Protection* 137, pp. 312–327. ISSN: 0957-5820. DOI: 10.1016/j.psep.2020.02.024. URL: https://www.sciencedirect.com/science/article/pii/S0957582019319226 (visited on 05/02/2024) (cit. on p. 23).

Manz, Pia et al. (Jan. 2021). "Decarbonizing District Heating in EU-27 + UK: How Much Excess Heat Is Available from Industrial Sites?" In: *Sustainability* 13.3. Number: 3 Publisher: Multidisciplinary Digital Publishing Institute, p. 1439. ISSN: 2071-1050. DOI: 10.3390/su13031439. URL: https://www.mdpi.com/2071-1050/13/3/1439 (visited on 02/05/2024) (cit. on p. 47).

Marguerite, Charlotte et al. (Mar. 2019). "Task 3: Review of concepts and solutions of heat pump integration." In: (cit. on pp. 10, 15).

Molar-Cruz, Anahi et al. (Sept. 1, 2022). "Techno-economic optimization of large-scale deep geothermal district heating systems with long-distance heat transport." In: *Energy Conversion and Management* 267, p. 115906. ISSN: 0196-8904. DOI: 10.1016/j.enconman.2022.115906. URL: https://www.sciencedirect.com/science/article/pii/S0196890422007026 (visited on 01/27/2024) (cit. on p. 48).

MVV Mannheim Wärmepumpe (2024). URL: https://www.siemens-energy.com/de/de/home/stories/mvv-mannheim.html,%20https://www.siemens-energy.com/de/de/home/stories/mvv-mannheim.html (visited on 04/12/2024) (cit. on p. 32).

NCEI (2024). *Hourly/Sub-Hourly Observational Data*. National Centers for Environmental Information (NCEI). URL: https://www.ncei.noaa.gov/maps/ (visited on 04/09/2024) (cit. on pp. 36, 37).

Nielsen, S. et al. (2018). *Comparison of heat pump design and performance for modern refrigerants*. DOI: 10.18462/IIR.GL.2018.1149. URL: http://iifiir.org/clientBookline/service/reference.asp?INSTANCE=EXPLOITATION&OUTPUT=PORTAL&DOCID=IFD_REFDOC_0023512&DOCBASE=IFD_REFDOC_EN&SETLANGUAGE=EN (visited on 02/07/2024) (cit. on pp. 24, 57).

Nowak, Thomas (2023). *EHPA_market_report_2023_Executive-Summary.pdf*. URL: https://www.ehpa.org/wp-content/uploads/2023/06/EHPA_market_report_2023_Executive-Summary.pdf (visited on 01/30/2024) (cit. on p. 49).

O'Shea et al., John (May 2019). *HeatNet_NWE_Transition_Roadmap_Report_Final_-_Digital.pdf*. URL: https://www.codema.ie/images/uploads/docs/HeatNet_NWE_Transition_Roadmap_Report_Final_-_Digital.pdf (visited on 10/26/2023) (cit. on pp. 5, 15, 50).

Ochsner, Karl (2021). *Internationaler-GWP-Kongress-Linz*. URL: https://grosswaermepumpen-kongress.com/wp-content/uploads/2021/09/210916_Internationaler-GWP-Kongress-Linz.pdf (visited on 10/24/2023) (cit. on p. 42).

Odgaard et al., Anders (2020). *Oversigt-over-store-varmepumper-dec-2020-Engelsk.pdf*. URL: https://planenergi.dk/wp-content/uploads/2020/12/Oversigt-over-store-varmepumper-dec-2020-Engelsk.pdf (visited on 08/25/2023) (cit. on p. 10).

Ommen, Torben et al. (2019). *Generalized COP estimation of heat pump processes for operation off the design point of equipment*. DOI: 10.18462/IIR.ICR.2019.0648. URL: https://iifiir.org/datacite_notices/34719 (visited on 05/29/2023) (cit. on p. 8).

Paardekooper, Susana et al. (Oct. 5, 2018). *Heat Roadmap Europe 4: Quantifying the Impact of Low-Carbon Heating and Cooling Roadmaps*. Report. Publication Title: Heat Roadmap Europe 4. Aalborg Universitetsforlag (cit. on pp. 2, 86).

Paris Agreement (Dec. 12, 2015). URL: https://treaties.un.org/Pages/ViewDetails.aspx?src=IND&mtdsg_no=XXVII-7-d&chapter=27&clang=_en (visited on 10/26/2023) (cit. on p. 1).

Piel et al., Eloi (Dec. 2022). *Large heat Pumps in District Heating and Cooling systems*. URL: https://www.euroheat.org/static/c254bdc8-5b3b-4765-9a552f6f27af2253/V18-Technology-Report-Large-heat-pumps-in-District-Heating-and-Cooling-systems.pdf (visited on 10/23/2023) (cit. on p. 7).

Pieper, Henrik, Igor Krupenski, et al. (Sept. 1, 2021). "Method of linear approximation of COP for heat pumps and chillers based on thermodynamic modelling and off-design operation." In: *Energy* 230, p. 120743. ISSN: 0360-5442. DOI: 10.1016/j.energy.2021.120743. URL: https://www.sciencedirect.com/science/article/pii/S0360544221009919 (visited on 05/26/2023) (cit. on p. 44).

Pieper, Henrik, Vladislav Mašatin, et al. (Mar. 18, 2019). "Modelling framework for integration of large-scale heat pumps in district heating using low-temperature heat sources: A case study of Tallinn, Estonia." In: *International Journal of Sustainable Energy Planning and Management* 20. ISSN: 2246-2929. DOI: 10.5278/ijsepm.2019.20.6. URL: https://journals.aau.dk/index.php/sepm/article/view/2737 (visited on 05/26/2023) (cit. on pp. 8, 52, 83, 86).

Pieper, Henrik, Torben Ommen, et al. (Aug. 2018). "Allocation of investment costs for large-scale heat pumps supplying district heating." In: *Energy Procedia* 147, pp. 358–367. ISSN: 18766102. DOI: 10.1016/j.egypro.2018.07.104. URL: https://linkinghub.elsevier.com/retrieve/pii/S1876610218302613 (visited on 05/24/2023) (cit. on pp. 23, 24, 26, 51).

Popovski, Eftim et al. (Aug. 1, 2019). "The role and costs of large-scale heat pumps in decarbonising existing district heating networks – A case study for the city of Herten in Germany." In: *Energy* 180, pp. 918–933. ISSN: 0360-5442. DOI: 10.1016/j.energy.2019.05.122. URL: https://www.sciencedirect.com/science/article/pii/S0360544219310047 (visited on 05/26/2023) (cit. on pp. 8, 82, 86).

Pursiheimo, Esa et al. (June 1, 2022). "Optimal investment analysis for heat pumps and nuclear heat in decarbonised Helsinki metropolitan district heating system." In: *Energy Storage and Saving* 1.2, pp. 80–92. ISSN: 2772-6835. DOI: 10.1016/j.enss.2022.03.001. URL: https://www.sciencedirect.com/science/article/pii/S2772683522000036 (visited on 02/05/2024) (cit. on pp. 27, 34).

Renewables Global Status Report (June 14, 2019). REN21. URL: https://www.ren21.net/reports/global-status-report/ (visited on 10/26/2023) (cit. on p. 1).

Rogié, Brice et al. (Dec. 2020). "Analysis of Cold Air Recirculation in the Evaporators of Large-Scale Air-Source Heat Pumps Using CFD Simulations." In: *Fluids* 5.4. Number: 4 Publisher: Multidisciplinary Digital Publishing Institute, p. 186. ISSN: 2311-5521. DOI: 10.3390/fluids5040186. URL: https://www.mdpi.com/2311-5521/5/4/186 (visited on 05/29/2024) (cit. on p. 49).

Schlosser, F. et al. (Nov. 1, 2020). "Large-scale heat pumps: Applications, performance, economic feasibility and industrial integration." In: *Renewable and Sustainable Energy Reviews* 133, p. 110219. ISSN: 1364-0321. DOI: 10.1016/j.rser.2020.110219. URL: https://www.sciencedirect.com/science/article/pii/S1364032120305086 (visited on 06/07/2023) (cit. on p. 12).

Schmitt, Alex (Apr. 11, 2022). *EU Energy Outlook 2050: How will the European electricity market develop over the next 30 years?* Energy BrainBlog. URL: https://blog.energybrainpool.com/en/eu-energy-outlook-2050-how-will-the-european-electricity-market-develop-over-the-next-30-years/ (visited on 05/19/2024) (cit. on pp. 29, 82).

Song, Mengjie et al. (Feb. 1, 2018). "Review on improvement for air source heat pump units during frosting and defrosting." In: *Applied Energy* 211, pp. 1150–1170. ISSN: 0306-2619. DOI: 10.1016/j.apenergy.2017.12.022. URL: https://www.sciencedirect.com/science/article/pii/S0306261917317361 (visited on 01/30/2024) (cit. on p. 49).

Stromkennzeichnung (2024). E-Control. URL: https://www.e-control.at/industrie/oeko-energie/stromkennzeichnung (visited on 05/06/2024) (cit. on p. 28).

Sulzer, Matthias et al. (Feb. 1, 2021). "Vocabulary for the fourth generation of district heating and cooling." In: *Smart Energy* 1, p. 100003. ISSN: 2666-9552. DOI: 10.1016/j.segy.2021.100003. URL: https://www.sciencedirect.com/science/article/pii/S2666955221000034 (visited on 10/26/2023) (cit. on pp. 5, 7, 43).

Totschnig, G et al. (2018). "Potentiale, Wirtschaftlichkeit und Systemlösungen für Power-to-Heat." In: (cit. on pp. 33, 34).

Vaclav, Smil (2023). *Energy Institute Statistical Review of World Energy*. Statistical review of world energy. URL: https://www.energyinst.org/statistical-review/home (visited on 10/26/2023) (cit. on p. 1).

Vannoni, Alberto et al. (Dec. 1, 2023). "Large size heat pumps advanced cost functions introducing the impact of design COP on capital costs." In: *Energy* 284, p. 129204. ISSN: 0360-5442. DOI: 10.1016/j.energy.2023.129204. URL: https://www.sciencedirect.com/science/article/pii/S0360544223025987 (visited on 02/08/2024) (cit. on pp. 5, 6, 23–25, 86).

Wegfall der EEG-Umlage entlastet Stromkunden — Bundesregierung (May 28, 2022). Die Bundesregierung informiert — Startseite. URL: https://www.bundesregierung.de/breg-de/themen/tipps-fuer-verbraucher/eeg-umlage-faellt-weg-2011728 (visited on 03/26/2024) (cit. on p. 30).

Wolf, Stefan (Feb. 8, 2018). "Integration von Wärmepumpen in industrielle Produktionssysteme : Potenziale und Instrumente zur Potenzialerschließung." In: DOI: 10.18419/opus-9593. URL: https://scholar.archive.org/work/stzr4fbsvbbqvdiawqda4q3ezu (visited on 08/25/2023) (cit. on p. 10).

Xiao et al., Shengqing (2020). *Xiao_Geothermie_Kongress_2020_Langfassung.pdf*. URL: https://www.der-geothermiekongress.de/fileadmin/user_upload/DGK/DGK_2020/Raum_1_Dateien/Xiao_Geothermie_Kongress_2020_Langfassung.pdf (visited on 05/29/2023) (cit. on p. 10).

Yang, Tianrun et al. (Apr. 1, 2021). "Seasonal thermal energy storage: A techno-economic literature review." In: *Renewable and Sustainable Energy Reviews* 139, p. 110732. ISSN: 1364-0321. DOI: 10.1016/j.rser.2021.110732. URL: https://www.sciencedirect.com/science/article/pii/S1364032121000290 (visited on 05/24/2023) (cit. on p. 27).

Yu, Huili et al. (Dec. 1, 2023). "Numerical investigation on operational performance of seawater-source heat pump system coupled with capillary-box heat exchangers." In: *Case Studies in Thermal Engineering* 52, p. 103724. ISSN: 2214-157X. DOI: 10.1016/j.csite.2023.103724. URL: https://www.sciencedirect.com/science/article/pii/S2214157X23010304 (visited on 01/27/2024) (cit. on p. 46).

Zheng, Wandong et al. (Jan. 15, 2015). "The thermal performance of seawater-source heat pump systems in areas of severe cold during winter." In: *Energy Conversion and Management* 90, pp. 166–174. ISSN: 0196-8904. DOI: 10.1016/j.enconman.2014.10.050. URL: https://www.sciencedirect.com/science/article/pii/S0196890414009315 (visited on 02/29/2024) (cit. on p. 32).

Zogg, Martin (2008). "History of Heat Pumps Swiss Contributions and International Milestones." In: (cit. on pp. 42, 52).